Hydrocarbons and NSO-compounds in oil-bearing fluid inclusions detected by FT-ICR-MS and their applications in petroleum systems

vorgelegt von
M. Sc. Geologe
Yufu Han
ORCID: 0000-0002-2580-916X

an der Fakultät VI – Planen Bauen Umwelt
der Technischen Universität Berlin
zur Erlangung des akademischen Grades

Doktor der Naturwissenschaften
- Dr. rer. nat. -

genehmigte Dissertation

Promotionsausschuss:

Vorsitzender: Prof. Dr. Thomas Neumann
Gutachter: Prof. Dr. Christian Hallmann
Gutachter: Prof. Dr. Wilhelm Dominik

Tag der wissenschaftlichen Aussprache: 12. April 2022

Berlin 2022

I dedicate this thesis to my parents!

"The unity of knowledge and action"

Yangming Wang (1472 – 1529)

ACKNOWLEDGEMENTS

First and foremost, I would like to sincerely thank my two supervisors Dr. Mareike Noah and Dr. Kai Mangelsdorf. Dr. Mareike Noah guided me through the organization process of my Ph.D. study, provided assistance during the sample collection, introduced me to the Fourier transform-Ion cyclotron resonance-mass spectrometry (FT-ICR-MS) analysis and data evaluation, and helped to improve the data interpretation by valuable discussions. Dr. Kai Mangelsdorf has given invaluable scientific opinions and constructive feedback on scientific results during manuscript preparation and publications. My profound gratitude also goes out to my principal supervisor Prof. Dr. Brian Horsfield, who provided me an opportunity to study in the Organic Geochemistry Section of the Helmholtz Centre Potsdam (GFZ) German Research Centre for Geosciences, defined my Ph.D topic, and offered his advice on academic topics and data publication. Special thanks go to Dr. Volker Lüders who opened for me the door to the world of fluid inclusion and gave me invaluable assistance throughout the preparation phase of fluid inclusion analysis. Special thanks also go to Dr. Stefanie Pötz for guiding me through the secrets of FT-ICR-MS. Without their strong support and great help, it would have been a much harder road to complete my study and this dissertation.

A big thanks goes to Cornelia Karger, Anke Kaminsky, Dr. Andrea Vieth-Hillebrand, Doreen Noack, Kristin Günther and Mirco Rahn. Their professional technical and/or scientific support and assistance were invaluable to my research.

Oil-bearing fluid inclusion samples are not always easy to obtain. Thus, I would like to express special debt of gratitude to the following persons for providing samples and permitting to publish the outcome: Dr. Nicole Guilhaumou (Museum d'Histoire Naturelle Paris), Dr. David Banks (University of Leeds), Stephen Becker (ExxonMobil Upstream Research Company), Dr. Alexander Hartwig (Aker BP ASA Norway), Dr. Joachim Rinna (Aker BP ASA Norway), Dr. Jon Erik Skeie (Aker BP ASA Norway), Dr. Félix Schubert (University of Szeged) and Sándor Körmös (University of Szeged).

My sincere gratitude is extended to Claudia Engelhardt and the Welcome Center of GFZ for their special help and assistance concerning work and life issues over the past years. Many thanks also go to staff members and students (past and present) of the Organic Geochemistry section in Potsdam: Huiwen Yue, Dr. Yuanjia Han, Dr. Yaling Zhu, Dr. Shengyu Yang, Priv. Doz. Dr. Hans-Martin Schulz, Mostafa Nasr Sayed Monged, Dr. Ricardo Ruiz Monroy, Roman Feal, Karsten Adler, Ferdinand Perssen, Michael Gabriel, Dr. Robert Ondrak, Dr. Nicolaj Mahlstedt, Dr. Volker Ziegs and Prof. Dr. Christian Hallmann.

The China Scholarship Council (CSC) and the Industry Partnership Progamme Polars in Fluid Inclusions (PIFI) are gratefully acknowledged for funding my study. Sophie Müller-Moewes and the Center for Junior Scholars (CJS) from the Technical University Berlin are also thanked for supporting me with a Short-term scholarship for foreign students (STIBET) degree completion grant enabling me to finish my thesis despite of delays related to the Covid-19 pandemic.

Finally, I would like to express my great gratitude especially to my beloved parents, brother and girlfriend for their loving support and great trust in me over these years.

LIST OF PUBLICATIONS

Articles:

(1) Han, Y., Noah, M., Lüders, V., Horsfield, B., Mangelsdorf, K., 2020. NSO-compounds in oil-bearing fluid inclusions revealed by FT-ICR-MS in APPI (+) and ESI (–) modes: A new method development. Organic Geochemistry, 149, 104113. *https://doi.org/10.1016/j.orggeochem.2020.104113*

(2) Han, Y., Noah, M., Lüders, V., Rinna, L., Hartwig A., Skeie J.K., Horsfield, B., Mangelsdorf, K.,2022. Geochemical characteristics of inclusion oils from the Skarv field A segment and their implications for the oil charge and leakage history. Marine and Petroleum Geology, 137, 105506. *https://doi.org/10.1016/j.marpetgeo.2021.105506*

(3) Han, Y., Noah, M., Lüders, V., Körmös S., Schubert F., Poetz S., Horsfield, B., Mangelsdorf, K. 2022. Fractionation of hydrocarbons and NSO-compounds during primary oil migration revealed by high resolution mass spectrometry: insights from oil trapped in fluid inclusions. International journal of Coal Geology, 254, 10397. *https://doi.org/10.1016/j.coal.2022.103974*

Posters:

(1) Han, Y., Noah, M., Lüders, V., Horsfield, B., 2018. Analysis of NSO compounds in oil-bearing fluid inclusions using ultra-high resolution mass spectrometry. ALAGO, Brazil, Poster.

(2) Han, Y., Noah, M., Lüders, V., Horsfield, B., 2019. NSO compounds in oil-bearing fluid inclusions – development of a clean-up method suitable for FT-ICR-MS analysis. IMOG, Sweden, Poster.

ABSTRACT

Oil-bearing fluid inclusions (FIs) are a widespread phenomenon in veins and vugs of petroleum systems. The occluded oils provide invaluable information on the composition and physical as well as chemical properties of these oils and on geochemical processes within the respective petroleum system. A specific advantage of fluid inclusions is that the trapped oils are protected against secondary processes impacting the petroleum system such as water washing, biodegradation, migration and drill mud contamination and, thus, fluid inclusions provide information on the original pristine petroleum charge. From an analytical point of view generally gas chromatography-flame ionization detector (GC-FID), gas chromatography-mass spectrometry (GC-MS) and gas chromatography-isotope ratio mass spectrometry (GC-IRMS) are applied to analyze the aliphatic and aromatic compounds of the FI oils and to solve the geological issues of the petroleum system. Less is known about co-occurring nitrogen, sulfur and oxygen (NSO)-containing compounds. NSO-compounds are components, which, due to their polarity, are prone to physical, chemical and biological interaction processes and therefore, are promising compounds for unravelling secondary alteration processes in petroleum systems. To explore the potential of the NSO fraction in FI oil research, a relatively new analytical technique has been applied here: the Fourier transform-ion cyclotron resonance-mass spectrometry (FT-ICR-MS) in combination with Atmospheric Pressure Photoionization in positive ion mode (APPI (+)) and Electrospray Ionization in negative ion mode (ESI (–)). The technique allows an extension of the analytical window of NSO components into the high molecular weight compound range.

Due to the high sensitivity of the FT-ICR-MS it was first necessary to develop an extremely thorough FI clean-up and sample preparation method. Then, in a second step, the application potential of the NSO fractions measured by FT-ICR-MS for FI research was explored in two case studies addressing the charge and leakage history in petroleum systems and petroleum fractionation during oil primary migration. In these studies, the data of the newly introduced FT-ICR-MS technique are combined in

a multi-analytical approach with microscopy, GC-MS and GC-IRMS data.

Due to the low compound yield in FIs, the FI compound inventory can easily be contaminated by compounds from outer surfaces and a thorough cleaning protocol is a prerequisite for FI oil research. Previous clean-up methods for host minerals are not suitable for the FT-ICR-MS analysis, and a more rigorous clean-up method had to be developed. For this purpose, two fluorite and two quartz samples, containing a high number of oil FIs, were selected to develop an improved clean up method for host minerals using Soxhlet and sonication apparatus with various inorganic and organic solvents used in sequence. Although not all contaminants from surrounding host mineral surfaces could be eliminated, the procedure enabled the external contaminants to be identified and thus to assess the level of contamination of individual NSO-compound classes. This allows a well-considered interpretation of the FT-results of FI samples including their contamination levels, especially for compounds measured in the APPI (+) but also in the ESI (–) mode. Furthermore, it was demonstrated that previously established NSO parameters developed for crude oils and sediment extracts can also be utilized in FI oil research.

In the first case study the oil charge and leakage history of the Skarv field A reservoir segment in the Haltenbanken region offshore Norway was elucidated. FI oils in quartz cements from the Jurassic Garn and Tilje Formation (Fm) sandstones representing the initial oil charge were compared to the corresponding adsorbed (Ad) residual oils on host mineral surfaces representing the current reservoir oil filling. The comprehensive biomarker, stable carbon isotope and NSO-compound analyses shows that both FI oils from the Garn and Tilje Fm and the Ad oil from the Tilje Fm derive from a similar source of similar age, whereas the Ad oil from the Garn Fm shows a lower maturity level and differences in facies indicators. The similar geochemical signals for the FI oils from the Tilje and Garn Fm point to a first charging from the same source rock most likely the late-Jurassic/earliest-Cretaceous Spekk Fm. The fact that the Ad oil in the Tilje Fm is similar to the respective FI oil indicates that the Tilje Fm was charged only once. In contrast, differences between the FI and Ad oils in the Garn Fm suggest that first charge oil has leaked and was replenished by a later oil

charge presumably from another less mature source of the Spekk Fm. The NSO data confirm the similarity between the FI oils of the Garn and Tilje Fm. However, due to very low NSO-compound contents in the Ad oils a comparison between the FI and Ad oil NSO-compounds for the two reservoirs using FT-ICR-MS was not possible in this case.

In the second case study, the fractionation of hydrocarbon (HC) and NSO-compounds during oil primary migration of the Hosszúhetény Calcareous Marl Formation (HCMF) in the Mecsek Mountains area (Hungary) was revealed, where FI oils represent expelled fluids and extracts from the HCMF source rock (SR) represent retained bitumen as verified by the similar biomarker proxies and stable carbon isotope data. The comparison of FT-ICR-MS results from the FI oils and SR extracts shows that O_1, N_1, N_1O_1 and S_1O_1 compound classes are preferentially retained in the SR bitumen, while S_1 compounds are preferentially expelled from SR. O_2 and HC compounds seem to show at first glance no preference. In addition, a deeper look into the NSO-compound classes reveals that compounds with a higher aromaticity are preferentially retained in SRs, which is especially true for compounds with a high number of double bond equivalents (DBEs) in the lower carbon number range. This indicates shorter alkyl side chains attached to the aromatic structures and thus a less pronounced shielding effect. Overall, this study provides significant indication that HC and NSO-compound fractionation during primary migration is influenced by the different functional groups with their associated polarities and by their molecular shape and size especially the degree of aromaticity.

ZUSAMMENFASSUNG

Ölhaltige Flüssigkeitseinschlüsse sind ein weit verbreitetes Phänomen in Gängen und Klüften von Erdölsystemen. Die eingeschlossenen Öle liefern wertvolle Informationen über die Zusammensetzung und physikalischen wie chemischen Eigenschaften dieser Öle sowie über geochemische Prozesse im entsprechenden Erdölsystem. Ein besonderer Vorteil von Flüssigkeitseinschlüssen besteht darin, dass die eingeschlossenen Öle vor verändernden sekundären Prozessen wie z. B. der Wasserauswaschung von Komponenten, dem biologischen Abbau, der Migration von Ölen und der Verunreinigung durch Bohrschlamm geschützt sind. Flüssigkeitseinschlüsse können damit unverfälschte Informationen über die ursprüngliche Erdölfüllung liefern. Aus analytischer Sicht werden im Allgemeinen Techniken wie die Gaschromatographie (mit einem Flammenionisationsdetektor, GC-FID), die Gaschromatographie-Massenspektrometrie (GC-MS) und die Gaschromatographie-Isotopenverhältnis-Massenspektrometrie (GC-IRMS) eingesetzt, um die aliphatischen und aromatischen Verbindungen der Öle in Flüssigkeitseinschlüssen zu analysieren und die geologischen Fragestellungen des Erdölsystems zu beantworten. Im Gegensatz zu aliphatischen und aromatischen Verbindungen ist nur sehr wenig über Stickstoff, Schwefel und Sauerstoff (NSO) enthaltende Verbindungen bekannt. Bei den NSO-Verbindungen handelt es sich um Komponenten, die aufgrund ihrer Polarität stark dazu neigen, physikalische, chemische und biologische Wechselwirkungsprozesse mit der Umgebung einzugehen. Sie sind daher vielversprechende Verbindungen, um anhand der Veränderung ihrer relativen Zusammensetzung sekundäre Alterationsprozesse in Erdölsystemen aufzudecken. Um das Potenzial der NSO-Komponenten in der Erforschung von Ölflüssigkeitseinschlüssen zu untersuchen, wird in dieser Arbeit eine relativ neue Analysetechnik angewandt: die Fourier-Transform-Ionen Zyklotron Resonanz-Massenspektrometrie (FT-ICR-MS) in Kombination mit Atmosphärendruck-Photoionisation im positiven Ionenmodus (APPI (+)) und Elektrospray-Ionisation im negativen Ionenmodus (ESI (–)). Gleichzeitig ermöglicht diese Technik eine Erweiterung des Analysefensters von NSO-Komponenten in den vorher nicht

erfassten hochmolekularen Bereich.

Aufgrund der hohen Empfindlichkeit des FT-ICR-MS ist es zunächst erforderlich, eine neue Reinigungs- und Probenvorbereitungsmethode für die Untersuchung von Flüssigkeitseinschlüssen zu entwickeln. In einem zweiten Schritt wird das Anwendungspotenzial der mit der FT-ICR-MS Technik bestimmten NSO Komponenten in zwei Fallstudien untersucht, die sich mit der Befüllungs- und Leckagegeschichte in einem Erdölsystem und der Erdölfraktionierung während der primären Ölmigration befassen. In diesen Studien werden die Daten der neu eingeführten FT-ICR-MS Methode mit herkömmlichen Daten der Flüssigkeitseinschlussanalyse wie der Mikroskopie, GC-MS und GC-IRMS kombiniert.

Aufgrund der in der Regel geringeren Menge an Verbindungen in Flüssigkeitseinschlüssen kann diese Zusammensetzung leicht durch Komponenten von der äußeren Oberfläche des Wirtsminerals verunreinigt werden. Aus diesem Grund ist ein gründliches Reinigungsprotokoll eine zentrale Voraussetzung für die Erforschung von Flüssigkeitseinschlüssen. Bisherige Reinigungsmethoden für Wirtsminerale sind für die FT-ICR-MS Analyse nicht geeignet, und es musste eine rigorosere Reinigungsmethode entwickelt werden. Es wurden zwei Fluorit- und zwei Quarzproben, die eine große Anzahl von Ölflüssigkeitseinschlüssen enthielten, ausgewählt, um eine verbesserte Reinigungsmethode für die Wirtsmineralien zu entwickeln. Bei dieser Methode kommen verschiedene Extraktionsverfahren wie Soxhlet- und Ultraschallextraktion mit unterschiedlichen anorganischen und organischen Lösungsmitteln zum Einsatz. Obwohl nicht immer alle Verunreinigungen vollständig von den Wirtsmineraloberflächen entfernt werden konnten, ermöglicht das Verfahren die Identifizierung externer Verunreinigungen und damit die Bewertung des Verunreinigungsgrads einzelner NSO-Verbindungsklassen. Dies erlaubt eine ausgewogene Interpretation der FT-Ergebnisse aus Flüssigkeitseinschlüssen unter Berücksichtigung des Verunreinigungsgrades insbesondere für Verbindungen, die im APPI (+) aber auch im ESI (–) Modus gemessen wurden. Darüber hinaus konnte gezeigt werden, dass die zuvor bei der FT-Untersuchung von Rohölen und

Sedimentextrakten entwickelten NSO-Parameter auch in der Erforschung von Ölflüssigkeitseinschlüssen verwendet werden können.

In der ersten Fallstudie wurde die Ölfüllungs- und Leckagegeschichte des Skarv-Feldes A in der Haltenbanken-Region vor der norwegischen Küste untersucht. Ölflüssigkeitseinschlüsse in Quarzen aus den Sandsteinen der jurassischen Garn- und Tilje Formation (Fm), die die ursprüngliche Ölfüllung darstellen, wurden mit den entsprechenden adsorbierten Resten von Ölen auf den Wirtsmineraloberflächen verglichen, die die aktuelle Ölfüllung des Reservoirs repräsentieren. Die umfassenden Analysen von Biomarkern, stabilen Kohlenstoffisotopen und NSO-Verbindungen zeigen, dass sowohl die Ölflüssigkeitseinschlüsse aus der Garn- und Tilje Fm als auch das adsorbierte Öl aus der Tilje Fm aus einer ähnlichen Quelle mit vergleichbarem Alter stammen, während das adsorbierte Öl aus der Garn Fm einen niedrigeren Reifegrad und Unterschiede bei den Faziesindikatoren aufweist. Die ähnlichen geochemischen Signale für die Ölflüssigkeitseinschlüsse aus der Tilje- und Garn Fm deuten darauf hin, dass die Öle aus demselben Muttergestein stammen, höchstwahrscheinlich der spätjurassischen/frühkreidezeitlichen Spekk Fm. Die Tatsache, dass das adsorbierte Öl in der Tilje Fm dem aus den entsprechenden Flüssigkeitseinschlüssen ähnelt, deutet darauf hin, dass die Tilje Fm nur einmal befüllt wurde. Im Gegensatz dazu weisen die Unterschiede zwischen dem adsorbierten Öl und dem Öl aus den Flüssigkeitseinschlüssen in der Garn Fm darauf hin, dass das Öl der ersten Reservoirbefüllung bereits mittels tertiärer Migration aus der Fm migriert ist und durch eine spätere Ölcharge aufgefüllt wurde, die vermutlich aus einem anderen, weniger reifen Muttergestein der Spekk Fm stammt. Die FT-ICR-MS NSO-Daten bestätigen die Ähnlichkeit zwischen den Flüssigkeitseinschlussölen der Garn und Tilje Fm. Aufgrund der sehr geringen Gehalte an NSO-Verbindungen in den adsorbierten Ölen war ein Vergleich zwischen den NSO-Verbindungen der Flüssigkeitseinschluss- und adsorbierten Öle mittels FT-ICR-MS für die beiden Öllagerstätten in diesem Fall nicht möglich.

In der zweiten Fallstudie wurde das Fraktionierungsverhalten von Kohlenwasserstoffen und NSO-Verbindungen während der primären Ölmigration in

der kalkhaltigen Hosszúhetény Marl Formation (HCMF) im Mecsek-Gebirge (Ungarn) untersucht. Hierbei repräsentieren die Ölflüssigkeitseinschlüsse die primäre Ölmigrationsphase und die Extrakte aus dem HCMF-Muttergestein das zurückgehaltene Bitumen. Diese Öl-Muttergesteinsbeziehung wurde durch die Ähnlichkeit von Biomarkerparametern und stabilen Kohlenstoff-Isotopendaten bestätigt. Der Vergleich der Ergebnisse von Ölflüssigkeitseinschlüssen und Muttergesteinsextrakten zeigt, dass die Verbindungsklassen der O_1-, N_1-, N_1O_1- und S_1O_1-Komponenten bevorzugt im Muttergesteinsbitumen zurückgehalten werden, während S_1-Verbindungen bevorzugt aus dem Muttergestein migrieren. O_2- und Kohlenwasserstoffverbindungen scheinen auf den ersten Blick keine Präferenz zu zeigen. Darüber hinaus zeigt ein tieferer Blick in die NSO-Verbindungsklassen, dass Verbindungen mit einer höheren Aromatizität bevorzugt im Muttergestein zurückgehalten werden, was insbesondere für Verbindungen mit einer hohen Anzahl von Doppelbindungsäquivalenten (DBEs) im unteren Kohlenstoffzahlbereich gilt. Dies deutet auf kürzere Alkylketten an den aromatischen Strukturen und damit auf einen weniger stark ausgeprägten Abschirmungseffekt durch die Alkylseitenketten hin. Insgesamt liefert diese Studie deutliche Hinweise darauf, dass die Fraktionierung von Kohlenwasserstoffen und NSO-Verbindungen während der primären Migration von den verschiedenen funktionellen Gruppen und deren Polaritäten sowie von der Molekülform und -größe insbesondere dem Grad der Aromatizität beeinflusst wird.

CONTENTS

LIST OF FIGURES

UV light, and pale blue fluorescence of oil adsorbed on clay minerals. c) Bitumen adsorbed on the surface of quartz (marked by white circle) showing yellowish fluorescence under UV light, and pale blue fluorescence of oil adsorbed on clay minerals. d) Asphaltene-rich residues trapped in intergranular pores of sandstone of sample G1. e) Asphaltene-rich residues in figure 3.2d show yellow fluorescence under UV light, and pale blue fluorescence of oil adsorbed on clay minerals. f) Aqueous FIs in quartz from sample G1 under transmitted light, note that the liquid to vapor ratios are highly variable and inclusions can be all-liquid or contain large bubbles. g) Two oil inclusion trails in quartz from sample T1 showing yellow fluorescence under UV light (color in figure cannot reflect real fluorescence color under UV light), and pale blue fluorescence of oil adsorbed on clay minerals. h) Oil inclusion trail in quartz from sample T1 under transmitted light. i) Same oil FIs in figure 3.2h showing yellow fluorescence under UV light. j) Abundant irregularly-shaped oil FIs trapped in quartz from sample T1 showing yellow fluorescence under UV light. k) Oil FIs trapped in a growth zone in quartz from sample T1. l) Oil FIs from figure 3.2k show yellow fluorescence under UV light and pale blue fluorescence of oil adsorbed on clay minerals. Pl: pale blue; Y: yellow; Qz: quartz.

Figure 3.3. a) *n*-Alkane distribution patterns measured by GC-MS of adsorbed (Ad) oils from the Garn (Gx; red) and Tilje Fms (Tx; green) in the Skarv field A segment, Norway. b) *n*-Alkane distribution patterns of fluid inclusion (FI) oils from the Garn (Gx; blue) and Tilje Fms (Tx; magenta).

Figure 3.4. Mass trace *m/z* 191 and 217 chromatograms showing the distribution of hopanes, diasteranes and steranes in adsorbed (Ad) and fluid inclusion (FI) oils from the Garn (G1, G2 and G3) and Tilje (T1 and T2) Fms. Ts = 18α-trisnorneohopane; Tm = 17α-trisnorhopane; BNH = 28,30-bisnorhopane; Gm = Gammacerane.

Figure 3.5. Pie chart of elemental and compound class distributions in inclusion (FI) oils from the Garn (G1 and G2) and Tilje (T1) Fms. O_x = Compound class containing x oxygen atoms; HC = Hydrocarbon; N_y = Compound class containing y nitrogen atoms; N_yO_x = Compound class containing y nitrogen and x oxygen atoms; S_z = Compound class containing z sulfur atoms; S_zO_x = Compound class containing z sulfur and x oxygen atoms.

core molecule within every DBE class. Note that S_1 compounds with carbon numbers above 50 in the SR extract are not included due to instrumental resolving power limitations for S_1 compounds in the here investigated SR sample (see text).

Figure 4.9. a) Double bond equivalent (DBE) distributions of the O_1 compound class in the two source rocks (SR-1 and SR-2) extracts (red) and four fluid inclusion (FI-3 to FI-6) oils (blue). b) Normalized intensity distribution of the three DBE groups $DBE_{1–5}$ (low), $DBE_{6–15}$ (medium) and DBE_{15+} (high) for the O_1 class in the SR extracts (red) and FI oils (blue) with average value indicated. c) DBE versus carbon number plot of the O_1 class in a representative SR extract (SR-2). d) DBE versus carbon number plot of the O_1 class in a representative FI oil (FI-6). The normalized intensity (%) is expressed relative to the total monoisotopic ion abundance of the O_1 class. The magenta colored diagonal line delineates the minimum carbon number of a non-alkylated planar polycyclic aromatic core molecule within every DBE class.

Figure 4.10. a) Double bond equivalent (DBE) distributions of the O_2 compound class in the two source rocks (SR-1 and SR-2) extracts (red) and four inclusion (FI-3 to FI-6) oils (blue). b) Normalized intensity distribution of the three DBE groups $DBE_{1–5}$ (low), $DBE_{6–15}$ (medium) and DBE_{15+} (high) for the O_2 class in SR extracts (red) and FI oils (blue) with average value indicated. c) DBE versus carbon number plot of the O_2 class in a representative SR extract (SR-1). d) DBE versus carbon number plot of the O_2 class in a representative FI oil (FI-3). The normalized intensity (%) is expressed relative to the total monoisotopic ion abundance of O_2 class. The magenta colored diagonal line delineates the minimum carbon number of a non-alkylated planar polycyclic aromatic core molecule within every DBE class.

Figure 4.11. a) Double bond equivalent (DBE) distributions of the N_1 compound class in the two source rocks (SR-1 and SR-2) extracts (red) and four inclusion (FI-3 to FI-6) oils (blue). b) Normalized intensity distribution of the three DBE groups $DBE_{1–5}$ (low), $DBE_{6–15}$ (medium) and DBE_{15+} (high) for N_1 class in SR extracts (red) and FI oils (blue) with average value indicated. c) DBE versus carbon number plot of the N_1 class in a representative SR extract (SR-2). d) DBE versus carbon number plot of the N_1 class in a representative FI oil (FI-6). The normalized intensity (%) is expressed relative to the

LIST OF TABLES

0.65% < Ro < 1.35% (Radke and Welte, 1983); DBT/Ph= Dibenzothiophene/phenanthrene.

Table 4.1. Note: Ts = 18α-trisnorneohopane; Tm = 17α-trisnorhopane; C_{29}Ts = 18α-30-norneohopane; 22S/(22S + 22R) = C_{31} αβ-22S/(22S + 22R) hopanes; C_{35} homohopane index = $C_{35}/(C_{31}–C_{35})$ homohopanes; 20S/(20S + 20R) = C_{29} ααα-20S/(20S + 20R) steranes; ββ/(ββ + αα) = C_{29} αββ/(αββ + ααα) steranes; C_{27}/C_{29} sterane = C_{27} ααα-20R/C_{29} ααα-20R sterane; diasteranes/steranes = C_{27} βα-diasteranes/C_{27} (ααα + αββ) steranes; steranes/17α-hopanes = $C_{27}–C_{29}$ steranes/$C_{29}–C_{35}$ 17α-hopanes; methylphenanthrene index (MPI-1) = 1.5 × (3MP + 2MP)/(P + 9MP + 1MP); calculated vitrinite reflectance (Rc) = 0.6 × MPI-1 + 0.4 (for 0.65% < Ro < 1.35%; Radke and Welte, 1983).

Table S1. Relative abundance of the compound class data in figure 2.5. Note: nd. = not detectable or not determinable; HC = hydrocarbon; GE = Germany; TN = Tunisia; PK = Pakistan; MX = Mexico; APPI (+) = Atmospheric Pressure Photoionization in positive ion mode; ESI (–) = Electrospray Ionization in negative ion mode.

Table S2. Relative abundance of the DBE 5 groups of the hydrocarbon data in figure 2.9. Note: nd. = not detectable or not determinable; GE = Germany; TN = Tunisia; PK = Pakistan; MX = Mexico.

Table S3. Relative abundance of *n*-alkane distribution data in figure 3.3. Note: nd. = not detectable or not determinable; G = Garn Formation; T = Tilje Formation; Ad= adsorbed oil; FI = inclusion oil.

Table S4. Relative abundance of the compound class data in figure 3.5. Note: G = Garn Formation; T = Tilje Formation; FI = inclusion oil; HC = hydrocarbon.

Table S5. Compound specific carbon isotopic composition of *n*-alkane data in figure 3.6. Note: G = Garn Formation; T = Tilje Formation; Ad = adsorbed oil.

Table S6. Compound specific carbon isotopic composition of *n*-alkane data in figure 4.4. Note: nd. = not detectable or not determinable; SR = source rock extract; FI = inclusion oil.

Table S7. Relative abundance of the compound class data in figure 4.5. Note: nd. = not detectable or not determinable; HC = hydrocarbon; SR = source rock extract; FI =

inclusion oil.

Table S8. Normalized abundance of compound data in figure 4.13. Note: nd. = not detectable or not determinable; DBE = Double bond equivalent; HC = hydrocarbon; SR = source rock extract; FI = inclusion oil.

LIST OF ABBREVIATIONS

A/C	Acyclic/cyclic
Ad	Adsorbed
APCI	Atmospheric pressure chemical ionization
API	American Petroleum Institute grad
APPI	Atmospheric pressure photoionization
B	Magnetic field
BNH	28,30-bisnorhopane
BTs	Benzothiophenes
C_{29}Ts	C_{29} 18α-norneohopane
C_{30}*	17α-diahopane
IRMS	Initial ratio mass spectrometry
DBE	Double bond equivalent
DBTs	Dibenzothiophenes
DCM	Dichloromethane
EI	Electron ionization
ESI	Electrospray ionization
F'	Centrifugal force
F	Centripetal force
f	Cyclotron frequency
FD/FI	Field desorption/ionization
FID	Flame ionization detector
FIs	Fluid inclusions
Fm	Formation
FT-ICR-MS	Fourier transform-ion cyclotron resonance-mass spectrometry
FT-IR	Fourier-transform infrared
G	Garn Fm
GC	Gas chromatography
GC-MS	Gas chromatography-mass spectrometry
GE	Germany

Gm	Gammacerane
GOI	Grains containing oil inclusions
GOR	Gas to oil ratio
HC	Hydrocarbon
HCl	Hydrogen chloride
HCMF	Hosszúhetény Calcareous Marl Formation
HPLC	High performance liquid chromatography
IR	Infrared spectroscopy
kg	kilogram
kv	kilovoltage
LSB	Lower Saxony Basin
L-V	Liquid-vapor
m/z	Mass to charge ratio
ma	million years
MALDI	Matrix assisted laser desorption ionization
mg	milligram
min	minute
mL	milliliter
mm	millimeter
MP	Methylphenanthrene
MPI-1	Methyl Phenanthrene Index
MPLC	Medium pressure liquid chromatography
ms	millisecond
MVT	Mississippi Valley-type
MX	Mexico
NMR	Nuclear magnetic resonance
NSO-compounds	Nitrogen, sulfur and oxygen containing compounds
OM	Organic matter
P-blank	Procedural blank
Ph	Phenanthrene
PK	Pakistan

PVTX	Pressure-Volume-Temperature-Composition
Rc	Calculated vitrinite reflectance
Re	Vitrinite reflectance equivalent
Ro	Vitrinite reflectance
S-blank	System blank
SIM	Single ion monitoring
SR	Source rock
T	Tilje Fm
Tm	17α-trisnorhopane
TMIA	Total monoisotopic ion abundance
TN	Tunisia
ToF-SIMS	Time-of-flight secondary ion mass spectrometry
Ts	18α-trisnorneohopane
TSR	Thermochemical sulfate reduction
UCM	Unresolved complex mixture (UCM)
UV	Ultraviolet
v	velocity
v/v	volume/volume
VPDB	Vienna Pee Dee Belemnite
wt%	Percentage by weight
$\delta^{13}C$	Stable carbon isotope $^{13}C/^{12}C$ ratio relative to standard of the Vienna Pee Dee Belemnite
µL	microliter
µm	micrometer
ω_c	Angular cyclotron frequency

1. INTRODUCTION

1.1 Composition of Petroleum

Petroleum, thermogenically generated from organic matter over geological times in deeply buried source rock formations, is extremely complex by nature (Tissot and Welte, 1984; Horsfield, 1997; Robbins and Hsu, 2000). Petroleum mainly consists of hydrocarbons such as paraffins, naphthenes and aromatics and to a lesser extent of components containing hetero-atoms such as nitrogen, sulfur and oxygen (NSO) compounds. Furthermore, compounds of higher molecular complexity are present including asphaltenes which are rich in metals, particularly vanadium, nickel, and iron (Tissot and Welte, 1984; Robbins and Hsu, 2000). The relative compositions of these component groups are quite variable in petroleum, controlled by the nature of the organic source material (kerogen) as well as secondary evolution and alterations processes after petroleum generation. To unravel the various influences controlling petroleum compositions, numerous organic geochemical methods have been developed as outlined below (Dickinson, 1980; Pearson and Gharfeh, 1986; Wang and Fingas, 1997; Speight, 2001; Chen et al., 2015).

1.1.1 Factors controlling petroleum composition

The composition of petroleum depends initially on the nature of the organic matter (kerogen) type in the source rocks, the maturation stage at the time of petroleum expulsion and subsequently upon secondary evolution and alteration processes comprising migration of petroleum from the source to the reservoir rock, biodegradation of petroleum by microorganisms living in oil reservoirs, water washing of more water soluble compounds, secondary thermal cracking of generated petroleum hydrocarbons, thermochemical sulfate reduction (TSR) etc. (Tissot and Welte, 1984; Moldowan et al., 1985; Jones, 1987; Horsfield, 1997; Harayama et al., 1999; Cross et al., 2004; Peters et al., 2005). Some of these factors, such as the kerogen nature tend to make petroleums different, while some others, for example migration processes, tend to make crude oils more similar. Thus, the oil composition

is influenced by multiple factors (Tissot and Welte, 1984). Although it is difficult to identify a single factor that is clearly responsible for the distribution of petroleum constituents, the analysis of the petroleum constituents can shed light on these factors and the main factors are presented in the following part:

Organic matter type. The gross chemical composition of petroleum is initially controlled by the nature of the organic matter (kerogen) in the source rock. The definition of kerogen type I, II, III and IV showing different petroleum potential, can be expressed using H/C vs. O/C diagram, in which the hydrogen-rich type I and II kerogens are more oil-prone (van Krevelen, 1961; Tissot and Welte, 1984; Vandenbroucke and Largeau, 2007). The deposited organic matter is a complex mixture of lipids, carbohydrates, proteins, lignins and other organic matter components produced by different source organisms. Thus, different mixtures of source organisms depending on marine, terrigenous and lacustrine depositional conditions lead to different characteristic compositions of the organic matter in the source rocks (Tissot et al., 1974; Moldowan et al., 1985; Horsfield, 1997; Peters et al., 2005). For example, marine organic matter usually generates paraffinic-naphthenic or aromatic petroleum, while terrestrial organic matter generates more paraffinic or sometimes paraffinic-naphthenic petroleum (Tissot and Welte, 1984). High sulfur petroleum occurs more frequently in carbonate rich source rocks (Tissot and Welte, 1984; Vandenbroucke and Largeau, 2007). Biomarker distributions in petroleum, such as pristine, phytane, hopanes and steranes are useful tools to distinguish between different original source inputs and depositional environments (Tissot and Welte, 1984; Peters et al., 2005).

Thermal maturation. Petroleum compounds are metastable products which tend toward greater thermodynamic stability during maturation with increasing depth and associated rising temperature (Tissot and Welte, 1984; Peters et al., 2005). In addition to the absolute temperature controlling the thermal maturation, the time of exposure to that temperature can also affect petroleum composition, while the influence of pressure is likely to be considered subordinate (Tissot and Welte, 1984). With increasing maturation, petroleum components lose their functional groups (oxygen,

sulfur and nitrogen) and their carbon chain length become shorter resulting in an increasing amount of low molecular weight hydrocarbons (including hydrocarbon gases) at the expense of high molecular weight constituents (Tissot and Welte, 1984; Lewan, 1997). Thus, by releasing different compound distributions at different maturation stages the composition of petroleum depends also on the level of thermal maturity.

Migration. Considerable changes in the composition of petroleum are caused by the oil migration process. The expulsion of oil from the source rock is named primary migration, while the migration through the subsurface lithology (carrier rock) into the reservoir rock is called secondary migration and the leakage of oil from a petroleum reservoir is termed remigration or tertiary migration (Tissot and Welte, 1984). Less polar compounds, especially those of lower molecular weight, migrate preferentially into the reservoir rock, while polar NSO-compounds are preferably retained in the source rock. Thus, expelled and migrated oils are typically enriched in saturated and aromatic hydrocarbons, but depleted in NSO-compounds and asphaltenes compared with pristine oils in the source rocks (Leythaeuser et al., 1988a; Sandvik et al., 1992; Han et al., 2015). This compositional partitioning reflects the interaction of the individual petroleum constituents (with their different physicochemical properties) with the organic matter and mineral matrix of the source and carrier rocks and the porewaters along the migration pathways (Larter and Aplin, 1995).

Biodegradation. Biodegradation is a process leading to the alteration of petroleum due to the activity of microorganisms (Connan, 1984; Blanc and Connan, 1994; Peters et al., 2005). The degree of petroleum alteration depends on the intensities of the microbial activity and the time the petroleum is exposed to biodegradation, finally leading to different molecular compositions of the petroleum (Palme, 1993; Peters et al., 2005; Tissot and Welte, 1984). During this process, hydrocarbons are preferentially consumed by microorganisms while heteroatomic compounds are less susceptible resulting in their relative increase in the residual oils (Tissot and Welte, 1984; Peters et al., 2005).

1.1.2 Analysis of petroleum composition

Due to the complex composition of petroleum a separation of the investigated oil into fractions of different polarity is needed. The so-called SARA analysis is a common chromatographic separation that fractionates petroleum into saturated hydrocarbons, aromatic hydrocarbons, resins (NSO compounds), and asphaltenes (Robbins and Hsu, 2000; Andersen and Speight, 2001). After precipitation of asphaltenes with a large excess of a hydrocarbon solvent such as *n*-hexane or *n*-heptane (Mitchell and Speight, 1973; Theuerkorn et al., 2008), the remaining maltenes were further separated into an aliphatic, aromatic and NSO-compounds containing fraction using organic solvent of different polarity or a medium pressure liquid chromatography (MPLC) system (Radke et al., 1980). The separated petroleum fractions can then be measured by gas chromatography, gas chromatography-mass spectrometry, compound-specific carbon and hydrogen gas chromatography-isotope ratio-mass spectrometry and very recently by Fourier transform-ion cyclotron resonance-mass spectrometry.

Gas chromatography coupled with a flame ionization detector (GC-FID) is a highly efficient analytical instrument for separating individual petroleum components using a capillary column in an oven (Wang and Fingas, 1997; Speight, 2001). Main petroleum constituents especially *n*-alkanes, olefins, alkylbenzenes and even higher molecular weight paraffins (less than C_{40}) have extensively been studied and quantified using GC-FID. In addition to GC-FID, combinations of capillary GC with other techniques such as a pyrolysis system and a mass spectrometer (MS) are widely used to obtain compositional information from petroleum and its source rocks (Wang et al., 1994; Horsfield, 1989; Peters et al., 2005).

Gas chromatography coupled with a mass spectrometry (GC-MS) can be applied not only to detect individual petroleum compounds but also to identify the structure of compounds using the characteristic mass spectral fragmentation patterns (Peters et al., 2005). Additionally, minor components can be visualized by using characteristic mass traces of the respective compounds (e.g., for hopanes and steranes). Analogous to the GC-FID also quantitation of individual compounds relative to an added internal

standard can be obtained using GC-MS. Component information deduced from GC-MS, especially those of source and maturity related biomarkers, are widely used for characterizing the factors controlling petroleum composition, such as organic matter type, thermal maturation and biodegradation levels (Peters et al., 2005).

Gas chromatography coupled with isotope ratio mass spectrometry (GC-IRMS) is a valuable technique used to measure the relative abundance of stable isotopes of carbon, hydrogen, nitrogen or oxygen in individual compounds separated from petroleum (Hayes et al., 1990; O'Malley et al., 1994). The stable carbon and hydrogen isotopic compositions of *n*-alkanes are widely used to characterize oil-source correlations, thermal maturation, biodegradation and migration processes (Sofer et al., 1984; Tissot and Welte, 1984; Clayton, 1991; Dzou and Hughes, 1993; Cramer et al., 1998; Liao and Geng, 2009).

Recently, Fourier transform-ion cyclotron resonance-mass spectrometry (FT-ICR-MS) offers the highest available broadband mass resolution, mass resolving power, and mass accuracy to characterize the distribution of petroleum constituents by their elemental formulas (Marshall and Rodgers, 2008). A detailed description of this technique is provided in section 1.5.

Further techniques to unravel the petroleum composition and compound structure are high performance liquid chromatography (HPLC), ^{1}H and ^{13}C nuclear magnetic resonance (NMR) spectroscopy, infrared (IR) spectroscopy and Fourier transform infrared spectroscopy (FTIR). HPLC has been applied to analyze hydrocarbon group types of petroleum and was successfully utilized for the quantitative analysis of certain fractions (Pearson and Gharfeh, 1986; Sarowha et al., 1997). NMR has gained a prominent place in compositional and structural analysis of petroleum fractions, especially in determining the aliphatic and aromatic carbon and hydrogen distribution in complex petroleum mixtures (Dickinson, 1980; Hirasaki et al., 2003). IR provided the distribution of several structural and functional groups of petroleum components, and quantitative estimates of the various functional groups can be made using FTIR (Chen et al., 2015).

1.1.3 Samples used for petroleum composition analysis

To decipher the composition of petroleum, produced oils, drill stem test (DST) oils and reservoir core extracts are the most common samples used for analysis before or during petroleum production. Information on the petroleum composition is very valuable to identify the commercial value of an oil field, establish proper extraction and recovery ways, and study the geological background. For example, oil families in reservoir can be elucidated from intensive investigation of the geochemical composition of oil samples and source rock extracts. Although many benefits are gained from analyzing the current petroleum composition (affected by secondary alterations), these samples provide only minor information about the petroleum system history with its progressive oil charge and/or leakage and in-reservoir oil alteration events over time (George et al., 2007a). Additionally, the DST oils and reservoir core extracts can also be influenced by oil-based drilling mud contaminants interfering with the compositional evaluation. To overcome these restrictions, oils trapped in fluid inclusions (FIs) can be utilized, as they are isolated from secondary alterations by the host minerals, and therefore FIs represent a way to preserve pristine oils. The analyses of FI oils are a well-used method to trace alteration events in petroleum system (Horsfield and McLiman, 1984; Karlsen et al., 1993, 2004; George et al., 1996, 1997a, 1998, 2001, 2004a, 2007a, Volk et al., 2001, 2002, 2003, 2004, 2005a; Volk and George, 2019). Meanwhile, those routine analytical methods applied for conventional oil sample composition analyses and described above can also be used to evaluate the oil composition in FI (Munz, 2001; George et al., 2007a; Volk and George, 2019).

1.2 Oil-bearing fluid inclusions

Oil-bearing fluid inclusions (FIs), imbedded in minerals, contain aliquots of oil that was trapped within cavities during crystal growth as primary FIs or during recrystallization of secondary cracks in the presence of a fluid phase as secondary FIs (Fig. 1.1) (e.g., Burruss, 1981; Roedder, 1984; Goldstein and Reynolds, 1994; Munz, 2001). The formation process of primary oil FI is that the initially suspended oil

droplets in the saline brines became attached to the surface of the crystal during authigenic minerals growth (Roedder, 1984). If a crystal is fractured in the presence of an oil system, the oil will enter the fractures and trapped as secondary oil FI during recrystallization of the cracks (Roedder, 1984; Bodnar, 2003). These tiny "petroleum capsules" contain abundant physical and geochemical information on paleo oils that recorded direct evidence about characteristics of migrated and trapped petroleum at different times in the geological past (Volk and George, 2019). In recent decades, the analysis of oil FIs has become a significant and common means of studying the past oil fillings in petroleum systems (Burruss, 1981; Horsfield and McLimans, 1984; McLimans, 1987; Karlsen et al., 1993; Lisk et al., 1996; George et al., 1997a, 2004a; Munz, 2001; Volk and George, 2019).

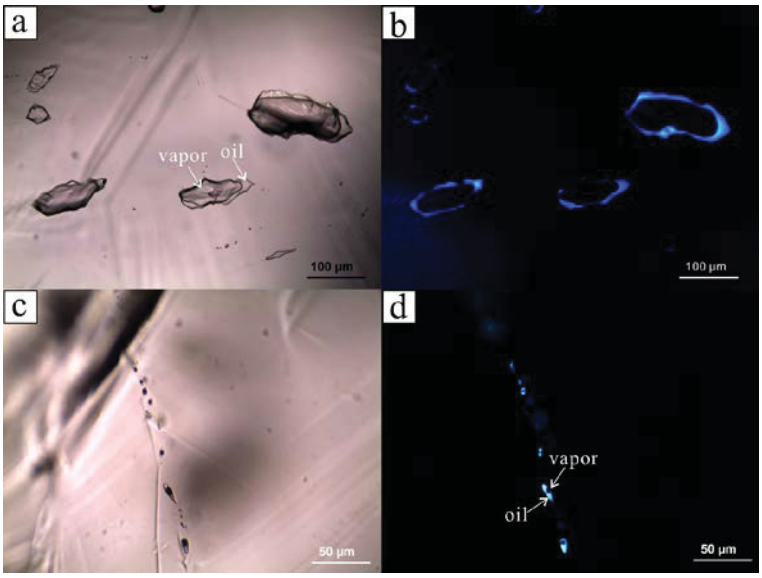

Figure 1.1 Photomicrographs of primary (a, b) and secondary (c, d) oil-bearing fluid inclusions under transmitted (a, c) and UV light (b, d). Samples from Csukma Formation in Mecsek Mountains of Hungary.

The size of oil FIs are typically in the range between <1µm to ~20µm (Kvenvolden and Roedder, 1971; Burruss, 1981; Volk and George, 2019), however, large-scale oil FIs (>100µm) are not uncommon and some of them are even visible to the naked eye (Ulrich, 1989; Guilhaumou et al., 1990; Suchý et al., 2010; Bejaoui et al., 2013). They are widespread in petroleum systems trapped in cements and/or fracture-fill mineralization hosted by a wide variety of different minerals, e.g., quartz,

carbonate and feldspar (Burruss, 1981; Roedder, 1984; Karlsen et al., 1993). Most of the oil FIs occur as secondary inclusions within detrital grains in clastic reservoirs (Munz, 2001; Volk and George, 2019). Many studies on oil FIs are conducted in sediment-hosted so-called Mississippi Valley-type (MVT) deposits and other hydrothermal derived fluids as well, where FIs are typically contained in fluorite, but also in barite, carbonate or sphalerite (Etminan and Hoffmann, 1989; Germann et al., 1995; Jochum et al., 1995a; Guilhaumou et al., 2000; Benchilla et al., 2003; González-Partida et al., 2003). In this FI formation process, petroleum that was generated from source rock migrated with hydrothermal brines and precipitate in veins and/or vugs of limestone (Etminan and Hoffmann, 1989; Benchilla et al., 2003; González-Partida et al., 2003). These oil FIs are mainly primary inclusions being sparse and randomly distributed and relatively large (Roedder, 1984). In contrast, studies on oil FIs in chalk and limestone reservoir have not been reported yet (Munz, 2001).

Oil FIs can occur in multiphases, such as liquid oil and vapor, and can as well as contain an aqueous phase and various kinds of solids, which is dependent on the conditions during the formation of the oil FIs (Munz, 2001; Burruss, 2003). Black or brown solids may be present within the oil liquid phase which is often interpreted as solid bitumen (Burruss, 2003). The composition of fluids in oil FIs can be complex. In addition to aliphatic and aromatic hydrocarbons (HC), NSO-compounds and organic gases such as methane and other low molecular weight HC, it can also contain inorganic gases such as CO_2, H_2S and N_2 (Roedder, 1984; Pang et al., 1998; Munz, 2001; Burruss, 2003). Methane is the simplest hydrocarbon compound that has been used to assess the maturation stage of trapped FI oils (Lüders et al., 2012; Lüders and Plessen, 2015). Higher molecular weight *n*-alkanes are preferential adsorbed on host minerals compared to lower molecular weight HC (Etminan and Hoffmann, 1989; George et al., 1997b, 1998). Similar to crude oils in source and reservoir rocks, a wide variety of biomarkers can be detected in FI oils such as *n*-alkanes, acyclic isoprenoids, steranes, diasteranes, terpanes, hopanes and aromatic steroids providing crucial information on source-, maturity- and biodegradation-related parameters to characterize petroleum systems (Karlsen et al., 1993; Nedkvitne et al., 1993; George

et al., 1997a, 1997b, 1998, 2001, 2004a, 2007a; Volk et al., 2002, 2003, 2005a; Pan et al., 2003; Cao et al., 2006).

As mentioned above, FI oils trapped in host minerals also contain a higher proportion of polar compounds than the associated reservoir oils (Karlsen et al., 1993; Macleod et al., 1993; Nedkvitne et al., 1993; Pang et al., 1998; Bhullar et al., 1999), which is caused by the preferentially adsorption of NSO-compounds onto charged mineral surfaces due to their higher polarity (Clementz, 1976; Horstad et al., 1990). The occurrence of polar compounds with lower molecular weight such as phenolic, carbazolic and benzocarbazolic compounds in FI oils has been reported by Peters et al. (2018) using GC-MS. When comparing polar compounds in FI oils with the associated crude oils Peters et al. (2018) suggested that water washing has partially remove those low molecular weight polar compounds before being trapped in FI. In contrast, very little compositional insight has to date been gathered on NSO-compounds in FI oils with higher molecular weight. The reason for this was the detection window of GC-MS covering compounds within a mass range of *m/z* 50–600 Da, which constrains the study of higher molecular weight NSO-compounds. In recent years the establishment of the FT-ICR-MS into the organic geochemical tool set significantly broadens the mass range detection ability compared to GC-MS allowing now the assessment of higher molecular weight aromatic HCs and NSO-compounds (Marshall and Rodgers, 2008). The pioneering work of Noah et al. (2018, 2019) was the first to demonstrate that FT-ICR-MS can be used to analyze NSO-compounds in FI oils, and it opens the analytical window to thousands of additional high molecular weight compounds not accessible before to solve geological and geochemical problems with the help of FI analysis.

1.3 Application potential of oil FIs in petroleum systems

Since oil FIs were mentioned for the first time in a scientific journal at the end of the 19th century (Reese, 1898), applications for the utilization of oil FIs to understand the evolution of petroleum accumulations within petroleum systems are widely exerted, especially during recent decades due to the development of various

sophisticated analytical approaches (Munz, 2001; George et al., 2007a; Volk and George, 2019). The great advantage of using FI oils is that the oil is physically isolated from the main pore system of the carrier and reservoir rock, and therefore subsequent events affecting the reservoir such as leakage and later charging, water-washing, biodegradation and contamination associated with drilling do not affect the composition of the sealed inclusion oil. The main subjects for the application of FI analysis in petroleum systems are the reconstruction of the oil charge and migration history or the reconstruction of the original oil phase after secondary alteration by analyzing the physical and chemical properties of the trapped and from this time on isolated oils in the FIs.

1.3.1 Oil charge history

Crude oil trap filling, leakage and recharge processes are common in petroleum systems over geological times, resulting into complex oil charge and leakage histories in many oil fields (Karlsen et al., 1993; Karlsen et al., 2004; George et al., 2007a). The paleo charged oil can be occluded in diagenetic cements, such as quartz overgrowths and in healed microfractures within detrital grains (Walderhaug, 1994; Munz, 2001; George et al., 2007a). Thus, oil trapped in FIs can be used to assess the complex reservoir filling, leakage and/or the secondary alteration histories of the reservoir oil compared to the original oil in the FI. In addition to the compositional analysis, physical characteristics such as homogenization temperature, generation stages and salinity are conventional tools to describe the oil charge (Parnell et al., 1998, 2001; Conliffe et al., 2017). Improved analytical methods, such as GC-FID, GC-MS and GC-IRMS, allow the compositional characterization of paleo oils in FI, which usually reflect the paleo oil charge.

Thus, FI oils trapped in current columns can be used to understand the evolution of petroleum systems when comparing with the geochemical signatures of co-occurring reservoir crude oil. The geochemical difference between FI oil and reservoir oil can reveal various oil charge histories. For example, the FI oil can derive from the same source as the corresponding reservoir oil, but shows a lower maturity. This reflects the progressive oil charging with an early charge signal in the FI and a later

charge signal in the reservoir oil (Karlsen et al., 1993; George et al., 1997a, 1997b, 1998; Bhullar et al., 1999; Volk et al., 2001, 2002; Shariatinia et al., 2013). Furthermore, compositional differences between FI and reservoir oils can reveal multiple source charges during geological time (Karlsen et al., 1993; Lisk et al., 1996; George et al., 1997a, 1998; Pan et al., 2003; Pestilho et al., 2018). In addition, FI oil and reservoir crude oil can also derived from the same source rock (Spekk Fm), but from different kitchen areas with source rocks expelling petroleum at different times (Karlsen et al., 2004).

Oil FIs are not only found in oil reservoirs, but also in dry structure of past filled reservoirs which have been drained due to later leakage. These inclusion oils offer the possibility of deducing the oil migration and charging history without accessing the actual reservoir oil and predicting the oil trapped in not yet breached structures, as indicated in several Australian basins (George et al., 1997b, 2007b; Volk et al., 2004), the Jeanne d'Arc Basin, offshore Newfoundland (Parnell et al., 2001) and the Haltenbanken Vest area, Norway (Karlsen et al., 2004, 2006). Karlsen et al. (2004) presented a study in which they used oil FIs from dry structures to develop a model for oil migration, overpressure development and paleo-leakage in the Haltenbanken Vest area.

After trapped in FIs, the secondary alteration processes e.g., biodegradation and water washing cannot affect the composition of FI oils which therefore, preserve paleo oil charge information. Non-biodegraded FI oils vs biodegraded crude oil and biodegraded FI oils vs non-biodegraded crude oil studies have been reported to elaborate the key geochemical information about the source and maturity of the original oil charge (Jensenius and Burruss, 1990; Lisk et al., 1996; George et al., 1998; Bhullar et al., 1999; George et al., 2004a; Volk et al., 2005a). Furthermore, oil FIs can preserve the original signatures of non-water washing crude oils (George et al., 2004a) and can be used to investigate the interaction and distribution of water dissolved compounds between the water and petroleum phase (Peters et al., 2018). In addition to that, trapped FI oil was used to help to identify the source rock of reservoir oils that have been contaminated by drilling mud (George et al., 2002).

1.3.2 Oil migration

As mentioned above primary oil migration refers to the expulsion of oil from the source rock into the carrier rock and the migration into the reservoir system is termed secondary migration (Tissot and Welte, 1984), while the leakage from the reservoir is called tertiary migration. Due to compound fractionation during the petroleum expulsion process and along the migration pathway caused by different physical properties of the various oil constituents and by secondary alteration processes such as water washing and biodegradation impacting the reservoir oil composition, oil trapped in reservoirs can have large compositional differences with the initially expelled or migrated oil (Leythaeuser et al., 1988a, 1988b, 1988c; Larter and Aplin, 1995). Thus, a great challenge is to retrace the composition and characteristics of the original reservoir oil. However, during oil migration part of the initially migrated oil can be trapped in fracture-filling minerals under certain condition, which offers the opportunity to decipher original oil characteristics and the oil migration process.

1.3.2.1 Primary migration

The transport within and the expulsion or release of oil compounds from source rocks are termed oil primary migration (Tissot and Welte, 1984). To evaluate the primary migration process, oil data from reservoir rock and interbedded source rock were investigated reflecting the expelled oil and retained bitumen, respectively (Tissot and and Welte, 1984; Leythaeuser et al., 1988a, 1988b, 1988c; Bodnar, 1990; Han et al., 2015). In these studies, shale-sandstone contacts were examined to elucidate the oil primary migration. Besides that, abundant oil FIs and solid bitumen have been found in bedding-parallel fibrous veins (beef and cone-in-cone), such as calcite and quartz, which indicate that the fibres grew while source rocks were generating oil and were always related to overpressure (Jochum et al., 1995b; Parnell et al., 2000; Volk et al., 2002; Cobbold et al., 2013; Zanella et al., 2015). Thus, comparison of oil from the same source rock either occluded in FIs, or accumulated in conventional reservoirs or retained as bitumen in the source rock allows to determine the compound fractionation during oil primary expulsion. Jochum et al. (1995b) reported preferential entrapment of low molecular weight *n*-alkanes in inclusions during primary migration

of hydrocarbons in the Posidonia shale. Parnell et al. (2000) documented that fracture-filling carbonates and sulphates in the Neuquén Basin, Argentina, contain abundant oil FI and solid bitumen, which were trapped during oil primary migration. Volk et al. (2002) reported about fibrous calcite healed fractures generated during early petroleum generation and migration in over-pressured sediments in the Barrandian Basin, Czech Republic. Zanella et al. (2015) indicated that liquid and solid hydrocarbons present as inclusions in fibrous calcite of Mesozoic shale in the Wessex Basin, SW England, suggested primary oil migration. Although the studies mentioned above already focused on the interplay between oil primary migration and oil trapped fibrous calcite FI, geochemical fractionation trends of specific compound classes during oil primary migration needs to be further evaluated in detail.

1.3.2.2 Secondary migration

The migration of expelled petroleum from the source rock through the carrier rock to the reservoir rock is referred to as secondary migration (Tissot and Welte, 1984; England et al., 1987). During oil secondary migration, migrated oil can be trapped as FIs within framework grains such as quartz and within diagenetic cements (McLimans, 1987; George et al., 2004b; Karlsen et al., 2004, 2006). The small volume of oil occluded as oil FIs along secondary migration pathways reflects an aliquot of the oil that has passed through the migration conduits. The petrographic and physical characteristics of oil FIs, such as PVT, microthermometry and fluorescence, are conventionally used to reflect the oil migration time and space condition (McLimans, 1987; Tseng et al., 2003; Schubert et al., 2007; Baron et al., 2008). Recently, the compositions of FI oils analyzed by GC-MS were widely used to elaborate oil secondary migration process. George et al. (2004b) reported that migration pathways across prospects or basins can be geochemically mapped by analyzing the oil trapped in FIs on oil migration pathways. Jin et al. (2008) reported episodic petroleum fluid migration by analyzing the petrographic and geochemical properties of oil FIs in calcite cements in fault zones of the northwestern margin of the Junggar Basin. Peters et al. (2018) suggested that the phenolic and carbazolic compounds in oil FIs could trace the secondary migration of oil. In addition to the

liquid components, Lüders and Plessen (2015) traced gas migration pathways of Posidonia shale using the isotopic composition of methane trapped in FIs.

In ore deposits, MVT type minerals and hydrothermal derived fluids can contain abundant oil and solid bitumen inclusions as well. When hydrocarbons were generated at the same time as the mineral forming brines and migrated together toward the rim of ore deposition, this type of mineralization is often associated with abundant oil FIs and solid bitumen, e.g., Pb-Zn sulfides in the Canning Basin, Western Australia (Etminan and Hoffmann, 1989), fluorite deposits in the Encantada-Buenavista, Mexico (González-Partida et al., 2003) and fluorite deposits in the Hammam Zriba, Tunisia (Benchilla et al., 2003). The presence of oil FIs inside of ore deposits has the strong potential to provide invaluable information on the oil generation and migration. For instance, based on FI research Etminan and Hoffmann (1989) reported that hydrocarbons trapped in MVT deposits were sourced and migrated from deeper kitchen areas in the Canning Basin and not from local source.

1.4 Analytical approaches for oil FIs

Comprehensive studies on the physical and chemical characteristics of oil FIs are not easy to conduct compared with crude oils and sediment extracts. Due to the small size and extremely low compound concentrations of FI oils, conventional analytical approaches often operate at the detection limit. In addition, due to the low extraction yield, oil and any other compounds from outer surfaces of the host minerals or compounds introduced by the laboratory preparation process can easily contaminate the chemical composition of FI oils. Thus, it is necessary to develop and apply a rigorous clean-up protocol and advanced analytical approaches to investigate oil FIs in a contamination-free or at least contamination-controlled manner. The analytical approaches for oil FIs have been review by Munz (2001), Burruss (2003) and Volk and George (2019). A brief compilation of these approaches is presented in the following paragraphs being divided into non-destructive and destructive techniques according to Munz (2001).

1.4.1 Sample preparation and clean-up

The first step to study FI is to prepare a doubly polished thin section to determine whether oil inclusions are present or not in the respective host minerals using microscopic techniques (Volk and George, 2019). Goldstein (2003) has given a detailed description about the preparation techniques for a doubly polished thin section, which is suitable for the inspection of oil FIs. The preparation of thin section is a prerequisite for both destructive as well as most non-destructive studies.

For most destructive studies elaborating the compositional characteristics of FI oils, the minimization of contaminants is required to avoid the interference with the FI oil composition. Additionally, to avoid mixing with other host minerals, purely sorted host minerals are needed as well. In petroleum systems most host minerals, such as quartz and carbonate minerals, occurred as cements in reservoir sandstones and separation techniques such as hand-picking, sink-floating and magnetic separation can be used to collect pure host mineral fractions (Karlsen et al., 1993, George et al., 2007a), while pure host minerals collected from veins and vugs can be cleaned directly. Quite similar rigorous cleaning protocols have been given by Karlsen et al. (1993), Jones and Macleod (2000) and George et al. (2007a). For non-carbonate minerals, the cleaning steps can be carried out as followed: rinsing of the host minerals in distilled water, followed by digestion in H_2O_2 and acids such as HCl, HNO_3, H_2SO_4, Aqua Regia and chromic acid, then various organic solvents (e.g., methanol, furan, chloroform and dichloromethane) are used to additionally clean the mineral surfaces (Karlsen et al., 1993; Jones and Macleod. 2000; George et al., 2007a; Volk and George, 2019). For the carbonate minerals, the application of any acid has to be avoided during the cleaning process, since acids would dissolve the host mineral and only organic solvent can be used (Volk et al., 2002; George et al., 2007a). The success of the cleaning process and thus the cleaning effectiveness can be assessed by comparing the compound inventory and intensity of the FI oils with those of the procedural system blank, which is usually the final cleaning rinse of the outer host minerals with an organic solvent (Jones and Macleod. 2000; George et al., 2007a; Volk and George, 2019).

After the cleaning procedure, the host minerals can be crushed by an on-line or an off-line crushing technique (George et al., 2007a). The on-line crushing is conducted in a close system by hand crushing or thermally decrepitation allowing the later detection of gases and light HCs in oil FIs (Lisk et al., 1996; George et al., 2007a; Volk and George, 2019). This technique connected with specific detector devices, such as mass spectrometry, can be used to reveal the molecular composition of gases and their isotope signatures (Horsfield and McLimans, 1984; Karlsen et al., 1993; Lüders et al., 2012; Lüders and Plessen, 2015). The off-line crushing is performed using pestle and mortar (Kvenvolden and Roedder, 1971; Karlsen et al., 1993; George et al., 1996; Jones and Macleod, 2000) or a special stainless steel crushing cylinder (Lisk et al., 1996; George et al., 2007a). During this process, the low molecular weight compounds, such as gases and light HCs in oil FIs will evaporate (George et al., 1998), while high molecular weight HC and polar compounds can be accessed.

1.4.2 Non-destructive analytical approaches

The physical properties of oil FIs can be characterized using plenty of non-destructive techniques in combination with doubly polished thin sections, including microscopy microthermometry, Pressure-Volume-Temperature-Composition (PVTX) modelling, fluorescence spectroscopy, and Raman and Fourier-transform infrared (FT-IR) spectroscopy.

Petrographic analyses. A transmitted-light microscope with a polariser and equipped with an ultraviolet (UV) lamp, is a fundamental equipment to study oil FIs. Due to the different optical characteristics, oil FIs can be easily distinguished from aqueous inclusions using UV lights (Roedder, 1984). Variations in the physical properties of oil FIs such as size, shape, gas to oil ratio (GOR), grains containing oil FIs (GOI), fluorescence color, the textural relationship and the classification of FIs can be determined (Burruss, 1981, 2003; Roedder, 1984; Mclimans, 1987; George et al., 2007a; Volk and George, 2019).

***Microthermometry*.** The minimum trapping temperature (homogenization temperature) of the oil FIs can be estimated by temperature induced phase changes

using microthermometric measurements (Shepherd et al., 1985; Burruss, 2003; Goldstein, 2003). The homogenization temperature of oil FIs are generally lower than those of coeval aqueous FIs (Roedder, 1984; Munz, 2001).

PVTX modelling. Calculating fluid densities and isochores, and estimating the pressure and temperature conditions of trapping is challenging for oil FI studies. The homogenization temperature, volumetric measurements determined by confocal laser scanning microscopy and chemical data are main parameters that need to be confirmed in PVTX modelling (Pironon et al., 1998; Aplin et al., 1999; Munz, 2001; Volk and George, 2019). Aplin et al. (1999) applied Pressure-Volume-Temperature (PVT) modelling software to determine the bulk composition, phase envelope, isochore and a range of physical properties of the trapped oil by choosing a range of different initial oil phase and titrant gas compositions (C_1–C_5).

Fluorescence spectroscopy. Fluorescence properties of oil are mainly caused by aromatic hydrocarbon and polar compounds. The relationship of API gravity and the fluorescence properties of oils has been well established (Hagemann and Hollerbach, 1986; McLimans, 1987; Stasiuk and Snowdon, 1997; Barwise and Hay, 1996; Volk and George, 2019). Oils with higher API gravity fluoresce in the blue end of the visible spectrum; in contrast oils of lower API gravity show a color shift towards the red end. In addition to the estimated API gravities, the assessment of the maturation stage of trapped oils using fluorescence colors has been discussed in many studies (Burruss et al., 1985; McLimans, 1987; George et al., 2001; Parnell et al., 2001).

Raman and FT-IR spectroscopy. Raman and FT-IR approaches are capable of detecting transitions between vibrational energy levels (Pironon and Barrés, 1990; Wopenka et al., 1990). The low molecular weight HCs, e.g., CH_4, can be accessed using Raman spectroscopy, while other compositions of oil are severely hampered by fluorescence emission, which is orders of magnitude higher than the Raman scattering (Wopenka et al., 1990). Functional groups such as -CH, $-CH_2$ and $-CH_3$ can be detected by FT-IR spectroscopy. The average alkane chain length has been estimated using the quantitative calculation of $-CH_2/-CH_3$ abundance based on peak area

(Pironon and Barrés, 1990; Bourdet et al., 2012).

1.4.3 Destructive analytical approaches

In order to obtain comprehensive compositional data from oil FIs, the destructive analytical methods have been developed. These methods include gas chromatography with a flame ionization detector (GC-FID), gas chromatography-mass spectrometry (GC-MS) and gas chromatography-isotope ratio mass spectrometry (GC-IRMS) for solvent extracts of FI assemblages trapped in host minerals and laser ablation GC-MS and Time-of-flight secondary ion mass spectrometry (ToF-SIMS) for intact individual oil FIs. For the destructive analytical techniques the clean-up and crushing methods described above are a prerequisite.

GC-FID. The gaseous and low molecular weight compounds crushed in on-line systems and the C_{15+} HCs crushed in off-line systems were analyzed using GC-FID (Horsfield and McLimans, 1984; Burruss, 1987; Karlsen et al., 1993; Volk et al., 2002). Horsfield and McLimans (1984) detected benzene and low molecular weight paraffins as well as whole oils using thermal decrepitation GC technique, thereby demonstrating the presence of paleo-oil and paleo-water legs in oil fields of the Middle East. Burruss (1987) described a method of on-line crushing and using a GC with a modified injector to analyze the released fluids. Later gas (C_1-C_5) compositions, saturated fractions and whole oils in the inclusions were detected using GC-FID after crushing (Karlsen et al., 1993).

GC-MS. To obtain more information on the chemical composition of oil FIs, Murray (1957) firstly used mass spectrometry, even though only low molecular HCs (C_1–C_8) were detected. Later, off-line crushing techniques in combination with GC-MS were widely applied to access a wide variety of aliphatic, aromatic and low molecular weight NSO-compounds in FI oils, which can be used to assess the geochemical characteristics of FI oils, such as maturation stages, oil sources and biodegradation levels (Karlsen et al., 1993, 1995, 2004, 2006; Nedkvitne et al., 1993; George et al., 1996, 1997a, 1997b, 1998, 2001, 2002, 2004a, 2007a; Volk et al., 2001, 2002, 2003, 2005a; Pan et al., 2003; Cao et al., 2006; Peters et al., 2018), and to trace

some Precambrian oils (Dutkiewicz et al., 2004; Volk et al., 2005b). To date, the analysis of the geochemical composition in FI oils by GC-MS becomes a conventional tool in studying petroleum system. Details on studying FI by GC-MS are presented in section 1.4.

GC-IRMS. Detailed carbon and hydrogen isotope signatures of hydrocarbon gases and *n*-alkanes in FI oils are detected using IRMS after crushing the host minerals (Karlsen et al., 1993; George et al., 1997a; Volk et al., 2004; Potter and Longstaffe, 2007; Lüders et al., 2012; Lüders and Plessen, 2015). George et al. (1997a) applied the carbon isotopic signature of C_{15+} *n*-alkanes from FI oils to study oil-oil or oil-source rock correlation. Lüders et al. (2012) and Lüders and Plessen (2015) accessed the maturation stage of trapped oils using the carbon isotope composition of methane from oil FIs.

Laser ablation GC-MS. Laser ablation systems connected with a GC-MS instrument were applied to obtain compositional information on intact (non-destructive) individual oil FIs. Various laser ablation systems, such as infrared Nd:YAG laser beam (Greenwood et al., 1998), femtosecond laser (Volk et al., 2010) and 193nm excimer (Zhang et al., 2012) have been introduced. Applying this technique, hydrocarbons similar to those from the host mineral crushing procedure can be obtained; however, some pyrolysis artefacts caused by the laser can occur (Greenwood et al., 1998).

ToF-SIMS. The composition and spatial distribution of organic molecules and chemical structures on surfaces of geological and biological samples can be analyzed using ToF-SIMS (Thiel et al., 2007). This approach in a combination with ion beams (Bismuth cluster) has been used to analyze the individual intact oil FIs, in which aliphatic and aromatic compounds were identified (Siljeström et al., 2010, 2013).

FT-ICR-MS. As discussed above the compositions of low molecular weight HCs and NSO-compounds in FIs have widely been used to investigate petroleum systems (Karlsen et al., 1993, 2004; George et al., 2007a; Volk and George, 2019). Whether high molecular weight HCs and NSO-compounds, a significant part of the oil fraction,

can be used in the same way, is currently the subject of scientific research (Noah et al., 2018, 2019). In recent years, the introduction of high-resolution mass spectrometry FT-ICR-MS into the organic geochemical analytical tool set (Marshall and Rodgers, 2008) opens the opportunity to access these high molecular weight HCs and NSO-compounds in FI oils, and broadens the analytical window by thousands of compounds not accessible before to study petroleum systems (Noah et al., 2018, 2019). Since this analytical method will play a central role in this thesis, the FT-ICR-MS technique and its application potential in petroleum research is described more detailed in the following chapter.

1.5 Fourier transform-ion cyclotron resonance-mass spectrometry (FT-ICR-MS)

1.5.1 Fundamentals of FT-ICR-MS

Since Thomson (1913) conducted the first mass spectrometer to obtain mass spectra of O_2, N_2, CO, CO_2 and $COCl_2$ in 1912, mass spectrometry has undergone countless improvements to increase resolution and mass detection ability (de Hoffmann and Stroobant, 2007). As one of the most powerful mass spectrometers, Fourier transform-ion cyclotron resonance-mass spectrometry (FT-ICR-MS) was firstly introduced by Comisarow and Marshall in 1974 (Comisarow and Marshall, 1974a, 1974b), it offers the highest available broadband mass resolution, mass resolving power, and mass accuracy (Marshall and Rodgers, 2008). Later, with the commercialization of FT-ICR-MS from low-field to high-field superconducting magnets with various ionization sources, such as 12T FT-ICR-MS produced by Bruker Daltonik GmbH, it sheds light on complex material matrixes, such as drugs, proteins and crude oils (Wanczek and Kanawati, 2019).

The general principle of FT-ICR-MS is based on the ion cyclotron theory proposed by Lawrence and Edlefsen (1930). When an ion with a distinct mass (m) and charge (q) is injected into a magnetic field (B) with a velocity (v), the ion will stabilize on a circular orbit due to the equality of centripetal force (F) and centrifugal force (F') (Fig 1.1).

$$F = qvB \tag{1}$$

$$F' = \frac{mv^2}{r} \tag{2}$$

Since the centripetal and centrifugal forces are in balance, equation 1 and 2 can be equated to equation 3

$$qvB = \frac{mv^2}{r} \tag{3}$$

The cyclotron frequency (*f*) of an ion on a circular orbit is equal to

$$f = \frac{v}{2\pi r} \tag{4}$$

According to the equation 3 and 4, angular cyclotron frequency (ω_c) is equal to

$$\omega_c = 2\pi f = \frac{v}{r} = \frac{q}{m}B \tag{5}$$

According to the equation (5) above, the mass-to-charge (*m/z*) ratio of an ion can be obtained by the measurement of the angular cyclotron frequency (ω_c). To measure the ω_c, the cyclotron is irradiated with an electromagnetic wave that has the same frequency as the ion, thereby exciting the ion cyclotron resonances. The "image current" induced by the ions circulating perpendicularly to the trajectory of the ions in the cell wall can be amplified and documented by the electrical device. These electrical signals contain information of all ions with different resonant frequencies, which can be transformed into the frequency spectrum through a Fourier transformation. Finally, according to the equation of frequency and *m/z* ratio (Eq. (5)), the mass spectrum with *m/z* as horizontal coordinate can be obtained (Fig. 1.2) (Comisarow and Marshall, 1974a, 1974b; de Hoffmann and Stroobant, 2007).

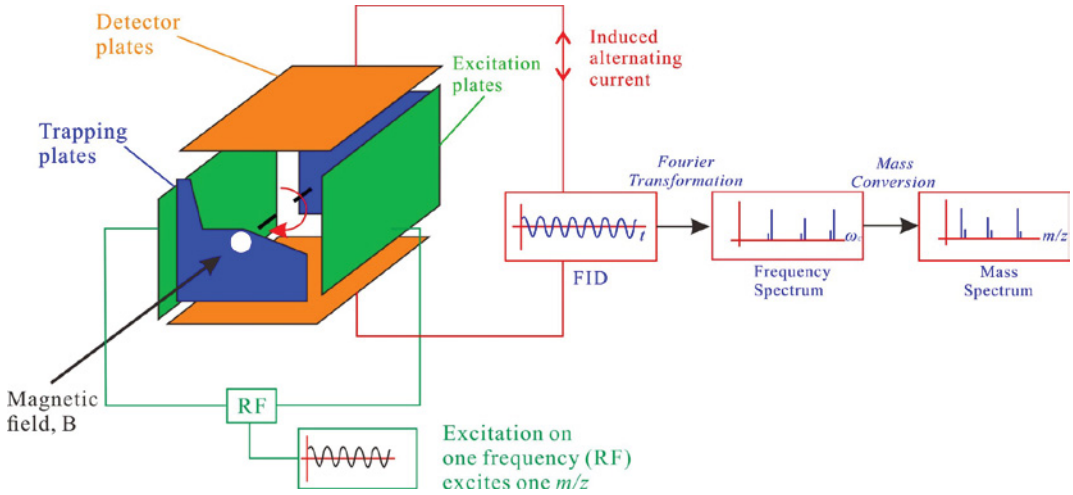

Figure 1.2 Sketch of an ion cyclotron resonance instrument (http://www.chm.bris.ac.uk/ms/fticrms.xhtml).

To access the various compounds with different structural and chemical properties in the different sample materials, a variety of ionization techniques are used for FT-ICR-MS, such as atmospheric pressure photoionization (APPI), field desorption/ionization (FD/FI), electron ionization (EI), atmospheric pressure chemical ionization (APCI), electrospray ionization (ESI), and matrix assisted laser desorption ionization (MALDI). Among them, ESI and APPI ion sources are widely used. ESI successfully introduced by Fenn et al. (1989), is a technique that is applying a strong electric field to a liquid to create an aerosol passing through a capillary tube under atmospheric pressure. By producing a spray the solvent can easily evaporate leaving behind the molecular target ions in the gas phase. In contrast to ESI, the APPI technique was recently introduced by Bruins and co-workers (Robb et al., 2000). Here the compound solution is vaporized by a heated nebulizer and interacts with photons emitted by a discharge lamp. Both ESI and APPI sources can work in positive and negative modes. In positive mode, it typically generates positive ions ($M + H^+$) by protonating (basic) neutrals, while in negative mode it generates negative ions ($M - H^-$) by deprotonating (acidic) neutrals (Marshall & Rodgers, 2008). While the ESI ionization works best for polar compounds, the big advantage for the APPI mode is that in addition to NSO-compounds also nonpolar compounds e.g., aromatic HCs can be ionized efficiently compared to other ionization modes.

For GC-MS the analytical window mainly covers compounds within a mass range of m/z 50−600 Da, while FT-ICR-MS enlarges the analytical window to compounds within a mass range up to m/z 2000 (Poetz et al., 2014) and this with an ultra-high mass resolution and mass accuracy (Marshall & Rodgers, 2008). The exact masses enable the calculation of the individual elemental composition ($C_cH_hN_nO_oS_s$) including double bond equivalents (DBE), whereby DBE is a measure for the number of rings and double bonds within a molecule. In this way thousands of elemental compositions can be assessed, allowing the FT-ICR-MS to become an excellent tool to characterize complex organic matter matrices not accessible before.

Except for the chemical and biological applications, this powerful tool has been successfully applied to characterize the elemental composition of various types of organic matter, such as organic matter in soils (Ohno et al., 2010, 2014; Guigue et al., 2016; Gan et al., 2021), dissolved organic matter in marine and different terrestrial water systems, groundwater and pore water (Koch et al., 2008; Minor et al., 2012, Schmidt et al., 2014; Islam et al., 2016; Rossel et al., 2016; Zhu et al., 2019), organic matter in coals (Wu et al., 2004; Rathsack et al., 2014; Zhu et al., 2019) and organic matter related to petroleum (Hsu et al., 1994; Guan et al., 1996; Qian et al., 2001; Hughey et al., 2002; Kim et al., 2005; Marshall & Rodgers, 2008; Shi et al., 2010; Poetz et al., 2014; Mahlstedt et al., 2016; Jiang et al., 2021; Yue et al., 2021).

1.5.2 Applications of FT-ICR-MS in petroleum systems

In the 1990s, petroleum was firstly measured by FT-ICR-MS using the ESI mode (Hsu et al., 1994; Guan et al., 1996), which starts a new era to characterize high molecular weight compounds in petroleum including NSO-compounds and HCs. Marshall and Rodgers (2004, 2008) proposed the term “Petroleomics”, which is the characterization of petroleum at the molecular level and they introduced the theoretical background and detailed analytical methods of the chemical composition in petroleum. Later, a variety of studies investigating the thermal maturity, oil migration, and secondary alteration processes have been published analyzing the NSO-compounds and (aromatic) HCs in crude oils and extracts from source, carrier and reservoir rocks using FT-ICR-MS (Hughey et al., 2004; Oldenburg et al., 2014;

Poetz et al., 2014; Liu et al., 2015; Mahlstedt et al., 2016; Han et al., 2018a, 2018b; Yue et al., 2021). In addition, Noah et al. (2018, 2019) firstly compared NSO-compound compositions in a FI oil, a produced oil, potential source rock extracts and reservoir rock extracts from the Üllés Field in the Pannonian Basin, Hungary, opening research into mineral-fluid interaction and the evolution of petroleum systems using NSO-compounds in FI oils. In the following, applications using FT-ICR-MS to solve geological and geochemical issues in petroleum system will be provided in more details.

Oil source. The composition of crude oil originally depends on the sedimentation history of the source rocks with its specific organic facies supply (Tissot and Welte, 1984). High molecular weight HCs and NSO-compound distributions in crude oils, originated from source rocks deposited under different environmental conditions, have been analyzed using FT-ICR-MS and different kerogen types and lithofacies have been discussed (Hughey et al., 2002; Wan et al., 2017; dos Santos Rocha et al., 2018). Hughey et al. (2002) analyzed three different crude oil types from North America, China and the Middle East, in which they presented various elemental compositions partly depending on their origin. Wan et al. (2017) found an increased abundance of oxygenated compounds and degree of condensations from Type I to III kerogens, while the carbon number range for N_1 species decreased. Furthermore, dos Santos Rocha et al. (2018) suggested that remarkable differences of hetero-atomic compounds in lacustrine and marine crude oils from different off-shore Brazilian basins were controlled by the respective kerogen types. For elucidating the impact of source inputs, more studies are needed in future, since secondary alteration events such as thermal maturation and biodegradation can also alter the compound composition significantly (Kim et al., 2005; Poetz et al., 2014;).

Thermal maturity. Parameters for the assessment of thermal maturity based on HCs and NSO-compounds from crude oil and sediment extracts have been widely discussed and successfully established. N_1 compounds, especially pyrrolic nitrogen, have been widely studied using the ESI (–) mode and relationships between the compositions of selected DBE classes and thermal maturity have been intensely

discussed (Hughey et al., 2004; Oldenburg et al., 2014; Poetz et al., 2014; Mahlstedt et al., 2016; Hosseini et al., 2017; Ziegs et al., 2018). For example, Hughey et al. (2004) pointed out that with the increasing oil maturity, condensation and aromatization of N_1 compounds increase, while alkyl side chains decrease. Oldenburg et al. (2014) suggested a maturity assessment tool using N_1 compounds, that linear relationship between oil maturity and the position of individual oils shows within triangular plot established by the relative distribution of DBE 9 (carbazoles), 12 (benzocarbazoles) and 15 (dibenzocarbazoles). In addition to the conventional biomarker maturity parameters from crude oil and sediment extracts measured by GC-MS, Noah et al., (2020) developed a new thermal maturity parameter for the maturity assessment of overmature shales based on polycyclic and heterocyclic aromatic compounds detected by FT-ICR-MS in the APPI (+) mode. Besides the natural samples, artificial pyrolysis experiments using immature or low mature source rock to simulate polar compound compositions at different maturation stages have been conducted recently (Zhang et al., 2016; Cui et al., 2021). Zhang et al. (2016) reported that NSO-compounds became more dealkylated and aromatic with increasing pyrolysis temperature from 335 ℃ to 600 ℃. Cui et al. (2021) found that the relative abundances of N_1 compounds first decreased but later increased when rising the pyrolysis temperature from 400 ℃ to 520 ℃.

Biodegradation. High concentrations of oxygen-containing compounds, especially of phenols and carboxylic acids, might point to the occurrence of biodegradation in crude oils or sediment extracts (Meredith et al., 2000; Hughey et al., 2002; Kim et al., 2005). The compositional difference of polar compounds in oils at different levels of biodegradation have been accessed in many studies (Kim et al., 2005; Hughey et al., 2007; Liao et al., 2012; Pan et al., 2013; Martins et al., 2017; Oldenburg et al., 2017; Liu et al., 2018). Among these studies, it turned out that the A/C (acyclic/cyclic) ratio ($A/C = \sum O_{2,\,DBE1}/\sum O_{2,\,DBE2+3+4}$), introduced by Kim et al. (2005), is an appropriate parameter to indicate potential biodegradation levels of crude oils. This is caused by the increase in the abundance of saturated acids with lower DBE due to the increasing of the degree of biodegradation. Meanwhile this parameter is widely used and confirmed (Hughey et al., 2007; Noah et al., 2015;

Martins et al., 2017). For example, Hughey et al. (2007) reported that the degree of biodegradation of oils qualitatively estimated using the A/C ratio are well correlated to those biodegradation index established according to biomarker.

Oil migration. The compositional differences of NSO-compounds between retained bitumen in source rocks and expelled fluids in reservoirs were applied to elucidate the compound fractionation during oil migration (Mahlstedt et al., 2016; Han et al., 2018a, 2018b; Yue et al., 2021). Mahlstedt et al. (2016) reported the preferential expulsion of smaller compounds into the crude oils and an enhanced content of cyclic compounds with a higher degree of aromatization within the retained fluids. Yue et al. (2021) discussed the variations of HCs and NSO-compounds induced by the lithofacies in three different petroleum systems, revealing that nitrogen-containing compounds are preferentially retained by biogenic quartz, while the more polar acidic oxygen-containing compounds are preferably retained by clay minerals during oil primary migration. In addition to natural samples, various pyrolysis experiments have been used to simulate the fractionation of polar compounds during oil expulsion, such as open-system pyrolysates (Mahlstedt et al., 2016), semi-open pyrolysis (Pan et al., 2019) and hydropyrolysis (Jiang et al., 2021). Furthermore, the fractionation of NSO-compounds caused by secondary oil migration has been reported for Duvernay-sourced oils in Canada by Liu et al. (2015), showing a significant relative decrease of O_2, N_1O_1 and N_1O_2 species as well as relative increase of O_1 species in the crude oil during migration.

Thermochemical sulfate reduction (TSR). TSR is a process in which hydrocarbons react with sulfate to produce CO_2 and H_2S in relatively hot (>100 ℃) non-clastic reservoirs, which can significantly affect compositional and isotopic organosulfur compounds distribution through the oxidative process or by back reactions of hydrocarbons with H_2S or elemental sulfur (Orr, 1974; Walters et al., 2015). FT-ICR-MS is very helpful to characterize the high molecular organosulfur compounds formed during the TSR process. Li et al. (2011) suggested that large amounts of sulfur ethers, thiophenes, and benzothiophenes with low DBE values and low thermal stability detected in the Ordovician oils of the Tarim Basin (China) might

be produced by the TSR process. Walters et al. (2015) reported that TSR lead to the generation of more condensed sulfur species containing one or more sulfur atoms being part of a single or multiple thiophenic cores.

1.6 Research perspective and structure of the dissertation

Building upon the pioneering work of Noah et al. (2018, 2019) this dissertation aims to explore the potential of the FT-ICR-MS technique to be utilized for the elucidation of the geochemical compositions of oils trapped in FIs. To achieve these goals, the following objectives are addressed:

1) Due to its ultra-high sensitivity, the FT-ICR-MS technique is prone to minimal traces of contamination from outer surfaces of host minerals and from the laboratory preparation process as well. Thus, first of all it is necessary to develop a sophisticated clean-up method for the investigation of FI oils with the FT-ICR-MS based on existing conventional cleaning procedures (Karlsen et al., 1993; George et al., 1998, 2007a; Jones and Macleod, 2000) developed for the analysis of FI oils by GC-FID and GC-MS.

2) After the establishment of a suitable method for the analysis of FI oils by FT-ICR-MS, the central scientific objective of this thesis will be the evaluation whether and, if yes, in which way high molecular weight HC and NSO-compounds can provide crucial information on the evolution of petroleum systems especially on the charging and migration history. Data interpretation will be conducted in a combined approach joining and comparing FT-ICR-MS data with conventional biomarker and isotope data obtained by GC-MS and GC-IRMS, respectively. The information potential of high molecular weight HC and NSO-compounds measured by FT-ICR-MS will be explored in two case studies.

This cumulative thesis includes five chapters. Chapter 1 introduces into the general background of the factors causing different petroleum compositions, the conventional methods applied for the analysis of petroleum compositions, sample types used for conventional analysis, the presence and formation of oil FIs, the

analytical approaches to analyze FI, the application of oil-containing FI in petroleum system research as well as the fundamentals of the FT-ICR-MS analysis and its application in petroleum geochemistry. Subchapter 1.6 addresses the research objectives of this dissertation comprising the development of an appropriate analytical procedure to use FT-ICR-MS for FI analysis and to evaluate the application potential of this technique in FI research using the example of two case studies. Chapter 2 describes the developed method for the use of FT-ICR-MS in FI research. Chapter 3 and 4 represent the two case studies dealing with the reconstruction of the oil charging history and the compound fractionation during primary migration. Chapter 5 presents a summary of the thesis and provides an outlook on the potential of the developed approach for future applications. Chapter 2 was published in Organic Geochemistry, Chapter 3 was published in Marine and Petroleum Geology, and Chapter 4 was published in International Journal of Coal Geology. Publication data and status as well as the contribution statements of the individual authors are presented in the following section:

Chapter 2 describes the development of an appropriate method to analyze FI with the FT-ICR-MS and GC-MS as well. Two fluorite samples originating from MVT-type deposits in Tunisia and Mexico, and two quartz samples from sediments in Germany and ore deposits in Pakistan were selected. These samples were cleaned using a newly developed method for the FT-ICR-MS analysis of FIs. The procedure allowed to assess the level of contamination of different compound groups ranging from not suitable over conditionally suitable to fully suitable for further data interpretation. Finally, potential applications of information obtained from FI analysis by FT-ICR-MS have been discussed. Y. Han, M. Noah, V. Lüders, B. Horsfield and K. Mangelsdorf were involved in the design of the experiments. Y. Han did the laboratory work and the data analysis, collection and evaluation. Y. Han wrote the draft version of the manuscript, which was finalized with the help of all co-authors. The samples examined in this publication were collected by V. Lüders.

Chapter 3 forms the first case study where the oil charge and leakage history in Skarv field A segment, North Sea, was examined. Five FI oils and associated adsorbed

oils on outer surfaces of FI were chosen from the Garn and Tilje Fm in the Haltenbanken area. Biomarkers and NSO-compounds in adsorbed and FI oils were analyzed using GC-MS and FT-ICR-MS in APPI (+) mode. The results allow the development of oil migration and leakage models in this area by comparing the compositional characteristics of the adsorbed and FI oils. Y. Han, M. Noah, B. Horsfield and K. Mangelsdorf were involved in the design of the experiments. Y. Han did the laboratory work and the data analysis, collection and evaluation. Y. Han wrote the draft version of the manuscript, which was finalized with the help of all co-authors. V. Lüders, A. Hartwig, J. Rinna and J.K. Skeie contributed to the sample collection and A. Hartwig, J. Rinna and J.K. Skeie provided valuable background information on the study area.

Chapter 4 describes the second case study in which the fractionation of the HC and NSO-compounds during oil primary migration in the Hosszúhetény Calcareous Marl Formation (HCMF), Hungary was investigated. Two SR extracts, representing retained bitumen, and six FI oils from calcite veins, representing the expelled oil, were selected and compared. Biomarkers and stable carbon isotopes were analyzed using GC-MS and GC-IRMS to establish oil-source rock correlations. In order to examine compositional fractionation processes of petroleum HC and NSO-compounds, SR extracts and FI oils were analyzed using FT-ICR-MS in APPI (+) mode. It could be demonstrated that HC, S_1, O_1, O_2 and N_1 classes show characteristic differences caused by fractionation processes during primary migration. Y. Han, M. Noah, V. Lüders, S. Poetz, B. Horsfield and K. Mangelsdorf were involved in the design of the experiments. Y. Han did the laboratory work and the data analysis, collection and evaluation. Y. Han wrote the draft version of the manuscript, which was finalized with the help of all co-authors. F. Schubert and S. Körmös contributed to the sample collection and writing as well.

2. NSO-COMPOUNDS IN OIL-BEARING FLUID INCLUSIONS REVEALED BY FT-ICR-MS IN APPI (+) AND ESI (–) MODES: A NEW METHOD DEVELOPMENT[1]

2.1 Abstract

The origins of hydrocarbons occurring in oil-bearing fluid inclusions (FIs) have been studied in detail over the last four decades, but very little is known about co-occurring nitrogen, sulfur and oxygen (NSO)-containing compounds. Here, we outline a new method for gathering valuable information on NSO-compounds using the Fourier transform-ion cyclotron resonance-mass spectrometry (FT-ICR-MS) in combination with Atmospheric Pressure Photoionization in positive ion mode (APPI (+)) and Electrospray Ionization in negative ion mode (ESI (–)). A key element was to develop a rigorous acid-free cleaning protocol to make oil inclusions from a broad range of host materials accessible to the very sensitive FT-ICR-MS technique. Although oil contamination from surrounding organic matter could not be entirely eliminated, the procedure enables distinction of external contaminants and identification of affected NSO-compound classes allowing a conditional interpretation of the FT-results of FI samples, especially for compounds measured in the APPI (+) mode. First insights into the high molecular weight hydrocarbons (HCs) and NSO-compounds in FI oils are presented here using examples from Germany, Tunisia, Pakistan and Mexico.

Keywords: NSO-compounds; oil-bearing fluid inclusion; clean-up method; FT-ICR-MS

---

1 *This chapter has been published as: Han, Y., Noah, M., Lüders, V., Horsfield, B., Mangelsdorf, K., 2020. NSO-compounds in oil-bearing fluid inclusions revealed by FT-ICR-MS in APPI (+) and ESI (–) modes: A new method development. Organic Geochemistry, 149, 104113 (postprint), https://doi.org/10.1016/j.orggeochem.2020.104113.*

2.2 Introduction

Oil-bearing fluid inclusions (FIs) hosted in minerals such as fluorite, quartz or carbonates contain aliquots of oil that were trapped within cavities during crystal growth as primary FIs or during recrystallization of secondary cracks in the presence of a fluid phase (e.g., Burruss, 1981; Roedder, 1984; Goldstein and Reynolds, 1994; Munz, 2001). In general, petroleum FIs are trapped in cements, and/or fracture-fill mineralization hosted by sedimentary rocks. Abundant oil-bearing FIs are reported from sediment-hosted Mississippi Valley-type (MVT) deposits, where they are typically contained in fluorite, but also in barite, carbonate or sphalerite (Etminan and Hoffmann, 1989; Guilhaumou et al., 2000; Benchilla et al., 2003; González-Partida et al., 2003). The geochemical information received from the analysis of FIs oils has been used to compare present and paleo-oils (early oil charges) and to examine migration events and alteration processes that have affected the composition of the oil (Horsfield and McLimans, 1984; Bodnar, 1990; Lisk et al., 1996; George et al., 1997a, 2004a; Volk and George, 2019). The great advantage of using FI oils is that the oil is physically isolated from the main pore system of the reservoir rock, and therefore events affecting the reservoir such as leakage, water-washing, biodegradation and contamination associated with drilling do not affect the composition of the inclusion oil. Comprehensive reviews of FI oil analyses and applications have been published by George et al. (2007a) and Volk and George (2019).

The composition of fluids in oil FIs is complex, with components including gases (such as CH_4, CO_2 and N_2), higher molecular weight HCs (aliphatic and alkylaromatic), NSO-compounds (containing nitrogen, sulfur or oxygen heteroatoms), and water (Roedder, 1984; Pang et al., 1998; Burruss, 2003). Murray (1957) was the first to unravel the composition of FIs-occluded oils, employing mass spectrometry to analyze light HCs and gases. Since then many different analyses have been applied to unravel the bulk composition of included oils, such as gas chromatography with a flame ionization detector (GC-FID) (Horsfield and McLimans, 1984), gas chromatography-mass spectrometry (GC-MS) (Karlsen et al., 1993; George et al., 1997a) and high performance liquid chromatography (HPLC) (Pang et al., 1998).

Techniques for analyzing individual oil inclusions also have been developed, such as time-of-flight secondary ion mass spectrometry (ToF-SIMS) using an ion gun (Siljeström et al., 2010, 2013), GC-MS with an on-line femtosecond laser (Volk et al., 2010), and GC-MS with an on-line excimer laser (Zhang et al., 2012). Aliphatic, aromatic and tetra- and pentacyclic hydrocarbons as well as low molecular weight NSO-compounds, such as phenols and carbazoles (Ruble et al., 1998; George et al., 2004a; Peters et al., 2018) were the main target classes under study.

As compared to crude oils, inclusion oils are preferentially enriched in polar compounds (Karlsen et al., 1993; Nedkvitne et al., 1993), because they are more readily adsorbed on mineral surfaces during inclusion formation (Crocker and Marchin, 1988; Pang et al., 1998; George et al., 2007a). Yet, very little compositional insight has to date been gathered on high molecular weight NSO-compounds in FI oils. Here, we utilize the Fourier transform-ion cyclotron resonance-mass spectrometer (FT-ICR-MS) with its ultra-high mass accuracy and detection reach to high *m/z* to study NSO-compounds in FI oils, identifying molecular formulae and resolving thousands of compounds that are inaccessible to GC-FID and GC-MS (Marshall and Rodgers, 2004, 2008). Many geological questions have been addressed using this instrument recently, such as organic matter maturation (Hughey et al., 2004; Oldenburg et al., 2014; Poetz et al., 2014), biodegradation (Kim et al., 2005; Hughey et al., 2007; Liao et al., 2012; Seidel et al., 2016; Martins et al., 2017; Oldenburg et al., 2017), oil migration (Liu et al., 2015; Han et al., 2018a; Ziegs et al., 2018), as well as oil and source rock correlation (Mahlstedt et al., 2016). Thus, this powerful instrument also could offer a new approach to shed light on polar compounds trapped in FI oils.

The indigenous organic matter surrounding FIs, and contaminants from drilling and sampling adhering on the surface or in microcracks of host minerals, may affect inclusion oil analysis. In previous studies, strong acids such as HCl and chromic acid were applied to clean host minerals (George et al., 2007a). However, this method is clearly unsuitable for carbonate minerals. For carbonate rocks various organic solvents, like dichloromethane and other solvent mixtures, have been used to

repetitively wash host minerals using Soxhlet, sonication or vacuum solvent extractions (Karlsen et al., 1993; George et al., 1998, 2007a; Jones and Macleod, 2000). Such clean-up procedures have successfully been used prior to the GC-MS analysis of FI oils (Jones and Macleod, 2000; Volk et al., 2002; George et al., 2007a). Noah et al. (2018, 2019) were the first to demonstrate that FT-ICR-MS can be used to analyze NSO-compounds in fluid inclusion oils contained in quartz, applying the clean-up methods developed by George et al. (2007a). Noah et al. (2018, 2019) compared FT-ICR-MS derived NSO-compound compositions in a FI oil, a produced oil, potential source rock extracts and reservoir rock extracts from the Üllés Field in the Pannonian Basin, Hungary. They found elevated abundances of NSO-compounds in FI oils compared to crude oils, which may reflect the greater affinity of NSO-compounds to polar mineral surfaces, where oils can be trapped on crystal imperfections. Furthermore, they demonstrate that FT-ICR-MS can be used as a tool to provide detailed information on NSO-compounds in FI oils. First high resolution mass spectrometry results showed systematic variations in NSO-compound composition between different sample types. This opened an exciting domain of research into mineral-fluid interaction and the evolution of petroleum reservoirs.

Initial extraction experiments in our study showed that the conventional cleaning methods developed for GC-MS do not always provide the level of purity needed for the very sensitive FT-ICR-MS technique and that additional cleaning steps are needed. Furthermore, conventional methods often use strong acids which cannot be applied to host crystals that react with acids, namely fluorite and carbonates.

Thus, in this study an acid-free clean-up and preparation procedure is presented that is suitable for all host mineralogies. It eliminates organic contaminants adhering to host mineral surfaces and thereby enables polar compounds in FI oils to be analyzed using FT-ICR-MS in APPI (+) and ESI (–) modes. These ionization modes were selected because they are the most common in crude oil characterisation and because they provide the broadest range of compound polarities and ionization efficiencies. Four representative samples with microscopically characterised oil-inclusions in different host minerals were chosen for the method development to

characterise occluded NSO-compounds in FI oils.

2.3 Material and Methods

2.3.1. Sample set and geological background

Oil can be trapped in fluid inclusions hosted in different minerals formed in various sedimentary settings (Roedder, 1984). For example, fracture-fill mineralization may contain abundant FIs that contain instantaneously generated oil (Roedder, 1984; Etminan and Hoffmann, 1989; Benchilla et al., 2003). The samples studied here originated from two MVT-type deposits in Tunisia and Mexico and consist of fluorite. In addition, quartz samples from two occurrences, namely quartz veins hosted by Triassic sandstones from Germany and vugs from an ore deposit in Pakistan were studied (Fig. 2.1). Detailed geological information on each sample is provided in Table 2.1.

Table 2.1. Geological information about host minerals in various area

Sample name	Host mineral	Location	Formation Time	Host rock	Potential source rock
GE	quartz	Germany	Late Jurassic-Early Cretaceous	Triassic sandstone	Lower Jurassic Posidonia shale
TN	fluorite	Tunisia	Late Tortonian-Pliocene	Campanian and Tithonian series limestones	Triassic-Permian sediments
PK	quartz	Pakistan	Early Oligocene	Upper Jurassic limestones	Lower Jurassic sediments
MX	fluorite	Mexico	Tertiary	Upper Cretaceous shale and carbonates	Upper Jurassic Calcareous shale and carbonates

2.3.1.1 Quartz sample from Germany

Colorless quartz from veins hosted in an Upper Triassic sandstone from the Lower Saxony Basin (LSB) located in north-western Germany hosts abundant oil and gas-bearing inclusions. The oil inclusions show liquid-vapor (L-V) homogenization at mean temperatures of 137.1 °C (Fig. 2.1a). The formation of quartz was triggered by fluid migration in response to tectonic movements of the LSB. A period of rifting and wrench tectonics occurred during the Late Jurassic and Early Cretaceous (Betz et al., 1987). During this period oil migrated and was preserved as FIs in quartz fracture-fill mineralization. The oil trapped in quartz was considered to be sourced from Lower

Jurassic Posidonia shale (Lüders et al., 2012) which is the most important source rock for oil (and gas) in the LSB (Lüders and Plessen, 2015 and references therein).

Figure 2.1. Photographs of fluid inclusion samples: a) quartz vein material from a Upper Triassic sandstone (Germany, GE); b) fluorite from Campanian series limestones (Tunisia, TN); c) quartz from Upper Jurassic limestones (Pakistan, PK); d) fluorite from Upper Cretaceous shale and carbonates (Mexico, MX).

2.3.1.2 Fluorite sample from Tunisia

The Tunisian fluorite sample is colorless and hosts large oil fluid inclusions with sizes up to 400 µm (Fig. 2.1b). The fluorite mineralization in north-eastern Tunisia occurs along the Zaghouan and Hammam Jedidi faults, which have been tectonically active since the Late Miocene (Bouhlel et al., 1988). In the Late Tortonian-Pliocene, petroleum that was generated from Triassic-Permian sediments migrated with hydrothermal brines into the Campanian series and Tithonian series limestones in Hamman Zriba (Benchilla et al., 2003). The mineral association is similar to MVT-type deposits (Cathles and Smith, 1983). Bouhlel et al. (1988), distinguished between three styles of fluorite mineralization in this area: white vein-type fluorite (F1 type), massive purple fluorite (F2 type) and massive white fluorite in cavities and open vugs

(F3 type). All fluorite types contain abundant oil-rich FIs. In the current study, a F3 fluorite sample was investigated. Homogenization temperatures of petroleum FIs vary between 173 °C and 194 °C ± 10 °C and salinities between 13 to 22% (Guilhaumou et al., 2000; Benchilla et al., 2003).

2.3.1.3 Quartz sample from Pakistan

The quartz crystals from Pakistan exhibit prominent prismatic or steep rhombohedral habits with dark material trapped inside (Fig. 2.1c). L-V homogenization of oil-bearing FIs in the temperature range between 121.8 and 162.8 °C was measured. Oil-bearing FIs hosted in fluorite and quartz were reported in the Koh-i-Maran region (Pakistan) (Benchilla et al., 2003). In the early Oligocene, oil generated from Lower Jurassic sediments and migrated with brines into the Upper Jurassic limestones. Bipyramidale quartz crystals from the Koh-i-Maran region resemble the well-known “Herkimer diamonds” (Ulrich, 1989).

2.3.1.4 Fluorite sample from Mexico

The purple fluorite sample from Encantada-Buenavista, Mexico is prone to crack along its cleavage and has an intense petroleum odor after cracking (Fig. 2.1d). During the Tertiary, oil and aqueous fluids penetrated a network of fractures in Upper Cretaceous shales and carbonates resulting in the precipitation of fluorites rich in oil FIs. Fluorite mineralization was similar to those described for Tunisia and other MVT-type deposits. L-V homogenization temperatures of FIs hosted in fluorite were documented between 139.6 and 153.2 °C. Oil was considered to have been sourced from calcareous shale and carbonates of the Upper Jurassic and to a lesser extent by Tertiary and Cretaceous rocks (González-Partida et al., 2002, 2003).

2.3.2 Host mineral clean-up

For the clean-up procedure high-purity solvent and clean glassware were utilized. High-purity dichloromethane and methanol (99.9% hypergrade for LC-MC), sodium dithionite ($Na_2S_2O_4$), sodium bicarbonate ($NaHCO_3$) and sodium citrate ($Na_3C_6H_5O_7$) (>99% grade) were used. Extraction thimbles were ultrasonically pre-cleaned for 30 minutes using dichloromethane as solvent, followed by Soxhlet extraction with

dichloromethane for 24 hours. Glassware was cleaned using a commercial surfactant solution (Neodisher LabClean FLA), then heated to 450 °C in an oven and finally rinsed three times with DCM before utilization.

In the first clean-up step minerals were coarsely broken with a hammer, splitting along cracks and fractures, and the mineral fragments were washed using distilled water and then dried. Afterwards, a Waller solution (33% sodium dithionite, 28% sodium bicarbonate, 59% sodium citrate in distilled water) (Nichols, 2019) was added to oxidize iron and organic matter on the surface of the host mineral fragments. While the oxidizing ability of the Waller solution is weaker than the commonly applied chromic acid, it is from a safety aspect less harmful and, importantly also suitable for carbonate mineral clean-up. The host minerals were kept in the Waller solution for 3 hours followed by a sonication for 10 min. Subsequently, the mineral material was washed twice using distilled water and dried. This step was repeated three times.

In the second step, a modified multiple-cleaning procedure was established based on the protocol of George et al. (2007a). The minerals were washed in sequence with solvents or solvent mixtures with decreasing polarity. The host minerals were cleaned with 30 mL of methanol, followed by 30 mL of a mixture of dichloromethane (DCM) and methanol (93:7, v/v) and finally by 30 mL of DCM using ultrasonication for 10 min each time. Each washing step was conducted three times.

After these rigorous cleaning procedures, the final washing step with DCM was collected as a blank for conventional GC-MS analysis. However, it turned out that this blank was not suitable for FT-ICR-MS analysis, since it still contained some tiny mineral particles which were prone to block the transfer capillary (capillary for ion transfer from the ion source (ambient pressure) into the MS with high vacuum conditions) of the FT-ICR-MS. Thus, the solvent-cleaned host minerals were transferred into an extraction thimble within a Soxhlet apparatus and washed twice for 24 h with 250 mL DCM and methanol (99:1, v/v) at 50 °C. The solvent of the final washing step was collected, concentrated by a Turbovap system (Biotage) and dried under a N_2 stream. This clean-up solution is used as the procedural blank (P-blank).

Before measuring any sample, pure solvent was measured on the FT-ICR-MS system to obtain a system blank (S-blank) for comparison.

2.3.3 Extraction of inclusion oils

Cleaned host minerals were loaded into a crushing cylinder equipped with two stainless steel balls. The host minerals were crushed by shaking, after which the crushing cylinder remained stationary for 10 min. The mineral powder was transferred into pre-cleaned extraction thimbles. The steel balls and crushing cylinder were rinsed with DCM and methanol (99:1, v/v) and the washings were added to the Soxhlet thimble. Afterwards, the mineral powder was extracted by Soxhlet extraction for 24 h with 250 mL DCM and methanol (99:1, v/v) at 50 °C. Finally, the Soxhlet extract was concentrated by a Turbovap system and dried under a stream of N_2. The extracted FI oil was weighed and measured by FT-ICR-MS in both APPI (+) and ESI (–) modes.

2.3.4 Analytical methods

2.3.4.1 Microscopy

Doubly polished thin sections of the minerals were used to observe the oil FIs using a BX50 Olympus microscope with various objectives (5×, 10×, 20×, 50×) connected to a UV light device.

2.3.4.2 FT-ICR-MS measurement

Blanks and inclusion oils were measured using a 12T Solarix FT-ICR-MS from Bruker Daltonik GmbH (Bremen, Germany) in ESI (–) and APPI (+) mode. A detailed description of the equipment, mass calibration and data analysis for ESI (–) mode has been presented by Poetz et al. (2014). For ESI (–) mode, a stock solution of 1 mg/mL in methanol and toluene (1:1, v/v) was diluted with the same solvent mixture to give a final concentration of 100 μg/mL. Before analysis, 1 mL sample solution was mixed with 10 μL of a 25% aqueous NH_3 solution to facilitate the deprotonation of the molecules for analysis. The working parameters were as follows: nitrogen flow rate 4.0 L/min, temperature at 220 °C, nebulizing gas 1.4 bar, sample solution flow rate 150 μL/h, capillary voltage 3000 V, additional collision-induced dissociation voltage

of 70 V, ions accumulation time 0.05 s, transfer time 1 ms, 4 megaword data sets. A total of 200 mass spectra were accumulated in a mass range from *m*/*z* 147 to 1000. External calibration for ESI (–) mode was performed using an in-house fatty acid and polyethylene glycol sulfate mixture.

For measurements in APPI (+) mode, a concentration of 1 mg/mL in methanol and hexane (9:1, v/v) was diluted with the same solvent mixture to give a final concentration of 20 µg/mL. The working parameters were as follows: dry gas (N_2) flow rate 3.0 L/min and temperature 210 °C, nebulizing gas (N_2) 2.3 bar, sample solution flow rate 20 µL/h, capillary voltage 1000 V, additional collision-induced dissociation voltage of 30 V, ions accumulation time 0.03 s, transfer time 1 ms, 4 megaword data sets. A total of 300 mass spectra were accumulated in a mass range from *m*/*z* 147 to 1200. External calibration for the APPI (+) mode was done using a calibration mixture containing polyethylene glycol 400 and polyethylene glycol 600 (1:1) from Fluka.

In each spectrum, signals with a signal-to-noise ratio ≥ 12 were included for further data assessment. Formula assignment was done using the isotopes ^{1}H, ^{12}C, ^{13}C, ^{14}N, ^{16}O, and ^{32}S, with the upper thresholds N ≤ 2, O ≤ 8, and S ≤ 2 in APPI (+) mode and N ≤ 2, O ≤ 8 and S = 1 in ESI (–) mode; C and H were unlimited. If no chemical formula within the allowed mass error of 0.5 ppm was found, the peak was not included in the mass/formula list. For each $C_cH_hN_nO_oS_s$ compound, its double bond equivalent (DBE) value was obtained by calculating DBE = c – h/2 + n/2 + 1. Each DBE refers to the number of unsaturation or rings in the individual compound structure.

2.3.4.3 GC-MS measurement

Prior to GC-MS analysis 5α-Androstane and 1-ethylpyrene were added as internal standards. The FI oils were analyzed using a Trace GC Ultra coupled to a DSQ mass spectrometer (Thermo Electron Corp.). The GC was equipped with a Thermo PTV injection system and a SGE BPX5 fused silica capillary column (50 m × 0.22 mm i.d. and 0.25 µm film thickness). Helium was used as carrier gas. The GC

oven was ramped from 50 °C to 310 °C at a rate of 3 °C/min and held at the end temperature for a further 30 min. The injector temperature was programmed from 50 °C to 300 °C at a rate of 10°C/s. The MS was operated in electron impact ionization mode (EI) at 70 eV. Full-scan mass spectra were recorded over m/z 50-600 at a scan rate of 1.5 scans/s.

2.4 Results and discussion

2.4.1 Microscopic characterization of fluid inclusions

FI oil characteristics were studied using both transmitted and UV light (Fig. 2.2). The oil inclusions in fluorite samples TN and MX are pale yellow under transmitted light, making it easy to distinguish them from co-genetically trapped colorless aqueous FIs. In contrast, the inclusion oils in the quartz samples GE and PK were colorless (Fig. 2.2). Oil inclusions in samples GE and MX range from 10 μm to 50 μm, and were more abundant in the MX sample than in the GE sample. Globular oil inclusions were common in the TN sample with diameters up to 400 μm. Oil inclusions in the PK sample showed variable shapes, reaching several hundred micrometers in size and containing large vapor bubbles. Several examples of solid bitumen trapped in inclusions were documented (Fig. 2.2c) in the PK sample which may have formed during the transformation of oil to gas at high temperature (Burruss, 2003). Most oil FIs consisted of either gas and liquid (either oil or water), or three phases (gas, liquid and solid bitumen). It has generally been demonstrated that blue and white fluorescence of inclusion oils indicate higher maturity (Burruss et al., 1985; McLimans, 1987). Oil FIs in samples GE, TN, and PK were deep blue, pale blue and light blue, respectively, under UV light, while they were nearly white in sample MX. The blue to white fluorescence points to low density of the oil inclusions, reflecting high API gravity (Burruss, 2003). It is assumed that the oil trapped in inclusions was generated from a source rock whose maturity was ca. 0.93 %Rc (TN), 1.31 %Rc (PK), and 0.97 %Rc (MX), as estimated using MPI-1 ratios (Table 2.2). An %Rc value of about 0.78 for the GE sample (Table 2.2) was calculated on the base of carbon isotope ratio of oil-bearing fluid inclusions by Lüders et al. (2012).

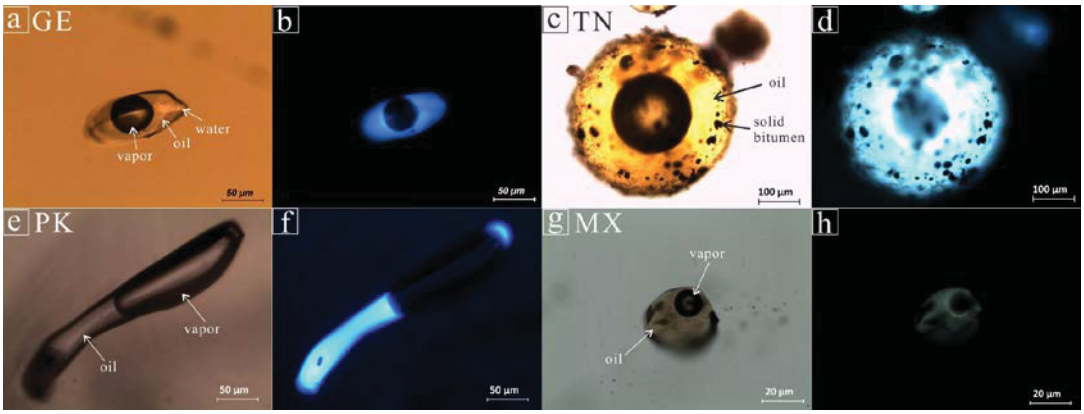

Figure 2.2. Photomicrographs of oil-bearing fluid inclusions under transmitted (a, c, e and g) and UV light (b, d, f and h). GE and PK: quartz sample from Germany and Pakistan, respectively. TN and MX: fluorite samples from Tunisia and Mexico, respectively (see Table 2.1).

Table 2.2. Extraction yields and maturity related ratios of FI oils.

Host mineral	Sample weight (g)	Extracted oil (mg)	Extracted oil (µg/g)	MPI-1	%Rc
GE-quartz	8.56	0.48	56	–	0.78[#]
TN-fluorite	2.38	0.38	159	0.88	0.93
PK-quartz	8.53	3.12	366	1.51	1.31
MX-fluorite	12.08	1.28	106	0.95	0.97

Note: GE and PK: quartz samples from Germany and Pakistan, respectively. TN and MX: fluorite samples from Tunisia and Mexico, respectively (see Table 2.1). Methylphenanthrene index (MPI-1) = 1.5 × [3MP + 2MP]/[P + 9MP + 1MP]; Calculated reflectance (%Rc) = 0.60 × MPI-1 + 0.40 (for 0.65 <%Ro < 1.35) (Radke and Welte, 1983). –: not detected; #: Phenanthrene was not detected in sample GE and thus, %Rc was calculated based on carbon isotope ratio of methane in oil inclusions (Lüders et al., 2012).

2.4.2 Extraction yields

The amounts of oils extracted from FI varied between 0.38 mg and 3.12 mg (Table 2.2). This resulted in extraction yields of 56–366 µg/g host mineral. The PK quartz sample showed the highest and the GE quartz sample the lowest extraction yield, while the MX and TN fluorite samples showed intermediate concentrations.

2.4.3 Contaminant assessment in fluid inclusion oils

The extracted oils, system blanks (S) and procedural blanks (P) were analyzed by FT-ICR-MS in the APPI (+) and ESI (–) modes. For the interpretation of the FT-ICR-MS data of the extracted FI oils it is especially important to identify indigenous signals and distinguish them from external sources. This is especially important because the occluded oils are present in low concentration. To assess the level of external components in the FI oil extracts, all signals detected were compared to the signals occurring in the S-blank and P-blank samples applying a Venn analysis (Oliveros, 2007) (Fig. 2.3). With this method, both unique and common signals from the different samples were revealed. Due to the ultrahigh resolution and sensitivity of the FT-ICR-MS organic compounds were detected even in the S-blank representing a measurement of a hypergrade solvent. However, the number of components common to the S-blank and the inclusion oils was small (0–19 signals) for both ionization modes, while the number of shared signals with all sample types were more abundant (68–229 signals). This most likely represented background signals of the measurement system. In contrast, the number of common signals between the FI oils and the P-blanks was significantly higher (101–504 signals). This might represent compounds still adhering on the mineral matrix even after the stringent clean-up procedure. On the other hand, it can also be argued that these signals included compounds which were present on the mineral surfaces as well as in the FI oils. However, there is no way to separate this and thus, to be on the safe side, these shared compounds were assessed as contaminants for the FI oils. Although there was a certain number of shared compounds between the P-blank and FI oil samples, in both ionization modes the number of unique compounds was typically highest for the extracted oils. One exception was the GE sample in the APPI (+) mode. The reason for this might be that this is the sample with the lowest extraction yields (Table 2.2).

The Venn diagram proved to be valuable providing a first assessment of the level of external contamination of the FI oils and to check how well the cleaning procedure had worked. On first inspection, the comparison of all assigned signals presented in Figure 2.3 suggests a successful cleanup for the processed FI samples.

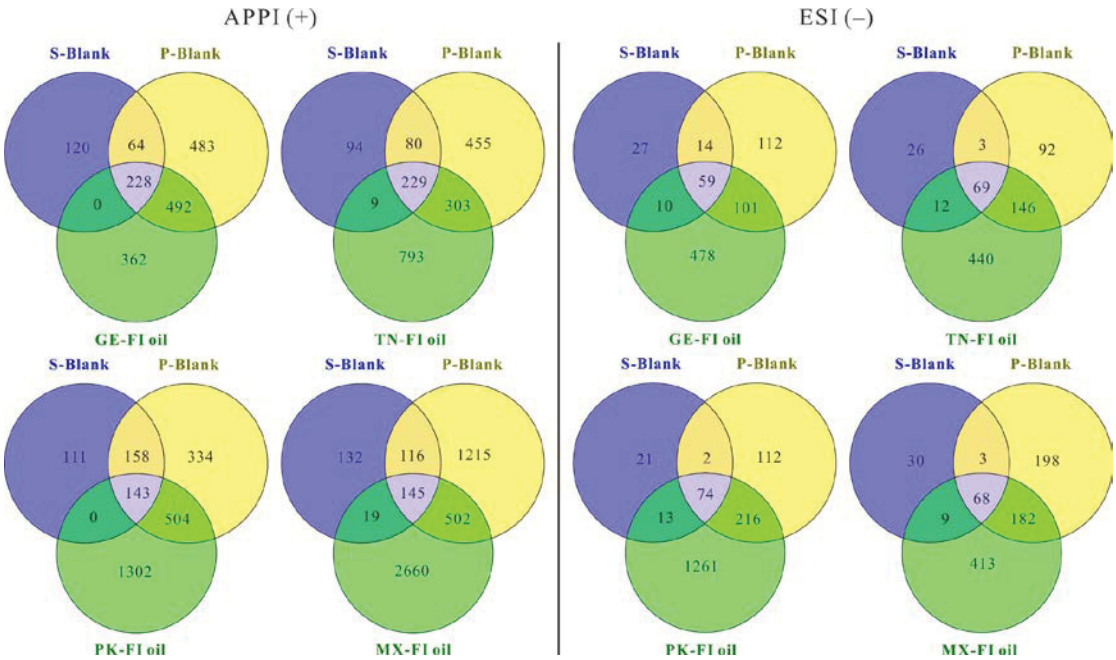

Figure 2.3. Venn diagrams showing the comparison of signals in system blank (S-blank), procedural blank (P-blank) and inclusion oils (FI). Non-overlapping areas indicate signals that are unique to a sample type, overlapping areas indicate common signals between two or all sample types. Left side FT-ICR-MS measurement in the APPI (+) mode and right side in the ESI (–) mode. GE and PK: quartz samples from Germany and Pakistan, respectively. TN and MX: fluorite samples from Tunisia and Mexico, respectively (see Table 2.1).

For a deeper assessment as to which compounds and compound classes can be used for further data interpretation, it is necessary to compare each compound class and its DBE distributions in the inclusion oils with those from the blanks. According to this comparison there were three different assessment categories defined: The assessment category I (high contamination level) is exemplified by the O_4 class in the GE sample measured in APPI (+) mode (Fig. 2.4). The comparison shows a very similar compound distribution for the extracted inclusion oil and both the S-blank and P-blank (Fig. 2.4a). Therefore, these compounds might have been introduced into the FI oil extract by contaminants still adhering on the mineral surface (P-blank) or by the solvent or measurement procedure (S-blank). These compound classes do not give reliable information on the oil and can be assessed as contamination.

Category II (low contamination level) was represented for instance by the HC species in the TN sample measured in the APPI (+) mode showing also a few distinct

compounds (red square in Fig. 2.4b) which were present in both blanks and the FI oil, but additionally a high number of HC compounds which were unique to the oil. Here only a selected part of the HC compounds was assessed as being contaminants, while the overwhelming remaining majority were considered as indigenous for the FI oil.

Category III (non-contamination level) was illustrated by the N_1 compound class from the MX sample measured in the ESI (–) mode. The corresponding S-blank and P-blank were completely free from N_1 compounds, indicating that the only source of these compounds is the FI oil itself (Fig. 2.4c).

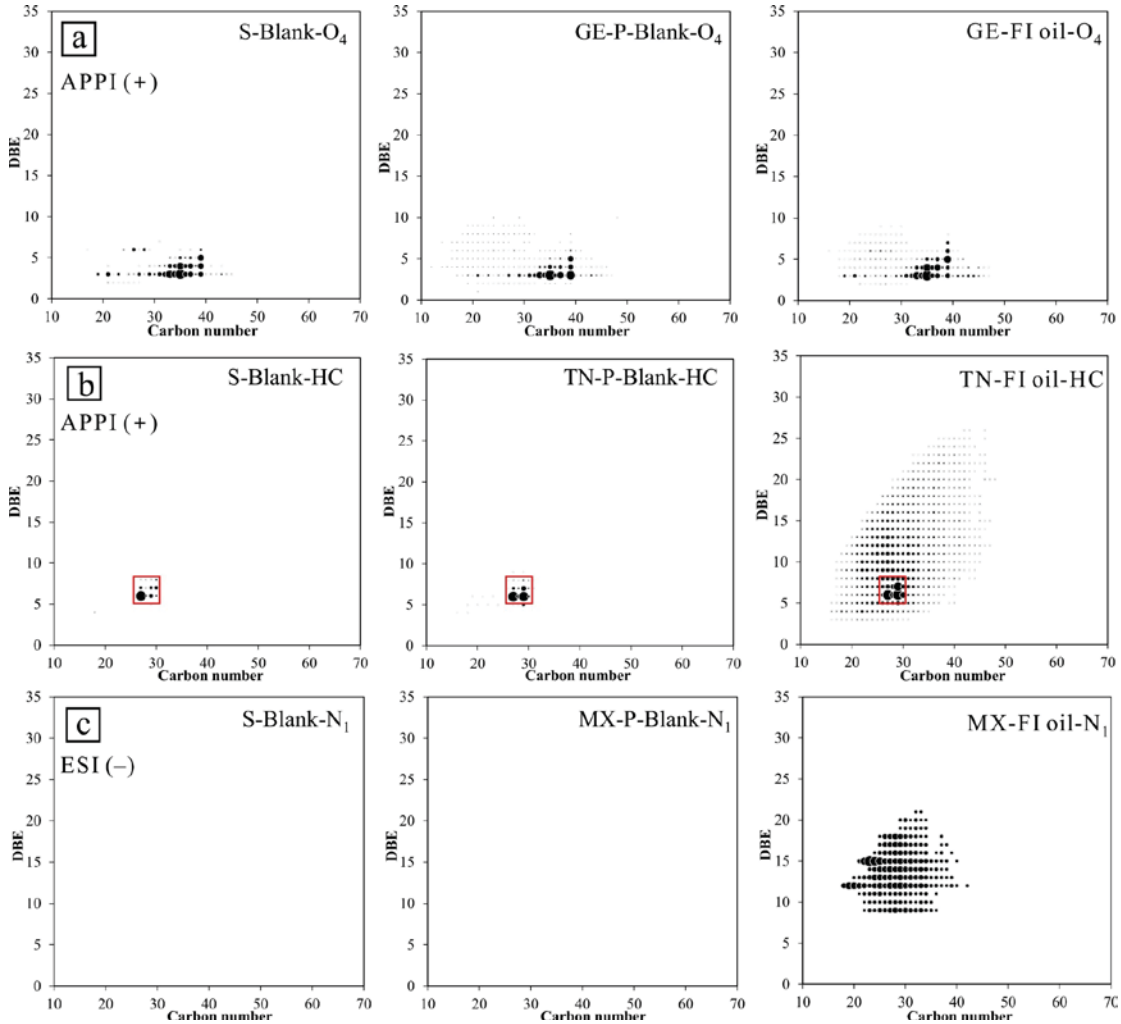

Figure 2.4. Double bond equivalent (DBE) vs carbon number plots of the: a) O_4, b) hydrocarbons (HC) and c) N_1 compound classes in the S-blank, P-blank and extract oil of: a) the GE quartz sample, b) TN fluorite sample measured by FT-ICR-MS in the APPI (+) mode as well as c) the MX fluorite sample measured in the ESI (–) mode.

In accordance with these three categories, the main compound classes were fully suitable or conditionally suitable (categories III and II, respectively) or unsuitable (category I) for further interpretation (Table 2.3). Thus, although contributions from external contamination sources cannot completely be avoided, the presented method shows that the level of contamination can be assessed and that the affected compound classes can be identified, thus enabling FI signals to be recognized. Figure 2.5a indicates that the dominant compound classes in APPI mode show no or only a low level of contamination (compare with Table 2.3). By contrast, in ESI (–) mode, only selected compound classes show an acceptable level of contaminants. Thus, although the Venn diagrams (Fig. 2.3) suggested a similar contamination level for the two ionization modes, the detailed compound class analysis (Table 2.3) indicates that the clean-up procedure worked much better for the compounds which can be measured in APPI (+) mode. A reason for this could be that compounds which are measurable in the ESI (–) mode usually show a much higher polarity and therefore adhere much better on mineral surfaces (Marshall and Rodgers, 2008). However, the Pakistan sample shows acceptable levels of contamination for almost all compound classes, (Table 2.3), and also the Mexican sample indicates for the dominating O_2 and N-classes that the clean-up procedures can partly be (partly) sufficient also for the ESI (–) mode. It is not very likely that this different behavior is dependent on the mineral matrix, since one quartz sample show massive contamination (GE) and the other not (PK). It is conceivable that the amount of extractable FI oil plays a more significant role for the compounds measurable in the ESI (–) mode. The amount of the GE and TN sample is significantly lower than for the MX sample and especially for the PK sample (Table 2.2), thus acidic contaminants, which are also common in the laboratory environments, have a much higher impact on the GE and TN samples. To conclude, the data suggest that only FI samples with a high extraction yield should be analyzed in the ESI (–) mode or that an even more intensive cleaning method is needed for the ESI (–) mode to reduce external contamination to an acceptable level. Nevertheless, considering the presented contamination assessment the presented method enables access to the NSO-compound fraction from FI oils allowing the investigation of their geochemical significance.

Table 2.3. Classification of the main compound classes in the investigated inclusion oils (see Table 2.1) with regard to their level of external contamination (after comparison with blanks).

Compounds classes	*APPI (+) mode*				*ESI (–) mode*			
	GE	TN	PK	MX	GE	TN	PK	MX
HC	II	II	II	II			#	
O_1	II	II	II	II	I	I	III	I
O_2	II	II	II	I	II	I	II	II
O_3	I	I	II	I	I	I	II	I
O_4	I	I	I	I	I	I	II	I
O_5	I	I	\	I	I	I	II	I
O_6	I	I	\	I	I	I	II	I
N_1	I	I	III	III	\	\	III	III
S_1	\	III	\	III			#	
S_2	\	I	\	III			#	
N_1S_1	\	\	\	III	\	\	\	III
N_1O_1	I	I	I	II	\	\	\	\
N_2O_2	I	I	I	I	I	I	I	I
S_1O_1	\	I	II	III	I	II	III	II

Note: I: detected compounds are not suitable for further interpretation (category I: highly contaminated), II: the overwhelming proportion of the compounds is unique to the FI oils (category II: low contamination level and conditionally suitable for further interpretation), III: compounds are unique to the FI oils (category III: not contaminated and fully suitable for further interpretation), \: no compounds detected, #: compounds not ionizable in ESI (–) mode.

2.4.4 NSO-compounds and HCs in inclusion oils as geochemical markers

In the following examples we demonstrate how compounds or compound classes from FI oils, assessed as suitable (category III) and conditionally suitable (category II) for further interpretation, can be applied to address various petroleum geological issues, namely characterization of intitial petroleum compositions, thermal maturity and biodegradation levels.

2.4.4.1 Characteristic compositions of inclusion oils

Fluid inclusion oil analysis can provide deep insights into the original oil composition which becomes especially important when reservoir oil is altered by subsequent processes. Figure 2.5a shows the distribution of low polarity NSO-

compounds and aromatic HCs detected in the four investigated FI oils using the APPI (+) mode. Comparing Figure 2.5a with Table 2.3 it becomes clear that the dominating compound classes (HC, O_1, O_2 and S_1) are not significantly affected by external contamination and that these groups can be used for further oil characterization and interpretation. In contrast, the high abundances of the O_4 compounds in the GE and TN samples might reflect external contamination. Overall, the compound inventory of the investigated FI oils showed a broad variability from pure HC to compounds with different numbers and combinations of heteroatoms (Fig. 2.5a) and differences between the investigated FI oils can clearly be recognized.

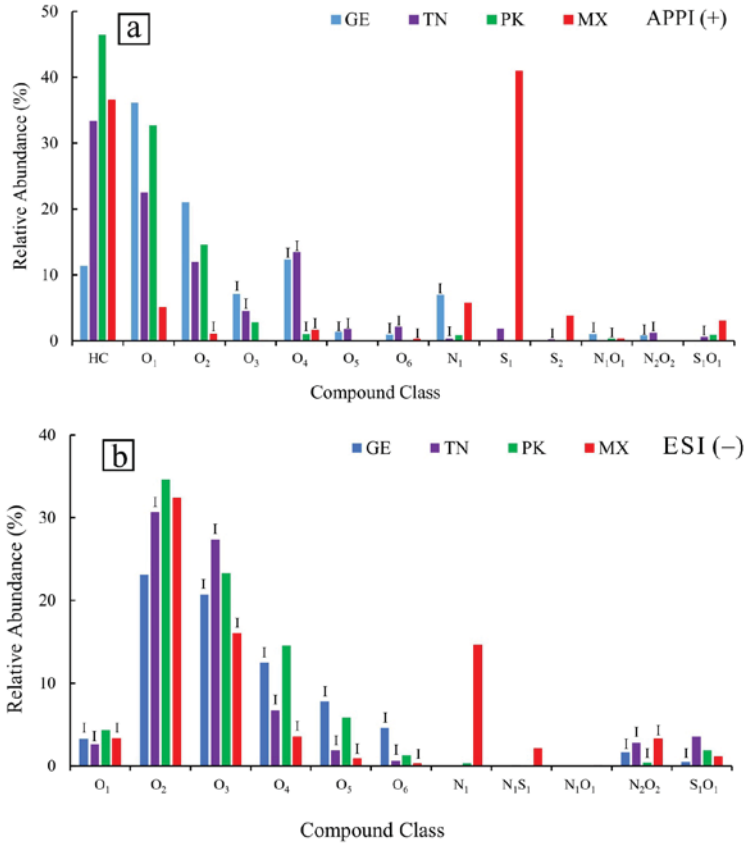

Figure 2.5. Relative abundance of the compound classes of the four investigated FI oils (see Table 2.1) measured by FT-ICR-MS in: a) the APPI (+) and b) ESI (–) mode. HC = hydrocarbons; element + number x = compounds bearing × heteroatoms. Strongly contaminated compound classes are marked with a "I" (contamination category I). For sample types see Table 2.1.

In the ESI (–) mode the acidic NSO-compounds are detected. Thus, the compound class distribution in all samples (Fig. 2.5b) was dominated by oxygen-

containing compounds, especially by O_2, O_3 and O_4 species. The N_1 species are major contributing classes as well. As discussed above in the ESI (–) mode residual contamination is a greater issue than in the APPI (+) mode. However, the level of contamination also seems to depend on individual sample characteristics and extraction yields of FI oils, since the PK FI oil shows only low and acceptable contamination levels, while the TN sample can essentially not be evaluated. However, with the exception of the TN sample the main compound class (O_2 class) can be used for further interpretation. The same is true for the N_1 class and for S_1O_1 species at least for the TN, PK and MX FI oils.

2.4.4.2 Thermal maturity assessed from inclusion oils

NSO-compound parameters that have been employed for assessing thermal maturity have been discussed in many studies based on nitrogen- and sulfur-containing compounds from reservoir petroleum. N_1 compounds, especially pyrrolic nitrogen, have been widely studied using the ESI (–) mode and relationships between N_1 compound compositions and thermal maturity have been established (Hughey et al., 2004; Oldenburg et al., 2014; Poetz et al., 2014; Mahlstedt et al., 2016). The same is true for S_1 compounds which have been studied in APPI (+) mode (Oldenburg et al., 2014; Walters et al., 2015) and ESI (+) mode (Li et al., 2011). In addition to the polar compounds, thermal maturity is also expressed in compositional changes of aromatic HCs detected in the APPI (+) mode (Purcell et al., 2006; Rodgers and Marshall, 2007), since thermal maturation promotes aromatization of the organic matter (Tissot and Welte, 1984).

Maturity assessment using nitrogen-containing compounds in inclusion oils

N_1 compounds were highly abundant in the MX FI oil, with DBE in the range from 9 to 21, and carbon numbers ranging from 19 to 42 (Fig. 2.4c). DBE 12 and 15 classes were preferentially enriched, and these compounds could be interpreted as consisting of a carbazole unit and additional benzene rings, such as benzocarbazoles and dibenzocarbazoles, respectively (Hughey et al., 2002; Shi et al., 2010; Oldenburg et al., 2014; Poetz et al., 2014). The DBE 9 group is interpreted as containing a

carbazole core unit with long alkyl chains as deduced in many studies (Hughey et al., 2002; Poetz et al., 2014). The abundance of the DBE 9 group was lower than those of the DBE 12 and 15 classes, which are interpreted to reflect carbazoles with one or two additional benzene rings, respectively. The N_1-DBE classes increase with increasing maturation due to ongoing aromatization (Hughey et al., 2004; Oldenburg et al., 2014). Thus, the N_1 species with DBE 9, 12 and 15 can be used to assess the maturity of the FI oil using a triangular plot (Oldenburg et al., 2014). The maturity of MX FI oil could therefore be assessed to be around 1 %Re (vitrinite reflectance equivalent) (Fig. 2.6). In corroboration with this result, the maturity of the MX FI oil calculated from the Methyl Phenanthrene Index (MPI-1) ratio (Radke and Welte, 1983) detected by GC-MS (Table 2.2) was 0.97 %Rc suggesting a good thermal maturity assessment from the FI oil for the MX sample.

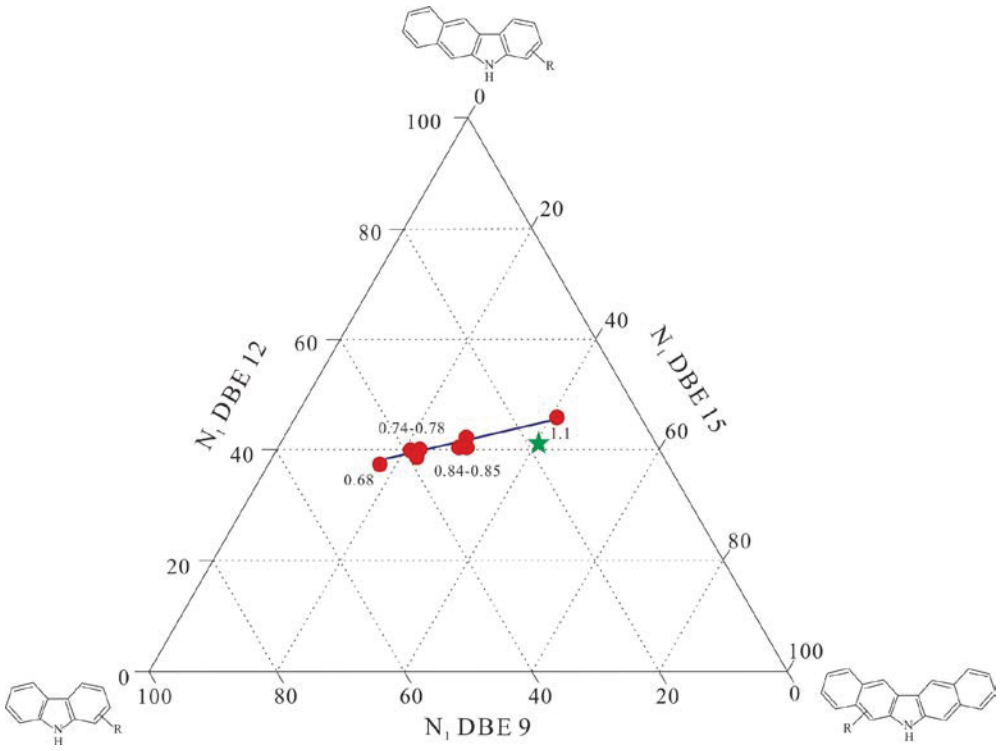

Figure 2.6. Triangular plot of N_1 DBE 9, DBE 12 and DBE 15 (modified after Oldenburg et al. (2014)) representing carbazoles with increasing number of aromatic rings, which is maturity dependent. The red circles are samples from Oldenburg et al. (2014) indicating different vitrinite reflectance ranges. The green star represents the position of the MX fluid inclusion oil sample. DBE = double bond equivalent. N_1 = compounds group containing one nitrogen.

Sulfur-containing compounds in inclusion oils as potential maturity markers

S_1 compounds in the MX sample had a broad DBE range from 1 to 26, and carbon numbers between 14 and 70 (Fig. 2.7). Compared to other reported crude oils (Purcell et al., 2007; Liu et al., 2010; Walters et al., 2015), the MX FI oil contained much broader carbon number and DBE ranges for the S_1 compounds. DBE 1 can be interpreted to be alkyl thiolanes (tetrahydrothiophenes) or alkyl thianes (tetrahydrothiopyrans), and DBE 2 with an additional fused naphthenic ring, while the DBE 3 class might bear a thiophene unit (Liu et al., 2018). DBE 4 and 5 classes presumably consist of thiophene with additional naphthenic rings. However, DBE 6 and DBE 9 classes were preferentially enriched probably containing compounds consisting of a thiophene unit and additional benzene rings such as known from benzothiophenes (BTs) and dibenzothiophenes (DBTs), respectively (Ho et al., 1974; Griffiths et al., 2013; Walters et al., 2015). The presence of DBTs was confirmed by GC-MS. In general, DBTs represent more thermally stable organosulfur compounds than do the low DBE S_1 compounds (BTs, thiophenes and alkylsulfides) (Ho et al., 1974; Manzano et al., 1997). It was observed that the abundance of low DBE S_1 compounds decreases with increasing maturity, while those of high DBE S_1 compounds increased in crude oil (Li et al., 2011; Oldenburg et al., 2014). Oldenburg et al. (2014) reported that low DBE sulfur compounds (lower than 5) were absent from maturity 0.68 %Ro to 1.1 %Ro. According to the N_1 compounds and MPI ratio shown above, the thermal maturity of the MX sample was roughly estimated around 1 %Rc. It is remarkable that despite its peak oil window maturity level, high abundances of S_1 species with low DBE values can still be observed. Two reasons might be responsible for this: (1) the aromatization process for the N_1 compounds is faster indicating different transformation gradients for N_1 versus S_1 compounds, or (2) the S_1 compound distribution might be influenced by prolific generation of lower DBE S_1 compounds. A conceivable process for the addition of low DBE S_1 compounds could be thermochemical sulfate reduction (TSR), during which low DBE organosulfur compounds are formed faster than they are destroyed, and similar cases have been described in studies reported by Li et al. (2011) and Walters et al., (2015). The TSR process has been confirmed in the MX fluorite by the presence of hydrogen

sulfide in fluid inclusions detected by Raman spectroscopy, and the presence of by-products from TSR such as calcite inclusions, solid bitumen (González-Partida et al., 2003; Tritlla et al., 2004). It is reasonable to deduce that TSR was responsible for the anomalous S_1 compounds distribution outlined above.

Our results show that S_1 compounds can be investigated in oil inclusions, and like the N_1 compounds, might also have the potential to act as maturity indicators. However, their maturity range of applicability and the factors influencing this parameter have still to be tested and evaluated with a larger number of sulfur-containing samples.

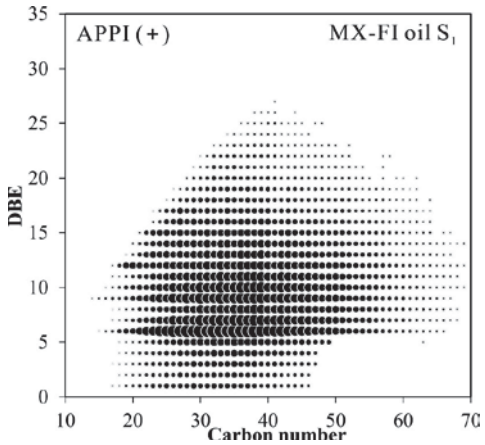

Figure 2.7. Double bond equivalent (DBE) vs carbon number plot of S_1 compounds in the MX sample measured in APPI (+) mode.

2.4.4.3 Hydrocarbons in inclusion oils

Due to ionization limitations, not all unsaturated and aromatic HCs can be ionized in APPI (+) mode (Marshall and Rodgers, 2008). Nevertheless, HCs were detected in all four investigated samples (Table 2.3). The carbon number range increases from the GE sample to the TN, PK and MX samples (Fig. 2.4b and 2.8). Thus, the PK and MX sample represent the broadest DBE and carbon number range. The DBE distribution of the GE FI oil showed a range from 3 to 13, while in the TN, MX and PK samples the upper DBE level was significantly higher, namely 26, 27 and 31, respectively (Fig. 2.4b and 2.8). This order is in accordance with the maturity assessment calculated by MPI-1 for the FI oils (GE (0.78 %Rc), TN (0.93 %Rc), MX

(0.97 %Rc) and PK (1.31 %Rc); Table 2.2), in which higher maturity inclusion oils shows higher DBE numbers. This indicates an increasing degree of aromaticity with increasing maturation.

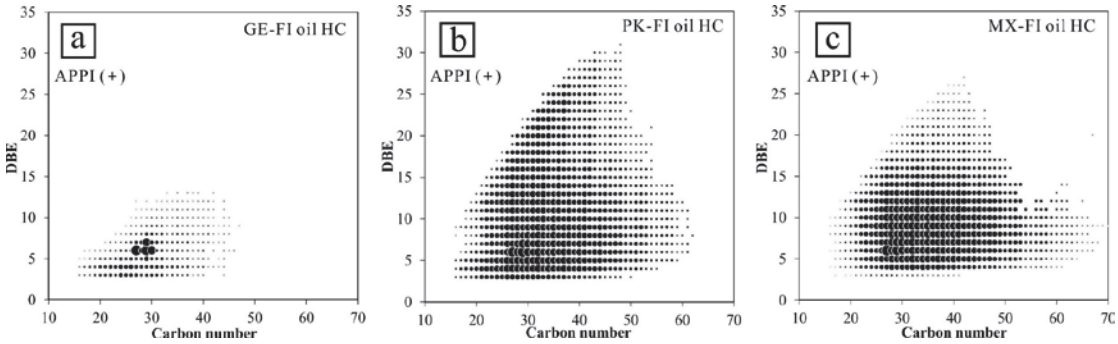

Figure 2.8. Double bond equivalent (DBE) vs carbon number plots of HC in the inclusion oil samples a) GE, b) PK and c) MX measured in the APPI (+) mode. For ample types see Table 2.1.

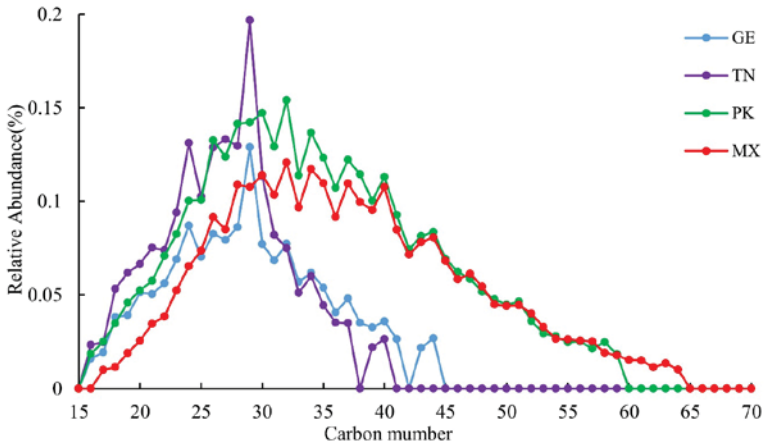

Figure 2.9. Carbon number distribution of the double bond equivalent (DBE) 5 groups of the aromatic hydrocarbons of the inclusion oil samples GE, TN, PK and MX. For sample types see Table 2.1.

Additionally, the carbon number range increases from the GE sample to the TN, PK and MX samples. Thus, the PK and MX samples represent the broadest DBE and carbon number range. In figure 2.9, different patterns in the carbon number distribution of the DBE 5 group of the four investigated samples are presented (Oldenburg et al., 2014). The GE and TN sample patterns ranged from 15 to 41 or 45 carbon atoms and showed a maximum at C_{29}. In contrast, the carbon number distribution in the PK and MX samples was broader ranging from 15 to 60 or 65

carbon atoms with a broad maximum between C_{25}-C_{40}. The GE and TN type distribution is similar to that reported for oils with a lower maturity and a maximum at C_{29} as well as a rapid decline from C_{29} to C_{30} (Oldenburg et al., 2014). In contrast, the PK and MX distribution pattern with the broader maximum around C_{33} resemble oils with higher maturity (Oldenburg et al., 2014). Thus, these data suggest that the PK and MX FI oils show a higher maturity than the GE and TN samples. In principle, this coincides with the calculated maturity assessment based on MPI-1. However, TN and MX show only low calculated maturity differences (TN 0.93 %Rc and MX 0.97 %Rc), but significant different DBE 5 group distributions (Fig. 2.9), indicating that factors other than thermal maturity (e.g., facies differences) might play a role for the different DBE 5 distributions.

2.4.4.4 Potential to infer biodegradation levels from inclusion oils

The particular strength of the FI method is to provide crucial information on the original oil composition and oil properties, especially when the reservoir oil has been altered by biodegradation. Importantly, the FI oils can also be used to search for early indications of oil biodegradation. Oxygen compounds, especially O_1 and O_2 compounds, measured by the ESI (–) mode have been widely studied and relationships between those compound class compositions and biodegradation have been demonstrated (Kim et al., 2005; Liao et al., 2012; Noah et al., 2015; Martins et al., 2017). It is known from previous ESI FT-ICR-MS based investigations of crude oils, that the abundance of O_2 species increase while those of the O_1 species decrease with increasing level of biodegradation (Kim et al., 2005; Hughey et al., 2007). Thus, the relative proportion of O_1 to O_2 compounds can provide a first hint for biodegradation. O_2 compounds are abundant, especially those from DBE 1 class representing acyclic carboxylic acids (Kim et al., 2005). In contrast, O_2 compounds with DBE 2, 3 and 4 represent mono-, bi- and tricyclic naphthenic acids (Kim et al., 2005; Noah et al., 2015). Kim et al. (2005) introduced the A/C (acyclic/cyclic) ratio ($A/C = \sum O_{2,\,DBE1} / \sum O_{2,\,DBE2+3+4}$) to estimate potential biodegradation levels of crude oil. The A/C ratio decreases with increasing biodegradation due to relative increase of cyclic acids and decrease of acyclic fatty acids. The A/C ratio has successfully been

applied to access biodegradation levels in petroleum reservoirs and at remediation sites (Kim et al., 2005; Liao et al., 2012; Noah et al., 2015; Martins et al., 2017).

Both the O_1 and O_2 compound classes were detected in the FI oil of the PK sample (Table 2.3). O_1 species are suggested to contain a hydroxyl functional group, with the DBE value ranges from 1 to 14 and carbon numbers range from 13 to 33 (Fig. 2.10a). O_2 species in the PK sample, representing the most abundant oxygen-containing compound class showed DBEs from 1 to 13, and carbon numbers range from 11 to 47 (Fig. 2.10b). O_2 species are strongly dominated by the DBE 1 group compounds, which represent carboxylic acids. While palmitic acid (C_{16}) and stearic acid (C_{18}) were detected in the blanks, O_2 species in the PK sample show overall only a low level of contamination (category II), and thus the O_2 data can be used to assess the A/C ratio. Compared with the findings in the literature about O_2 species (Kim et al., 2005; Liao et al., 2012; Noah et al., 2015; Martins et al., 2017) an A/C ratio of 1.6 indicates that the inclusion oil in the PK sample can be assessed as non-biodegraded during the time of trapping in the FIs. This result was confirmed by GC-MS data showing an unaffected *n*-alkane distribution pattern and the absence of an unresolved complex mixture (UCM). Although the investigated sample shows no indication of an early biodegradation, this example indicates that the respective compounds for a biodegradation assessment can be detected from some FI oils using the FT-ICR-MS. Thus, the new method shows high potential for indicating biodegradation in oil inclusions.

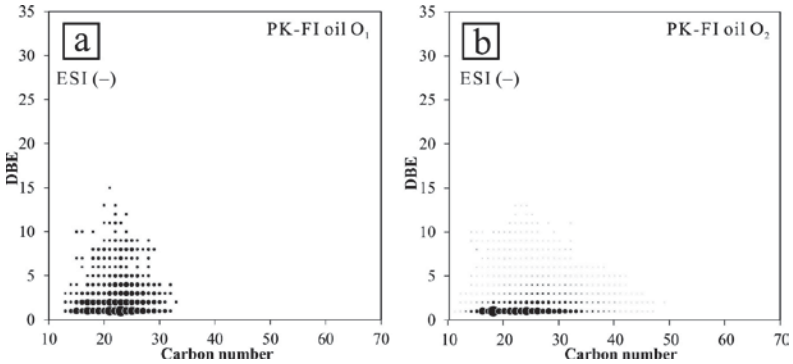

Figure 2.10. Double bond equivalent (DBE) vs carbon number plots of a) O_1 and b) O_2 compounds in the PK sample measured in ESI (–) mode.

2.5 Conclusion and outlook

A clean-up and crushing procedure for different host minerals has been developed, enabling biomolecules and NSO-compounds in oil-bearing fluid inclusions to be analyzed using FT-ICR-MS (APPI (+) and ESI (–) modes) and GC-MS as well. An additional putative benefit of the presented procedure is that it can also be applied to carbonate mineral hosts since it does not employ acids. Although external contamination cannot completely be removed by the clean-up procedure in all cases, especially where extraction yields are low, the developed method allows the contamination levels of different compound classes to be assessed and classified. This classification allows samples to be screened as to whether they are suitable or unsuitable for detailed interpretation. Data evaluation showed that the main compound classes are less influenced by external contamination especially in the APPI (+) mode and that their abundance in fluid inclusions allows established parameters for oil characterization to be determined. A new window is opened to investigate NSO-compounds in fluid inclusions with the FT-ICR-MS technique and to get more comprehensive information on petroleum or economic mineral emplacement.

2.6 Acknowledgements

The China Scholarship Council (CSC) is gratefully acknowledged for funding Yufu Han's research. We are indebted to Nicole Guilhaumou (Museum d'Histoire Naturelle Paris), David Banks (University of Leeds) and Stephen Becker (ExxonMobil Upstream Research Company) for providing sample material. We extend our gratitude to Cornelia Karger and Anke Kaminsky for their technical support. We are grateful to John Volkman, Herbert Volk, Paul Greenwood and an anonymous reviewer for their careful and constructive reviews of this paper.

3. GEOCHEMICAL CHARACTERISTICS OF INCLUSION OILS FROM THE SKARV FIELD A SEGMENT AND THEIR IMPLICATIONS FOR THE OIL CHARGE AND LEAKAGE HISTORY[2]

3.1 Abstract

The oil-bearing fluid inclusions (FIs) in reservoir sandstones in the Skarv field in the Haltenbanken region offshore Norway recorded a complex oil charge and leakage history. Inclusion oils, hosted in quartz cements, and corresponding adsorbed residual oils on mineral surfaces from the Jurassic Garn and Tilje Formation (Fm) sandstones have been investigated using coupled gas chromatography-mass spectrometry, coupled gas chromatography-isotope ratio mass spectrometry and, as a new technique for FI oil analysis, Fourier transform-ion cyclotron resonance-mass spectrometry. The biomarker, stable carbon isotope and nitrogen, sulfur and oxygen-containing compound results suggest that FI oils from both the Garn and Tilje Fms and adsorbed (Ad) oil from the Tilje Fm were derived from the same source, whereas Ad oil from the Garn Fm shows a lower maturity level and differences in facies indicators. The similar geochemical signals for the FI oils from the Garn and Tilje Fms point to a first charge from the same source rock i.e. the late-Jurassic/earliest-Cretaceous Spekk Fm (Oxfordian to Ryazanian age). The fact that the Ad oil in the Tilje Fm is also similar to the respective FI oil indicates that the Tilje Fm was charged only once. In contrast, differences between the FI and Ad oils in the Garn Fm suggest that first charged oil

---

2 This chapter has been published as: Han, Y., Noah, M., Lüders, V., Rinna, L., Hartwig A., Skeie J.K., Horsfield, B., Mangelsdorf, K.,2022. Geochemical characteristics of inclusion oils from the Skarv field A segment and their implications for the oil charge and leakage history. Marine and Petroleum Geology, 137, 105506 (postprint), https://doi.org/10.1016/j.marpetgeo.2021.105506.

has leaked and was replenished by a later charge sourced from a spatially different and less mature kitchen area of the Spekk Fm.

Keywords: Oil charge and leakage; biomarkers; NSO-compounds; Garn and Tilje Formations; Skarv field A segment

3.2 Introduction

Petroleum reservoirs have frequently undergone a complex oil charge and/or leakage history, which is not always evident from the present reservoir oil composition alone. Oil-bearing fluid inclusions (FIs) in the authigenic mineral cements of reservoir rocks can provide valuable insights into the early oil filling history of reservoirs over geological time (Horsfield and McLimans, 1984; Bodnar, 1990; Karlsen et al., 1993; Lisk et al., 1996; George et al., 1997a, 2004a; Volk and George, 2019). Moreover, subsequent events affecting the reservoir such as leakage, water-washing, biodegradation and contamination associated with drilling do not affect the original oil composition of the FIs. Thus, many case studies have been conducted to utilize compositional differences between inclusion oil, adsorbed oil on mineral surface and/or free reservoir oil to reconstruct the filling history of petroleum reservoirs (Karlsen et al., 1993, 2004; Wilhelms et al., 1996; Schwark et al., 1997; George et al., 1998; Pan et al., 2003; Cao et al., 2006; Volk and George, 2019). For instance, Karlsen et al. (1993) found that there were marked compositional differences between FI oils (hosted by quartz, feldspar and albite) and the oil presently in the North Sea Ula oil field, thus revealing a multiple charge history. George et al. (1998) indicated that initially charged oil in the Lower Cretaceous Barrow Group (Australia) was derived from a less mature, more calcareous source rock, deposited under more reducing conditions in contrast to the current reservoir oil. Additionally, biodegraded FI oil in contrast to non-biodegraded reservoir oil (Volk et al., 2005a) or non-biodegraded FI oil in contrast to biodegraded reservoir oil (George et al., 1998) were used to elaborate oil charge history.

The bulk composition of FI oils has previously been analyzed using gas chromatography with a flame ionization detector (GC-FID) (Horsfield and McLimans,

1984), coupled gas chromatography-mass spectrometry (GC-MS) (Karlsen et al., 1993; George et al., 1997a) and high-performance liquid chromatography (HPLC) (Pang et al., 1998). Indeed, GC-MS, alongside gas chromatography-isotope ratio monitoring mass spectrometry (GC-IRMS), were the main tools applied in the current study, but additionally Fourier transform-ion cyclotron resonance-mass spectrometry (FT-ICR-MS) (Noah et al., 2018; Han et al., 2020) was employed to document the composition of high molecular weight hydrocarbons and polar compounds containing nitrogen, sulfur and oxygen (NSO) atoms.

Authigenic cements including quartz, carbonate, albite and feldspar, of which especially quartz commonly bears oil FIs, have been widely reported in Jurassic sandstones of the Haltenbanken area offshore Norway (Ehrenberg, 1990; Robinson and Gluyas, 1992; Karlsen et al., 1993; Nedkvitne et al., 1993; Karlsen et al., 1995, 2004, 2006). The dissolution of quartz, during stylolite formation and to a lesser extent at grain contacts, is regarded as the most important source of quartz cements in this area (Walderhaug, 1990, 1994). Aliquots of oil are trapped within cavities during crystal growth as primary FIs or during recrystallization of secondary cracks in the presence of a fluid phase, and in the Haltenbanken area oil FIs mostly are located at the boundaries between quartz clasts and quartz overgrowths (Roedder, 1984; Walderhaug, 1990). The occurrence of oil FIs that formed during precipitation of quartz cement can help to shed light on oil charges emplaced in the early stages of reservoir filling. In that regard, Karlsen et al. (2004, 2006) examined the roles of faults and overpressure in the Halten Terrace area of Mid-Norway, but equivalent geochemical data for oil and gas fields in the more northerly part of Mid-Norway, such as the Skarv field of Haltenbanken, is sparse, meaning a full understanding of the generation, migration and alteration history is lacking.

In the study presented here, FI oils hosted by quartz cements and adsorbed (Ad) oils on mineral surfaces of Jurassic Garn and Tilje Formation (Fm) sandstones have been contrasted in order to elaborate the oil migration and charge history in the Skarv field (A segment). Hydrocarbons and NSO-compounds in FI and Ad oils were analyzed using GC-MS, GC-IRMS as well as FT-ICR-MS and the resulting data

points to complex oil charge and leakage events in the Garn and Tilje Fms.

3.3 Study area and samples

The Skarv field is located on the narrow SW-NE trending Dønna Terrace, which lies between the deeply buried and strongly overpressured Donna Terrace Basin to the west and the hydrostatically pressured shallower Sør High to the east (Fig. 3.1a). The terrace is bounded by the shallow Sør High to the east, and by complex fault zones to the west. The vertical displacement of both fault complexes is on the order of 2000 m, and each consists of faults, ramps and strongly tilted layers. Structurally the Skarv field is divided into several fault segments (segments A, B and C) by NW-SE trending faults and lie at sediment depth between 3300–3700 m (Riis and Wolff, 2020). The Skarv field is separated from the Idun field by a structural saddle (Fig. 3.1b). The Skarv segments produce gas and oil from Lower and Middle Jurassic reservoir sandstone in the Tilje, Ile and Garn Fms with gas/oil ratios of approx. 5,000 Sm^3/Sm^3, while the accumulation in Idun is much drier with a gas/oil ratio of approx. 25,000 Sm^3/Sm^3, suggesting either a strong fractionation of the hydrocarbon phase or alternatively generation from at least two different source rocks. The Spekk, Melke and Åre Fms are regarded as likely source rocks (Fig. 3.1c) in the region.

Twenty-three sandstone reservoir samples from two closely located wells separated by a distance of around several hundred meters in the Skarv field A segment were collected and checked for FIs using microscopy. Among all samples five contained sufficient amounts of oil FIs. Three of them (named G1, G2 and G3) are from the Garn Fm (Well 6507/5-1 middle Jurassic) and two of them (named T1 and T2) from Tilje Fm (Well 6507/5-A-4 H lower Jurassic) (Fig. 3.1b and Table 3.1). These samples comprised well-sorted, medium to coarse grain sandstones, with abundant oil FIs observed in the overgrowth zones, healed fractures or quartz trails (Fig. 3.2). After coarsely crushing these five samples and picking the quartz crystal fragments containing oil FIs, Ad oils on outer mineral surfaces were collected using solvent extraction. Finally, FI extracts were obtained after grinding the picked quartz crystals. Thus, for each sample two subsamples were obtained: a FI and an Ad oil

sample. The rigorous cleaning and separation procedures required to ensure FI-extract integrity are presented in detail in the following section.

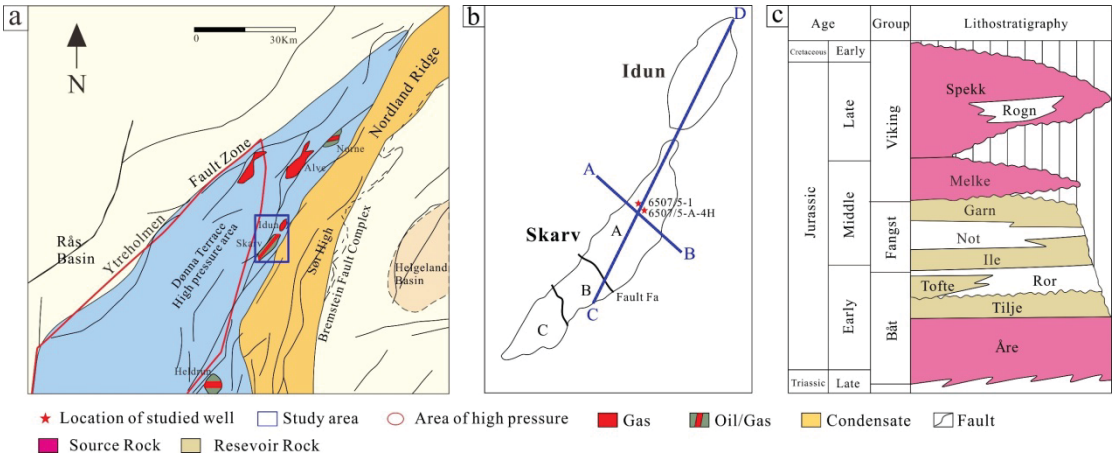

Figure 3.1. a) Structural map of the Skarv field study area (revised from Karlsen et al., 2004); b) map of Skarv and Idun field, including the positions of the studied wells 6507/5-1 and 6507/5-A-4 H. Blue line A-B is the seismic cross section in Figure 3.10a, and C-D in Figure 3.10b; c) Stratigraphic column of source rocks and reservoir rocks in the Jurassic Skarv area (revised from Karlsen et al., 2004). Source rocks are represented by coals from the terrestrial Åre Fm as well as marine shales in the Melke and Spekk Fms. Reservoir rocks are presented in the Garn, Ile, Tofte and Tilje Fms.

3.4 Analytical Methods

3.4.1 Sample preparation

Reservoir sandstones were coarsely broken with a hammer into smaller pieces since they were only poorly cemented. Afterwards the samples were extracted using Soxhlet extraction for 24 h with 250 mL dichloromethane (DCM) and methanol (99:1, v/v) at 50 °C to obtain the residual reservoir petroleum adsorbed on the mineral surfaces (termed as adsorbed or residual oil, Ad oil).

The extracted Ad oil was separated into two parts: one for GC-MS and GC-IRMS analysis and the other one for FT-ICR-MS analysis. The aliquot for the GC-MS and GC-IRMS measurement underwent asphaltene precipitation to obtain the *n*-hexane soluble maltene fraction. Subsequently, the maltenes were further separated

into aliphatic, aromatic and NSO-compounds containing fractions using a medium pressure liquid chromatography (MPLC) system (Radke et al., 1980) and finally, the fractions were measured with GC-MS and GC-IRMS. The aliquot of total extract for the FT-ICR-MS was measured directly.

3.4.2 Clean-up procedure and extraction of FI oils

After the Soxhlet extraction of the sandstone, quartz grains were picked, while fine minerals were discarded. Selected quartz particles were cleaned using the rigorous clean-up protocols developed by Han et al. (2020), which is suitable for both GC-MS and FT-ICR-MS analyses. The clean-up steps were slightly adjusted, as follows. Host minerals were washed with a Waller solution containing 33% sodium dithionite, 28% sodium bicarbonate, 59% sodium citrate in distilled water. Then host minerals were transferred into a Soxhlet extraction tube and washed twice (24h) with 250 mL DCM mixed with methanol (99:1, v/v) at 50 °C. Afterwards, the minerals were washed with three different organic solvents in the following order: methanol, blend of dichloromethane (DCM) and methanol (93:7, v/v), and DCM. The DCM extract from the last cleaning step was collected and residual particles were removed using a pre-cleaned thimble. This DCM extract was used as procedural blank for the respective sample.

Before continuing, the procedural blanks were measured by GC-MS and FT-ICR-MS and controlled for the amounts of remaining contaminants. The washing procedure was repeated until cleaning of the outer mineral surfaces was successful. Afterwards the cleaned quartz crystals were crushed in a small metal cylinder with two stainless steel balls, and finally, the FI oil in the powdered sample was extracted by a mixture of DCM and methanol (99:1, v/v) using Soxhlet extraction. Due to the overall low extraction yields (Table 3.1), the FI oils were directly measured by GC-MS and FT-ICR-MS without any further column fractionation (MPLC). The *n*-alkane abundance in the FIs was not sufficient to obtain reliable compound specific carbon isotope composition data.

3.4.3 Microscopic analysis

Doubly polished thin sections of the fracture filling minerals were studied for oil inclusion content using a BX50 Olympus microscope with various objectives (5×, 10×, 20×, 50×) connected to UV light source.

3.4.4 GC-MS

The aliphatic and aromatic hydrocarbon fractions obtained after MPLC fractionation of the Ad oils, the non-separated FI oils and procedural blanks were analyzed using a Trace GC Ultra coupled to a DSQ mass spectrometer (Thermo Electron Corp.). The GC was equipped with a Thermo PTV injection system and a SGE BPX5 fused silica capillary column (50 m × 0.22 mm ID and 0.25 µm film thickness). Helium was used as a carrier gas. The GC oven was programmed from 50 °C to 310 °C at a rate of 3 °C min^{-1}, followed by an isothermal phase of 30 min. The injector temperature was programmed from 50 to 300 °C at a rate of 10 °C s^{-1}. The MS was operated in electron impact ionization mode (EI) at 70 eV. Full scan mass spectra for compound identification were recorded from *m/z* 50 to 600 Da for the aliphatic fraction, and from 50 to 330 Da for the aromatic fraction at a scan rate of 2.5 scans s^{-1}. In addition to the full scan mode, aliphatic fractions were also measured in the SIM (single ion monitoring) mode to improve the sensitivity for specific biomarkers such as hopanes (*m/z* 191) and steranes (*m/z* 217).

3.4.5 FT-ICR-MS

Samples were measured using a 12 Tesla Solarix FT-ICR-MS from Bruker Daltonik GmbH (Bremen, Germany) in the atmospheric pressure photoionization (APPI) positive (+) mode. A solution of the extract with a concentration of 1 mg/mL in a mixture of methanol and hexane (9:1, v/v) was diluted with the same solvent mixture to give a final concentration of 20 µg/mL. The solutions were injected into the APPI source at a flow rate of 20 µL/h using a syringe pump (Hamilton). The analytes were ionized using a krypton lamb at 10.6 eV. The instrumental parameters for the APPI (+) mode were as follows: dry gas (N_2) flow rate 3 L min^{-1} and temperature 210 °C, nebulizing gas (N_2) 2.3 bar, capillary voltage 1000 V, additional

collision-induced dissociation voltage of 30 V, ions accumulation time 0.03 s, transfer time 1 ms and 4 megaword data sets. A total of 300 mass spectra were accumulated in a mass range from *m/z* 147 to 1200.

In each spectrum, signals with a signal-to-noise ratio ≥ 8 were included into the further data assessment. Formula assignment was done using the isotopes ^{1}H, ^{12}C, ^{13}C, ^{14}N, ^{16}O and ^{32}S, with the upper thresholds N ≤ 2, O ≤ 8, and S ≤ 2 in APPI (+) mode; C and H were unlimited. If no chemical formula within the allowed mass error of 0.5 ppm was found, the peak was not included into the mass/formula list. For each $C_cH_hN_nO_oS_s$ compound, its double bond equivalent (DBE) value was obtained by calculating DBE=c – h/2 + n/2 + 1, where c is the number of carbon, h of hydrogen and n of nitrogen atoms. DBE refers to the number of unsaturation or rings in the individual compound structure (Poetz et al., 2014).

3.4.6 GC-IRMS

Stable carbon isotope of *n*-alkanes was performed using an Agilent Technology 6890 GC coupled to a MAT 253 isotope ratio mass spectrometer (Thermo Fisher Scientific) via a combustion interface (GC-C/TC III, Thermo Fisher Scientific). Combustion was completed in a microvolume ceramic tube with CuO/Ni/Pt wires at 940 °C. Pyrolysis was performed in a microvolume ceramic tube at 1440 °C. The GC was equipped with a HP Ultra 1 column (50 m × 0.2 mm i.d., 0.33 µm film thickness). The temperature program started at 40 °C for 2 min and was then increased to 300 °C at 4 °C min^{-1} and held for 45 min. The injector was held at variable split ratios (splitless to split 1:50) and an initial temperature of 230 °C. During injection, the injector was heated to 300 °C at a rate of 700 °C min^{-1} and held at this temperature for the rest of the analysis time. $\delta^{13}C$ measurements of individual hydrocarbons are given in the delta notation relative to the Pee Dee Belemnite (PDB) standard. The quality of $\delta^{13}C$ determinations was checked by regular measurements of certified standards containing mixtures of *n*-alkanes (Chiron, Norway and A. Schimmelmann, Indiana University, USA). Standard deviations of triplicate measurements for $\delta^{13}C$ signatures were ≤ 0.5‰.

3.5 Results

3.5.1 Microscopic characterization of oil FIs

Oil FIs hosted in quartz were studied using microscopy with both transmitted and UV light (Fig. 3.2). Multiple types of oil FIs are commonly observed as trails and/or growth zones (Figs. 3.2a and 3.2g) in the studied samples. Oil FIs typically are mono-phase (only oil or bitumen) and two-phase (vapor and oil). The inclusions have ellipsoidal to irregular shapes and their sizes mostly range from 10 to 50 μm. Rarely, bigger inclusions with a length up to 100 μm were observed (Fig. 3.2i). The size of the gas bubble in the oil FIs can reflect the GOR (gas to oil ratio) of the trapped petroleum fluid (Bodnar, 1990; Karlsen et al., 2004). The oil FIs in sample T1 (Figs. 3.2i and 3.2l) represent low to medium GOR oils based on small gas bubble volumes. Besides oil FIs, abundant aqueous FIs are contained in sample G1. They commonly are arranged in secondary trails cross-cutting the quartz sample or occur in FI assemblages. Furthermore, some isolated inclusions that exhibit negative crystal shape were observed as well (Fig. 3.2f). Oil FIs in samples from the Garn and Tilje Fms show yellow fluorescence under UV light, while the Ad oils show pale blue fluorescence (Fig. 3.2).

Interestingly, asphaltene-rich residues with yellow fluorescence were observed in intergranular pores and quartz surfaces of sample G1 (Figs. 3.2c and 3.2e), but are not present in sample T1. The pale blue fluorescence points to low density of the Ad oils in the Garn and Tilje Fms, reflecting high API gravity (around 45°). In contrast, the yellow fluorescence of the FI oils in both Fms, reflects low API gravity (20°–30°) (Burruss, 2003). The low API gravity of the FI oils might be attributed to intense preferential adsorption of higher molecular-weight hydrocarbons onto mineral surfaces, which are finally captured in the FIs (George et al., 1998; Pang et al., 1998).

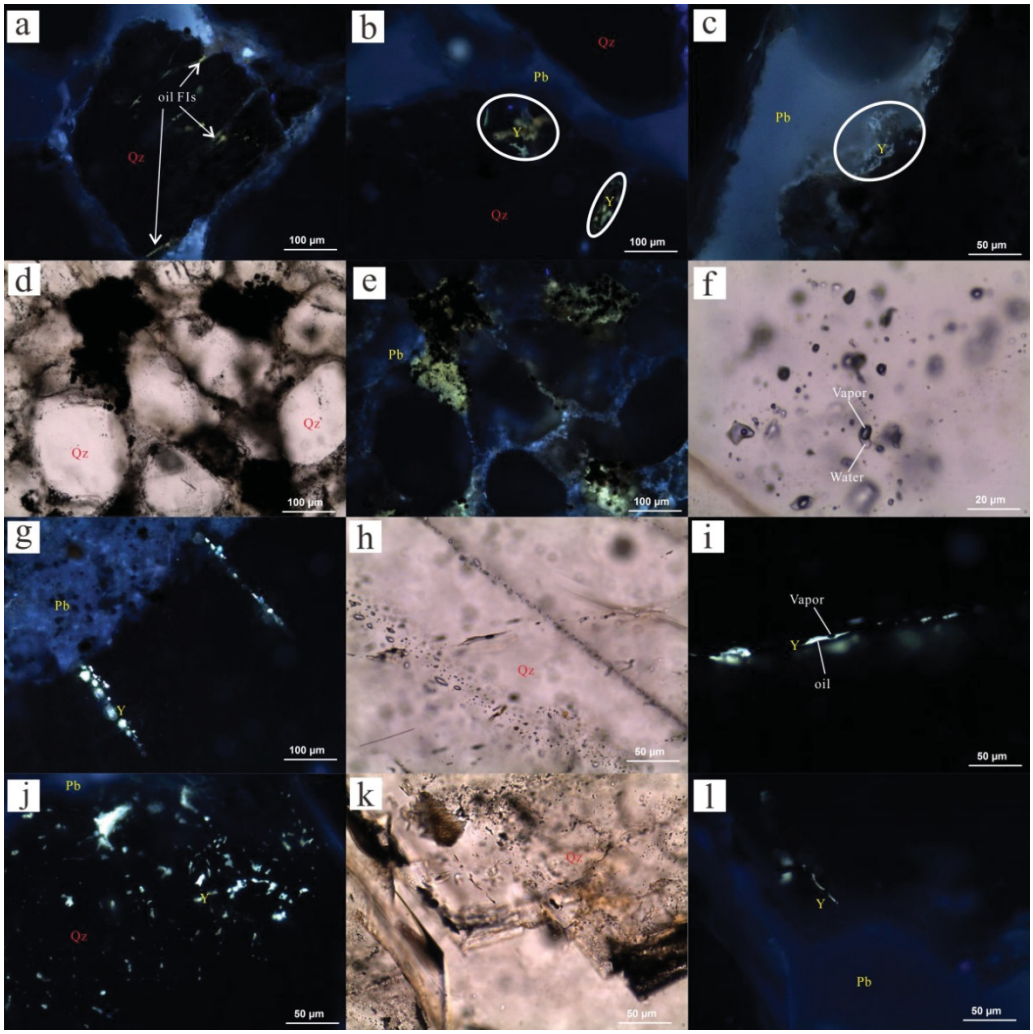

Figure 3.2. Photomicrographs of oil FIs from the Garn (a, b, c, d, e and f) and Tilje (g, h, i, j, k and l) Fm. a) Several oil FIs arranged along trails in a quartz crystal of sample G1 show yellow fluorescence under UV light. b) Cluster of oil FIs (marked by white circle) trapped in the growth zone of quartz (sample G1) showing yellow fluorescence under UV light, and pale blue fluorescence of oil adsorbed on clay minerals. c) Bitumen adsorbed on the surface of quartz (marked by white circle) showing yellowish fluorescence under UV light, and pale blue fluorescence of oil adsorbed on clay minerals. d) Asphaltene-rich residues trapped in intergranular pores of sandstone of sample G1. e) Asphaltene-rich residues in figure 3.2d show yellow fluorescence under UV light, and pale blue fluorescence of oil adsorbed on clay minerals. f) Aqueous FIs in quartz from sample G1 under transmitted light, note that the liquid to vapor ratios are highly variable and inclusions can be all-liquid or contain large bubbles. g) Two oil inclusion trails in quartz from sample T1 showing yellow fluorescence under UV light (color in figure cannot reflect real fluorescence color under UV light), and pale blue fluorescence of oil adsorbed

on clay minerals. h) Oil inclusion trail in quartz from sample T1 under transmitted light. i) Same oil FIs in figure 3.2h showing yellow fluorescence under UV light. j) Abundant irregularly-shaped oil FIs trapped in quartz from sample T1 showing yellow fluorescence under UV light. k) Oil FIs trapped in a growth zone in quartz from sample T1. l) Oil FIs from figure 3.2k show yellow fluorescence under UV light and pale blue fluorescence of oil adsorbed on clay minerals. Pl: pale blue; Y: yellow; Qz: quartz.

3.5.2 Extraction yield

High extraction yields ranging from 2179 to 5559 µg/g reservoir rock were recorded for the Ad oils (Table 3.1). Sample G3 shows the highest and sample T1 the lowest extraction yield, while the other samples show intermediate concentrations. In contrast, the yields of the extracted FI oils are much lower, ranging from 18.2 to 41.4 µg/g host mineral. The G1 host minerals show the highest and the T1 host minerals the lowest extraction yields. Aliphatic hydrocarbons are the dominating compound class among the Ad oils ranging from 83% to 95% followed by the NSO-compounds with 4%–16% and the aromatic hydrocarbons varying between 1% and 5%. As mentioned above, the FI oils were not separated into fractions of different polarity because extraction yields were so low.

Table 3.1. Background and compositional information on the selected samples from the Garn (G) and Tilje (T) Fms separated into fluid inclusion samples (FI) and adsorbed (Ad) oil samples from the respective petroleum reservoirs. Due to the low extraction yields FIs were not separated into an aliphatic, aromatic and NSO fraction.

Samples	G1-Ad	G1-FI	G2-Ad	G2-FI	G3-Ad	G3-FI	T1- Ad	T1-FI	T2-Ad	T2-FI
Well	6507/5/1						6507/5-A-4 H			
Depth (m MD)	3422.5		3432.8		3433.3		3684.5		3694.3	
Formation	Garn						Tilje			
Age	Middle Jurassic						Early Jurassic			
Aliphatic (%)	83.0	–	94.8	–	93.3	–	84.8	–	88.8	–
Aromatic (%)	1.3	–	1.4	–	1.1	–	5.0	–	4.3	–
NSO-compounds (%)	15.70	–	3.8	–	5.6	–	10.2	–	7.0	–
Sample weight (g)	27.0	14.5	26.0	9.9	32.0	15.6	32.0	13.2	35.0	20.5
extract weight (mg)	103.0	0.60	136.9	0.26	177.9	0.45	69.7	0.24	123.1	0.68
extract yield (µg/g)	3818	41.3	5267	26.2	5559	28.8	2179	18.1	3516	33.2

Note, –: no data obtained.

3.5.3 Molecular composition

3.5.3.1 n-Alkanes

Significant differences in *n*-alkane distribution patterns can be seen between FI and Ad oils (Fig. 3.3). The *n*-alkane distributions of the Ad oils range between the C_{13} and C_{37}. However, abundant *n*-alkanes essentially range between C_{13} and C_{20} for the Tilje Fm with a maximum at C_{17} and a bit broader between C_{13} and C_{25} for the Garn Fm with a maximum at C_{16}/C_{17}. The *n*-alkane patterns of the Ad oils within the same formations are very similar (Fig. 3.3a).

In contrast, the *n*-alkane patterns of the FI oils are much more different even when derived from the same formation (Fig. 3.3b). The *n*-alkanes in the FI oils from the Garn Fm range between C_{14}/C_{16} and C_{35}/C_{38} and from the Tilje Fm between C_{13}/C_{16} and C_{38}. The distribution of the abundant *n*-alkanes is much broader compared to the Ad oils and the maxima more variable plotting at C_{19}, C_{20} and C_{22} for the Garn Fm and C_{17} and C_{24} for the Tilje Fm. Low molecular weight *n*-alkanes also occur in FI oils (C_{13}–C_{18}), but this part of the fraction surely have been influenced by evaporation during the host mineral crushing procedure. Compared with the respective Ad oils, higher molecular weight *n*-alkanes are enriched in the FI oils, which might reflect preferential adsorption of longer waxy *n*-alkanes on host minerals (Etminan and Hoffmann, 1989; George et al., 1998).

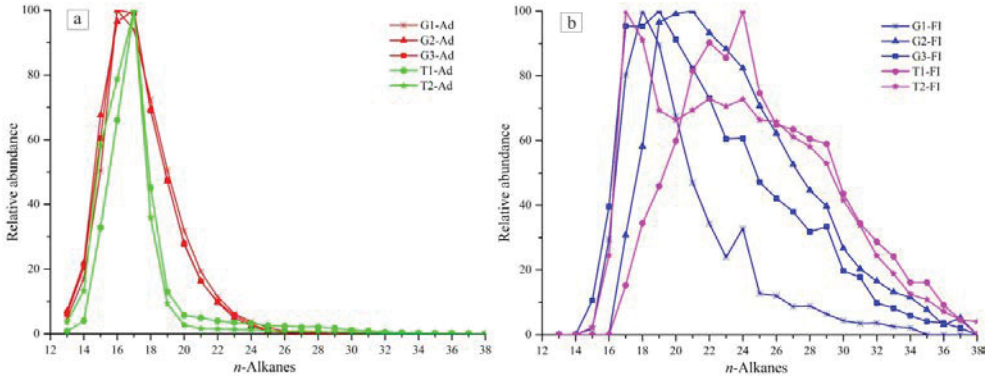

Figure 3.3. a) *n*-Alkane distribution patterns measured by GC-MS of adsorbed (Ad) oils from the Garn (Gx; red) and Tilje Fms (Tx; green) in the Skarv field A segment, Norway. b) *n*-Alkane distribution patterns of fluid inclusion (FI) oils from the Garn (Gx; blue) and Tilje Fms (Tx; magenta).

3.5.3.2 Hopanes and steranes

Hopanes and steranes from the Ad and FI oils were detected in SIM mode by GC-MS (see chromatograms in Fig. 3.4). Ad and FI oils show essentially the same hopane distribution for all samples containing Ts, Tm, 28,30-bisnorhopane (BNH), C_{29} and C_{30} hopanes and $C_{31–35}$ homo-hopanes. C_{29}αβ- and C_{30}αβ-hopanes are the most abundant hopanes in both Ad and FI oils. The presence of significant amounts of gammacerane is indicated in the G1-, G2- and G3-Ad and G1-FI oil samples, while in the other samples only trace amounts were detected.

Additionally, C_{27}–C_{29} steranes and diasteranes were detected in Ad and FI oils. In samples G1, T1 and T2, Ad and FI oils show similar sterane distributions and also the diasteranes look similar. In these samples, the C_{27} steranes are more abundant than the C_{28} and C_{29} steranes, and regular steranes are more abundant than diasteranes. In sample G2 and G3, there are clear differences between Ad and FI oils. In both Ad oils, C_{28} steranes are more abundant than C_{27} steranes and C_{29} steranes, and regular steranes are much more abundant than diasteranes. In contrast to the Ad oils of G2 and G3, the corresponding FI oils show similar steranes and diasteranes distribution again to the Ad and FI oils of G1, T1 and T2.

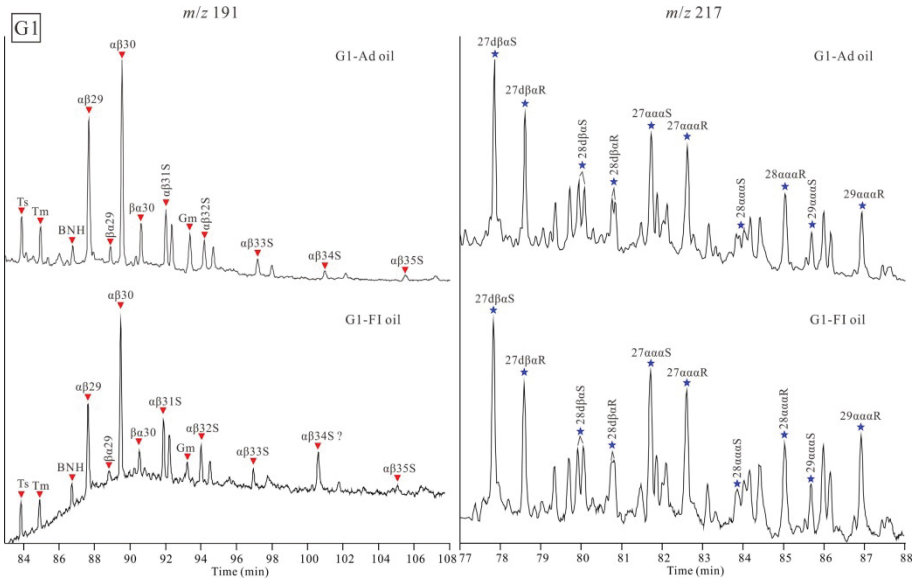

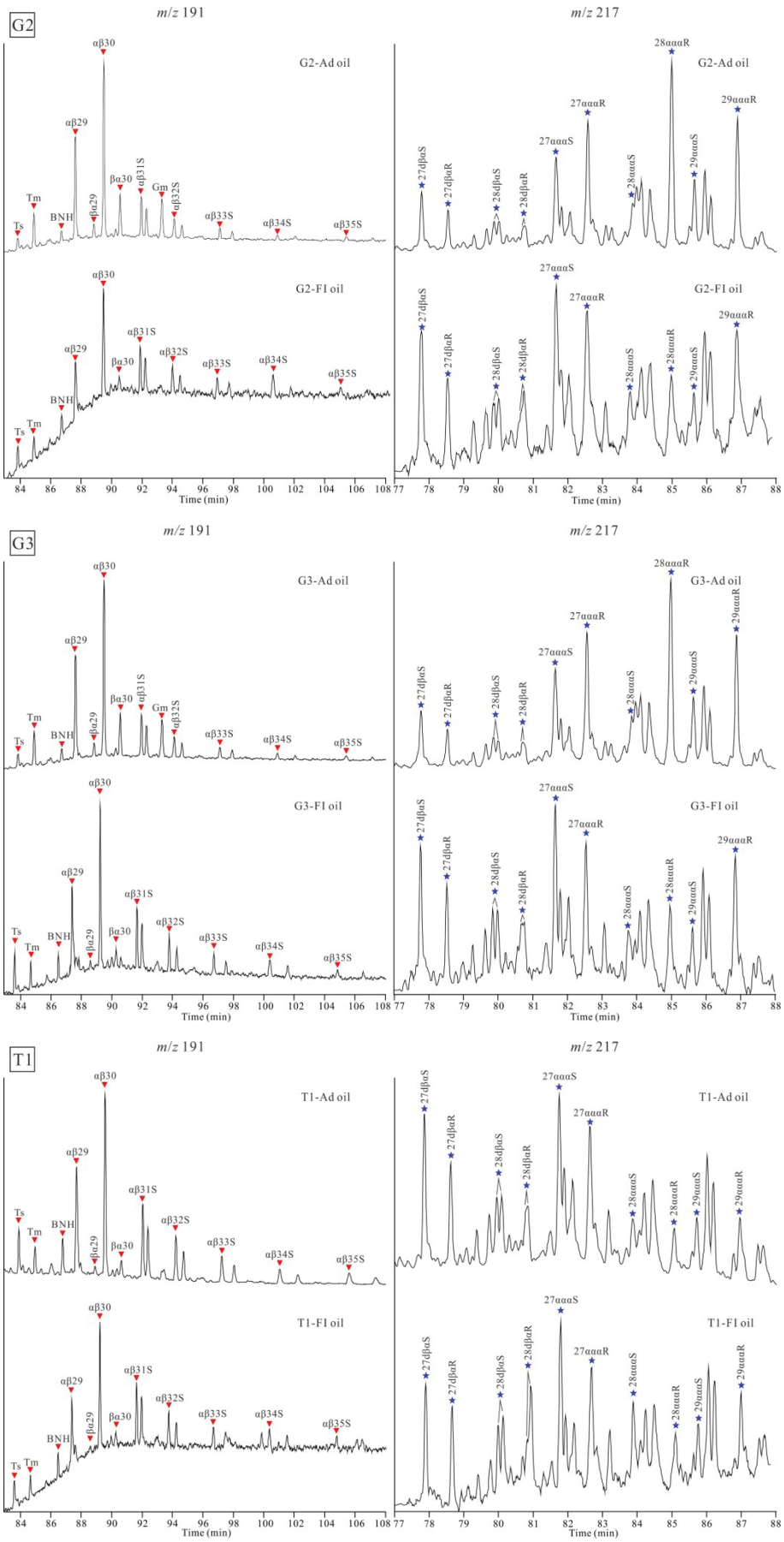
G2
m/z 191
m/z 217
G2-Ad oil
G2-FI oil
αβ30
αβ29
Tm
BNH
βα29
βα30
αβ31S
Gm
αβ32S
αβ33S
αβ34S
αβ35S
Ts
28αααR
27αααR
29αααR
27αααS
27dβαS
27dβαR
28dβαS
28dβαR
28αααS
29αααS
Time (min)
G3
G3-Ad oil
G3-FI oil
T1
T1-Ad oil
T1-FI oil

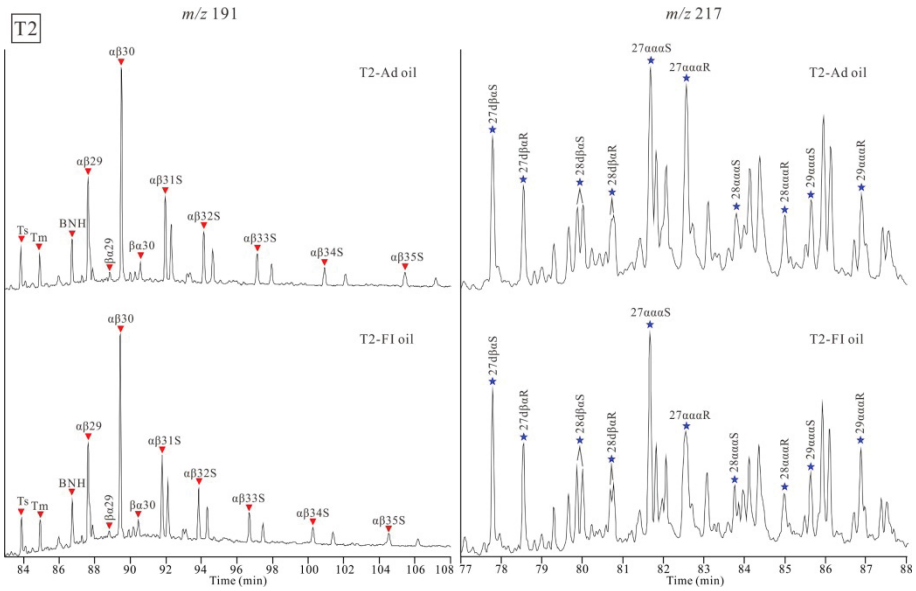

Figure 3.4. Mass trace *m/z* 191 and 217 chromatograms showing the distribution of hopanes, diasteranes and steranes in adsorbed (Ad) and fluid inclusion (FI) oils from the Garn (G1, G2 and G3) and Tilje (T1 and T2) Fms. Ts = 18α-trisnorneohopane; Tm = 17α-trisnorhopane; BNH = 28,30-bisnorhopane; Gm = Gammacerane.

3.5.3.3 Aromatic hydrocarbons

A few aromatic compounds such as phenanthrene, alkylphenanthrenes and alkyldibenzothiophenes, are present in the FI oils, whereas a higher diversity of aromatic hydrocarbons is present in Ad oils such as alkylnaphthalenes, alkylfluorenes and alkylbiphenyls. The different distributions of phenanthrene and methylphenanthrenes in Ad and FI oils are reflected by the variations in the methylphenanthrene index (MPI-1) and calculated reflectance (Rc) pointing to different maturation stages (Radke and Welte, 1983). In the FI oils from the Garn and Tilje Fms the MPI-1 varies between 0.66 and 0.74 and is similar to the values of the Ad oils from the Tilje Fm (MPI-1 = 0.73, 0.74 see Table 3.2). In contrast the maturity of the Ad oils from the Garn Fm is lower (MPI-1 = 0.55–0.63).

Table 3.2. Aliphatic and aromatic hydrocarbon parameters for fluid inclusion (FI) and adsorbed (Ad) oils from the Garn (G) and Tilje (T) Fms.

Sample Name	G1		G2		G3		T1		T2	
	Ad	FI	Ad	FI	Ad	FI	Ad	FI	Ad	FI
Hopanes										
Ts/(Ts + Tm)	0.56	0.55	0.25	0.50	0.28	0.62	0.62	0.56	0.56	0.52
C_{31}αβ-22S/(22S + 22R) hopanes	0.55	0.55	0.58	0.56	0.58	0.54	0.58	0.55	0.59	0.52
C_{29}Ts/C_{29}αβ-hopane	0.15	0.18	0.09	0.22	0.09	0.26	0.23	0.22	0.23	0.27
C_{30}*/C_{30}αβ-hopane	0.05	0.10	0.02	0.09	0.03	0.09	0.07	0.11	0.06	0.09
Gammacerane/C_{30}αβ-hopane	0.24	0.11	0.28	0.03	0.27	0.02	0.03	0.03	0.02	0.02
Moretane/C_{30}αβ-hopane	0.23	0.18	0.24	0.17	0.25	0.15	0.11	0.23	0.11	0.12
28,30-bisnorhopane /C_{30}αβ-hopane	0.10	0.18	0.08	0.21	0.07	0.18	0.20	0.21	0.21	0.24
Steranes/hopanes	0.75	0.44	0.59	0.39	0.57	0.41	0.50	0.28	0.53	0.36
Steranes										
C_{29}ααα-20S/(20S + 20R) steranes	0.36	0.31	0.32	0.30	0.34	0.27	0.46	0.43	0.45	0.43
C_{29}αββ/(αββ + ααα) steranes	0.49	0.50	0.37	0.54	0.40	0.48	0.63	0.60	0.62	0.58
%C_{27} steranes	45	41	31	38	32	39	44	40	44	41
%C_{28} steranes	28	26	36	27	35	25	23	26	24	24
%C_{29} steranes	28	32	33	34	33	36	33	34	32	35
Diasteranes/steranes	1.13	1.02	0.43	0.68	0.38	0.63	0.70	0.66	0.51	0.72
C_{30} sterane index	0.06	0.06	0.06	0.11	0.06	0.13	0.12	0.13	0.11	0.11
Aromatics										
Methylphenanthrene index (MPI-1)	0.63	0.70	0.55	0.72	0.54	0.66	0.74	0.74	0.73	0.72
Calculated vitrinite reflectance, %Rc	0.78	0.82	0.73	0.83	0.73	0.80	0.84	0.84	0.84	0.83
DBT/Ph	0.00	0.37	0.03	0.42	0.07	0.25	0.24	0.28	0.35	0.34

Note: Ts = 18α-trisnorneohopane; Tm = 17α-trisnorhopane; C_{29}Ts = 18α-30-norneohopane; C_{30}* = 17α-diahopane; Moretane = C_{30}βα-hopane; %C_{27} steranes = C_{27}/(C_{27}–C_{29}) steranes; %C_{28} steranes = C_{28}/(C_{27}–C_{29}) steranes; %C_{29} steranes = C_{29}/(C_{27}–C_{29}) steranes; C_{30} sterane index = C_{30}/(C_{27}–C_{30}) steranes; Methylphenanthrene index (MPI-1) = 1.5 × (3MP + 2MP)/(P + 9MP + 1MP); Calculated vitrinite reflectance (%Rc) = 0.6 × MPI-1 + 0.4 (for 0.65% < Ro < 1.35% (Radke and Welte, 1983); DBT/Ph= Dibenzothiophene/phenanthrene.

3.5.3.4 High molecular weight hydrocarbons and NSO-compounds

Based on the similarities deduced from the GC-MS data (G2 is very similar to G3 and T1 to T2) three representative reservoir samples (Ad and FI oils of sample G1, G2 and T1) were selected for APPI (+) FT-ICR-MS analysis. The number of individual signals measured by APPI (+) FT-ICR-MS is strongly different between Ad and corresponding FI oils. In the Ad oils of G1 and G2, 630 and 771 signals were detected, respectively, whereas FI oils show much higher signal numbers for both samples

ranging from 3466 (G1) to 3610 (G2). In the samples from the Tilje Fm the signal numbers are with values of 1027 (T1-Ad) and 4769 (T1-FI) significantly higher. In general, FT-ICR-MS measurements can be well applied to samples that contain a high number of NSO-compounds and broad range of compound classes (Marshall and Rodgers, 2008). However, the Ad oils investigated here are light oil dominated as indicated by the high aliphatic hydrocarbon contents (83%–95%, see Table 3.1) and only bear lower amounts of NSO-compounds (4%–15%). Thus, due to the low number of detected signals in the Ad oils compared to the FI oils, the FT-ICR-MS analysis focuses only on the FI oils. In the following, percentages of the total monoisotopic ion abundance (TMIA) are used to express the relative abundance of compound classes in the FI oils. To assess the level of external contamination of the FI oils during the sample preparation the procedure outlined by Han et al. (2020) is applied to the FI oils. A comparison of the FI oils with the blank results indicates that the O_4 class is highly contaminated and cannot be used for further data evaluation and is therefore excluded.

The outer circle of the FT-ICR-MS pie charts (Fig. 3.5) visualizes the different elemental classes, namely oxygen (O_x), nitrogen (N_y), nitrogen-oxygen (N_yO_x), sulfur (S_z), sulfur-oxygen (S_zO_x) containing compounds and hydrocarbons (HCs). Although with some proportional variations all three FI samples are dominated by O_x, N_y, N_yO_x, and HCs. These four elemental classes make up 91.1%–96.5% of the detected compounds. In sample G1-FI the N_yO_x compounds (36.4% TMIA) are the most abundant class followed by O_x (26.4% TMIA), N_y (25.5% TMIA) and HC (8.2% TMIA) classes. In sample G2-FI the O_x (40.1% TMIA) class dominates followed by N_yO_x (36.4% TMIA), HC (17.3% TMIA) and N_y (10% TMIA) classes and in sample T1-FI the most abundant class are again the O_x (32.9% TMIA) compounds followed by N_yO_x (27.2% TMIA), N_y (18.3% TMIA) and HC (12.8% TMIA) classes. The inner circle provides additional information on compounds with different numbers of hetero-atoms in the respective compound class. Some variations especially between G1-FI and the other samples is visual for the N_1O_1 compound abundance and the G2-FI sample appears to have a higher relative proportion of O_1 compounds.

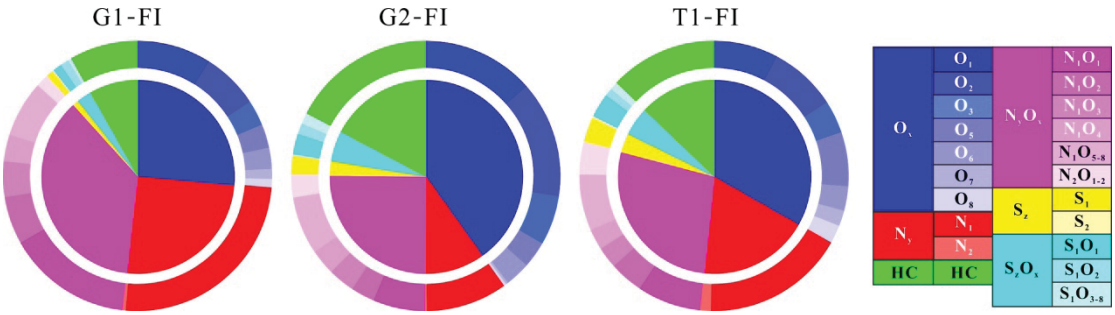

Figure 3.5. Pie chart of elemental and compound class distributions in inclusion (FI) oils from the Garn (G1 and G2) and Tilje (T1) Fms. O_x = Compound class containing x oxygen atoms; HC = Hydrocarbon; N_y = Compound class containing y nitrogen atoms; N_yO_x = Compound class containing y nitrogen and x oxygen atoms; S_z = Compound class containing z sulfur atoms; S_zO_x = Compound class containing z sulfur and x oxygen atoms.

FT-ICR-MS measurements with Electrospray Ionization in negative mode (ESI (–)) have also been applied. The ESI (–) mode is more prone to detect acidic compounds, while the APPI (+) mode mainly detects aromatic compounds of low-polarity. Compared to the APPI-data the ESI-data show a significant lower number of compounds and compound class variations. For instance, acidic nitrogen compounds, often used to access organic matter maturation (Hughey et al., 2004; Poetz et al., 2014), are essentially absent. Thus, since there is no additional information from the ESI (–) measurements, we present only the APPI (+) data here.

3.5.3.5 Stable carbon isotope of n-alkanes in Ad oils

Due to the low extraction yield of the FI oils, stable carbon isotope compositions of *n*-alkanes were only measured in selected Ad oils (sample G1, G2 and T1). Stable carbon isotopic composition for *n*-alkanes is a useful tool for oil-source correlation, since *n*-alkane carbon isotope signatures of oil is primarily controlled by the source rock depositional setting (Bjorøy et al., 1994; Murray et al., 1994). The isotopic ratios for the C_{14}–C_{28} *n*-alkanes in samples G1-Ad and G2-Ad range from −27.9‰ to −31.8‰ and from −27.3‰ to −32.5‰, respectively. The similar carbon isotope pattern of the individual *n*-alkanes clearly indicates that the Ad oils in sample G1 and G2 originated from a similar source (Fig. 3.6). In contrast, the Ad oil obtained from Tilje Fm (T1) shows a quite different carbon isotope distribution for the C_{16}–C_{32} *n*-alkanes in the

range between −26.9‰ to −35.1‰. Especially in the C_{16}–C_{23} range the *n*-alkanes are significantly depleted in ^{13}C relative to the Garn samples (Fig. 3.6). Thus, the different *n*-alkane profiles in the Ad oils from the Garn and Tilje Fms are considered to indicate different sources with different depositional characteristics.

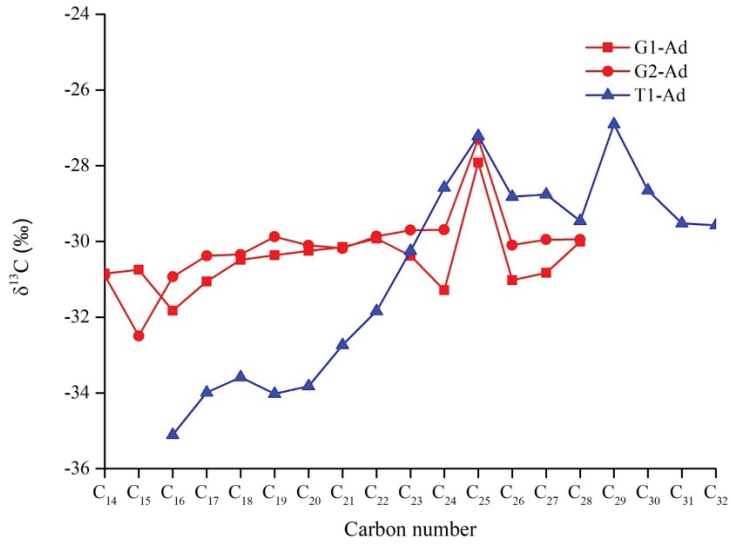

Figure 3.6. Carbon isotopic signatures of *n*-alkanes in the adsorbed (Ad) oils from the Garn (G1 and G2) and Tilje (T1) Fms.

3.6 Discussion

3.6.1 Sources of FI oils compared to reservoir Ad oils

Three potential Jurassic source rocks are present in the Haltenbanken region, namely the marine dominated Spekk and Melke Fms and the terrestrial dominated Åre Fm (Cohen and Dunn, 1987; Karlsen et al., 1995, 2004). The presence of C_{30} 4-desmethylsteranes, the sterane distributions with a dominance of C_{27} steranes and the steranes/hopanes ratio (Table 3.2) in both the Ad and FI oils from the Garn and Tilje Fms clearly implies the input of marine organic matter to the source rock (Peters et al., 2005). Therefore, the coaly Åre Fm dominated by C_{29} steranes (Karlsen et al., 2004) cannot be the source of the oils in the Garn and Tilje Fms here. The occurrence of BNH is common in reservoir oils of the North Sea sourced by the Spekk Fm, providing another indication that the Ad and FI oils in the Garn and Tilje Fms originated from the Spekk Fm as well (Grantham et al., 1980; Karlsen et al., 1995).

The Melke Fm also has petroleum generation potential in other Norwegian Sea petroleum systems, however it is less efficient compared with the Spekk Fm in the Haltenbanken region (Heum et al., 1986; Karlsen et al., 2004), because Heum et al. (1986) reported that the Melke Fm does not release more than 1.5 kg of petroleum/t rock, while the release of petroleum from the Spekk Fm was estimated as 30–35 kg of petroleum/t rock. Considering that the Spekk Fm is the most prolific source rock in this area, it is the most likely that the Spekk Fm is the petroleum source rock for the oils in the Garn and Tilje Fms.

Despite of some smaller variations, the biomarker distribution of the source parameters within the group of Ad and FI oils in the Garn Fm looks quite similar, but very different when comparing both groups (Fig. 3.7a). In contrast, in the Tilje Fm the source related parameters look more similar between the Ad and FI oils and they are also quite similar to the FI oils of the Garn Fm (Figs. 3.7a and 3.7b). This implies that the FI oils from the Garn and Tilje Fms as well as the Ad oil from the Tilje Fm were derived from a similar kitchen area of the Spekk Fm, and that the Ad oil from the Garn Fm was derived from another source area of the Spekk Fm, which reflects somehow different depositional conditions.

The source difference of the Ad and FI oils in Garn Fm is for instance clearly indicated by the gammacerane index, which is highly specific for water-column stratification (commonly due to hypersalinity) during source rock deposition (Sinninghe Damsté et al., 1995). Higher gammacerane values point to increased water salinity during time of deposition. In the Ad and FI oils from the Tilje Fm and the FI oils from the Garn Fm, the gammacerane index is usually very low (0.02–0.03). Only the G1-FI oil shows a slightly increased index value (0.11). In contrast, in the Ad oils from the Garn Fm the gammacerane index is significantly higher (0.24–0.28) (Table 3.2, Fig 3.7a). This indicates that the Ad oils from the Garn Fm derived from a source rock interval deposited under higher water salinity conditions than the FI oils from the Garn and Tilje Fms as well as the Ad oils of the Tilje Fm. Thus, it is most conceivable that the discrepancies between the source related biomarker parameters of the Ad and FI oils in the Garn Fm were derived from different oil charges originated from

spatially different kitchen areas in the Spekk Fm (Xu, 2003), which may include some sub-basins deposited under higher water salinities. In the Gyda Field in the southern Norwegian section of the North Sea, Pedersen et al. (2006) reported about DST-oil (well 2/2-5 oil) sourced from hypersaline facies from the Viking group (a formation equivalent to the Spekk Fm) of Upper Jurassic age. They proposed that these source rocks were formed in two possible ways (Pedersen et al., 2006): 1) influenced by saline runoff from exposed Permian salt diapirs, they may have accumulated in lagoons along the Upper Jurassic coastline or 2) they may have formed under the impact of hypersaline seafloor conditions caused by heavy, saline water blanketing the seafloor, overlain by normal marine water. In our study area the Haltenbanken region there are also salt induced structures that were believed to have formed over the Triassic salt during the Late Jurassic (Jackson & Hastings, 1986; Karlsen et al., 1995). These salt structures, which commonly formed parallel to basement faults, developed along rim synclines of the Melke Fm and perhaps also Spekk Fm (Jackson & Hastings, 1986). Thus, such runoff scenarios of salt diapirs can also be proposed as a model for the formation of sub-basins in the Spekk Fm impacted by hypersaline and reducing conditions in the Haltenbanken region.

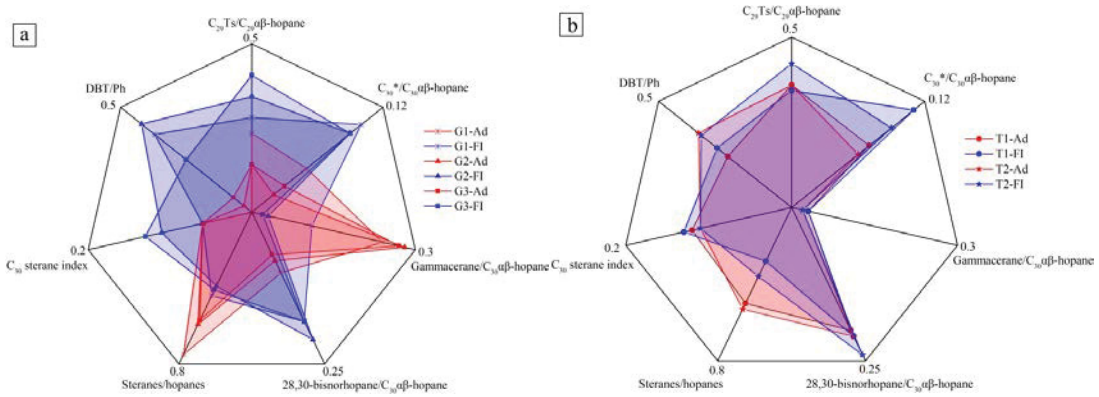

Figure 3.7. Spider diagrams showing the variation in source related biomarker parameters in adsorbed oils (Ad) and inclusion oils (FI) from the a) Garn and b) Tilje Fms. For explanation of the abbreviations see Table 3.2. The parameters are scaled from 0 to the value on the axis.

The source difference indicated by the biomarkers between the Ad oils in Garn and Tilje Fms can be confirmed by the stable carbon isotopic compositions of *n*-alkanes shown in figure 3.6. Moreover, the Ad oil of sample G1 seems to be slightly

different in some parameters (e.g., C_{29}Ts/C_{29}αβ-hopane and diasteranes/steranes) from those of G2- and G3-Ad oils. The microscopic analysis reveals for the G1-Ad oil an abundant pale blue fluorescence, however additionally asphaltene-rich residues with yellow fluorescence are present in the intergranular pores (Fig. 3.2e). These residues were not observed in samples G2 and G3. Thus, the extract of the reservoir rock G1 might contain both adsorbed oil and bitumen from these asphaltene-rich residues, which might represent remains from an initial petroleum charge. This bitumen mixture might be the reason for some different biomarker parameters between the G1- and G2- as well as G3-Ad oil samples (Fig. 3.7 and Table 3.2). However, although there are some differences presumably caused by the asphaltene-rich residues, overall the G1-Ad oil is still quite similar to the Ad oil composition in samples G2 and G3. This similarity is supported by the *n*-alkane carbon isotopic signatures of the G1- and G2-Ad oil samples (Fig. 3.6).

3.6.2 Maturity of FI oils compared to Ad oils

The main maturity related parameters are shown in Table 3.2 and Figure 3.8. In the Garn Fm all oils are beyond the early oil generation window, as the homo-hopane ratios (e.g., C_{31}αβ-22S/(22S + 22R) hopanes) have reached equilibrium. Other hopane and sterane maturity parameters e.g., Ts/(Ts + Tm), diasterane/steranes, Moretane/C_{30}αβ-hopane and C_{29}ααβ/(ααβ + ααα) steranes of samples G2 and G3 clearly indicate that the Ad oils are less mature than the corresponding FI oils (Fig. 3.8a). Another parameter, the C_{29}ααα-20S/(20S + 20R) maturity ratio, is equivocal and give conflicting information which may be due to the difference of depositional environment of the source rock of Ad and FI oils outlined above. In general, the distribution pattern of aromatic hydrocarbons changes with an increasing degree of maturation (Radke and Welte, 1983). Consistent with most of the sterane and hopane derived maturity parameters, in our samples the phenanthrene maturity ratios, e.g., MPI-1 and Rc, also suggest that G2 and G3 Ad oils are less mature (G2-Ad 0.73 %Rc and G3-Ad 0.73 %Rc) than the corresponding FI oils (G2-FI 0.80 %Rc and G3-FI 0.83 %Rc). The Rc value of the G1-Ad oil (0.78 %Rc) is slightly higher than for the G2- and G3-Ad oils but still lower than the corresponding FI oils (0.82 %Rc). As

discussed before, G1-Ad oil represents presumably a mixture of bitumen from an initial and later oil charge, which could also explain the discrepancies in the maturity parameters when compared to the G2- and G3-Ad oils (Fig. 3.8a and Table 3.2). In conclusion, the majority of the maturity indicators in the samples from the Garn Fm indicate that the Ad oils G1, G2 and G3 are less mature compared to their corresponding FI oils.

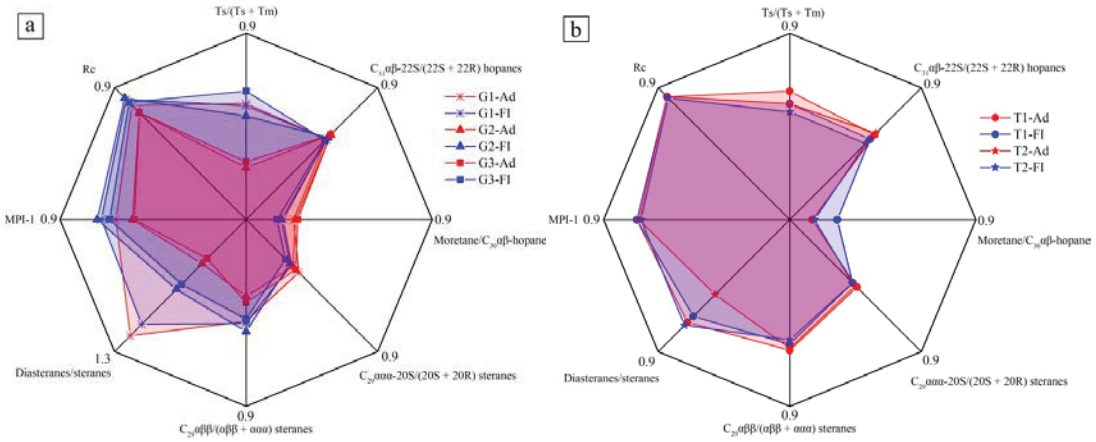

Figure 3.8. Spider diagrams showing the variation in maturity related parameters in adsorbed oils (Ad) and inclusion oils (FI) from the a) Garn and b) Tilje Fms. For explanation of the abbreviations see Table 3.2. The parameters are scaled from 0 to the value on the axis.

However, in contrast to Garn Fm samples, Ad and FI oils from the Tilje Fm originate from a source rock deposited under similar marine environmental conditions (Fig. 3.7b). This implies that the maturity related parameters in Tilje Fm are less affected by varying depositional environments. Except of two smaller deviations (diasteranes/steranes of T2-Ad and moretane/C_{30}αβ-hopane of T1-FI), most of the maturity related biomarker ratios are similar for the Ad and FI oils from the Tilje Fm (Fig. 3.8b) indicating a similar maturation stage for these oils.

The maturity parameters of the Ad and FI oils from Tilje Fm are also quite similar to the FI oils from the Garn Fm (Figs. 3.8a and 3.8b). The Rc values of the FI oils from Garn Fm (0.80–0.83 %Rc) are in the same range to those in the FI and Ad oils from the Tilje Fm (0.83–0.84 %Rc). In contrast the Ad oils from the Garn Fm (0.73–0.78 %Rc) are, as discussed above, of lower maturity (Table 3.2). The

differences in the maturation stage between the Ad oils from the Garn Fm to the other oil types confirm the different origin of the Garn Ad oils as suggested from the source assessment and carbon isotope distributions of *n*-alkanes (Figs. 3.6 and 3.7a).

3.6.3 Similarities of FI oils from Garn and Tilje Fms revealed by FT-ICR-MS

The source and maturity assessments based on biomarker parameters clearly indicate (Figs. 3.7 and 3.8), that FI oils from Garn and Tilje Fms were derived from a similar source. The FT data also indicate similar dominating component classes for the three FI samples G1, G2 and T1. However, the measurements also show variable abundances between these compound classes, which might on a first view contradict the biomarker results. Due to their higher polarity NSO-compounds interact more pronouncedly with the lithological matrix, and thus are much more affected by retention on mineral surfaces, water washing, biodegradation and fractionation during migration (Dubey and Waxman, 1991; Larter and Aplin, 1995). Therefore, variations in the relative abundance of different compound classes might be expected when comparing different inclusion oils from different reservoirs units. Such compound heterogeneities even within the same reservoir are indicated when comparing the two Garn FI oils (G1 and G2, Fig. 3.5). Thus, quantitative assessments are less indicative than qualitative evaluation. To assess the qualitative composition of the NSO-compounds in the FI oils, van Krevelen diagrams have been prepared plotting the hydrogen/carbon (H/C) ratio against different elemental contents (H, N, S, and/or O) normalized on the carbon content (Fig. 3.9) (Kim et al., 2003; Rodgers and Marshall, 2007; Marshall and Rodgers, 2008). Plots of these ratios have been previously used to determine biodegradation levels, asphaltene evolution and crude oil comparison (Kim et al., 2005; Klein et al., 2006; Rodgers and Marshall, 2007). The H/C value represents the aliphatic character of the detected compounds while the N or O to C ratios indicate the relative proportion of the respective heteroatoms with regard to the molecular carbon structure. Within the plot different numbers of hetero-atoms are color-coded.

For the $O_{1–3}$ classes in the FI oils from Garn Fm (G1-FI and G2-FI) and Tilje Fm (T1-FI) most of the signals are located in an area constrained by H/C ratios between 0.6 and 2.1 and O/C ratios between 0 and 0.2 (Fig. 3.9a). From the data distribution it is obvious that there are large similarities among the $O_{1–3}$ classes for the three FI oils. Although the overall distribution of the N_1 compounds look also fairly similar, a closer look shows that the N/C ratio is slightly lower in the T1-FI oil indicating a lower abundance of N_1 compounds with shorter carbon chain length than in the FI oils from the Garn Fm (Fig. 3.9b). For the N_1O_1 compounds the overall distribution is also similar with some slight differences at higher N/C ratios (Fig. 3.9c).

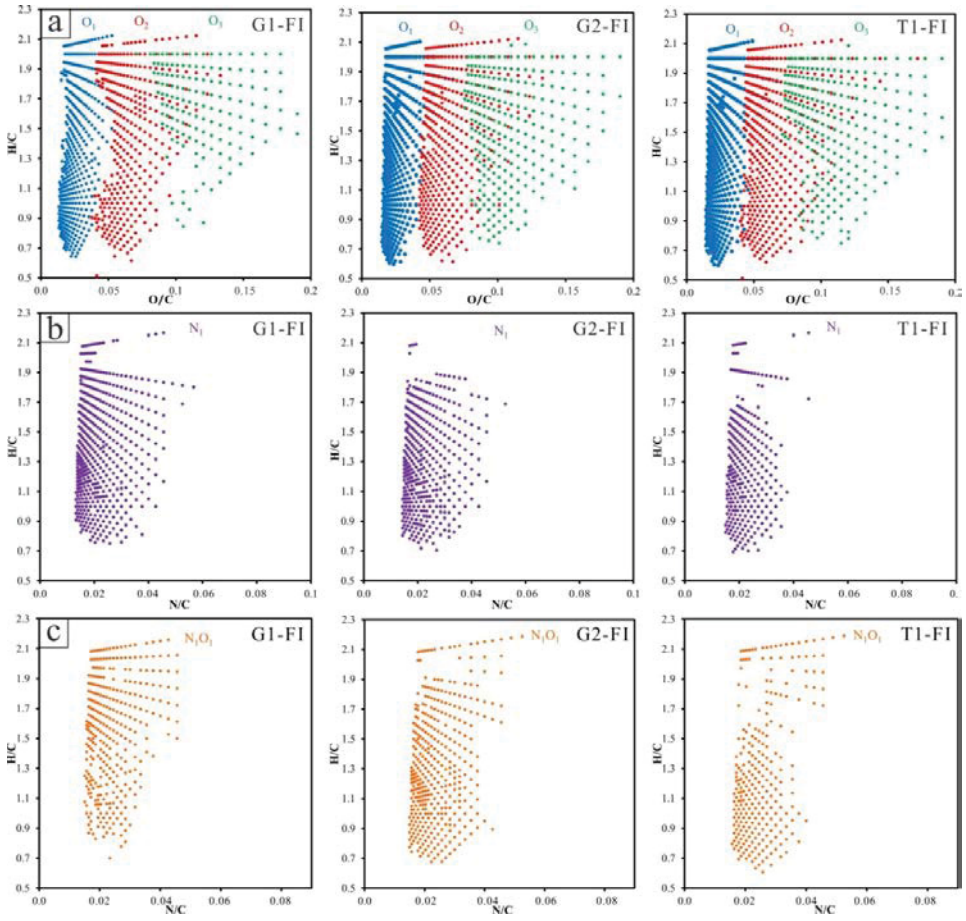

Figure 3.9. Van Krevelen diagrams of the H/C vs. O/C or N/C ratios of the a) $O_{1–3}$, b) N_1 and c) N_1O_1 class compounds detected in APPI (+) mode of G1-, G2- and T1-fluid inclusion (FI) oils.

Thus, for the FI oils of the Garn and Tilje Fms the qualitative composition of the main NSO-compound classes ($O_{1–3}$, N_1, N_1O_1) match each other well, with only subordinate deviations (e.g., N_1, T1-FI). Therefore, the NSO-compounds from the FI

oils support the interpretation from the aliphatic biomarkers that the FI oils in the Garn and Tilje Fms originate from a similar source.

3.6.4 Implications for the oil charge and leakage history

FI oils are geological capsules protecting its content from subsequent geological and biological transformation processes (George et al., 2007a; Volk and George, 2019) and preserving initial oil filling information (George et al., 1998). Thus, geochemical similarities and diversities between reservoir Ad and FI oils in the Garn and Tilje Fms can provide valuable information to elucidate the oil charge and leakage history of the Skarv field A segment in the Haltenbanken region.

3.6.4.1 Initial oil charge

The occurrence of abundant oil FIs with similar source and maturity characteristics in quartz clasts and quartz overgrowths formed during quartz cementation suggests that an initial oil charge from a similar source has migrated and trapped in the Garn and Tilje reservoirs. The source related biomarkers of the FI oils point to a marine source rock and the Spekk Fm is regarded as the most likely source rock in this region. In most areas of the Skarv field A segment the Spekk Fm (depth of 3178–3194 m in well 6507/5-1) has a maturity of approximately 0.5 %Ro-equivalent (data from well 6507/5-1 report), which is inconsistent with the oil maturity observed for the FI oils from the Garn and Tilje Fms (0.80–0.84 %Rc) (Table 3.2). Thus, the initial oil charge must have originated from a deeper buried part of the Spekk Fm and consequently be subjected to a higher thermal regime. According to the geological structure and burial history (Kazankapov, 2019), the Skarv field is confined to the more deeply buried and extensively faulted regions to the west, where the Spekk Fm is currently in the oil window with depth around 4400–4500 m (Fig. 3.10a). At this depth the Spekk Fm was nearly at refractory gas generation stage (Cohen and Dunn, 1987), and a large amount of petroleum has been generated and expelled. In this region the Åre Fm has exceeded the oil window as well, however the source related biomarkers in the FI oils did not indicate hydrocarbon characteristics expelled from the Åre Fm.

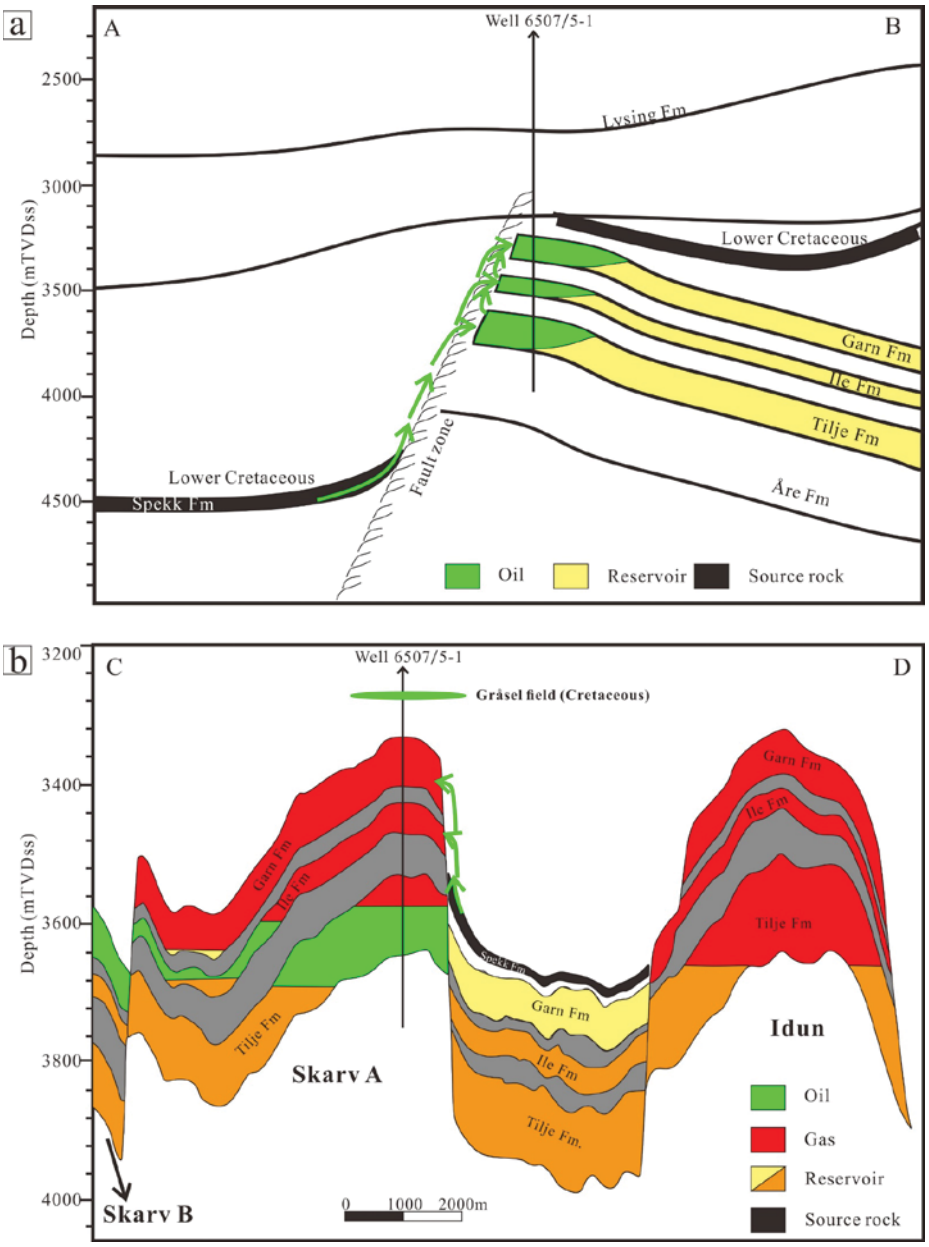

Figure 3.10. a) Sketch showing the initial oil charge pathway from Spekk Fm in the deeper western region along faults to the reservoirs in the Skarv field A segment (revised from Karlsen et al., 2004). b) Sketch showing the potential pathway of the second oil charge into the Garn Fm of the Skarv field A segment. Respective seismic lines A-B and C-D see figure 3.1b.

Thus, initial oil is suggested to be sourced from the Spekk Fm in the deeper western region migrating upwards along faults into the Skarv field (Fig. 3.10a). The similar source and maturation stage for the FI oils from the Garn and Tilje Fms, and for the Ad oil from the Tilje Fm, as outlined above, imply that the initial oil has reached and filled both the Garn and Tilje Fms. Moreover, the enriched longer chain

n-alkanes (C_{26+}) (Fig. 3.3) in the FI oils of the Tilje Fm suggest that the initial oil reached the Tilje Fm before the Garn Fm. When the migrated oil reached the deeper Tilje reservoir along the fault, the longer chain, less mobile *n*-alkanes were preferentially retained in the charged oil of the Tilje Fm (Larter and Aplin, 1995). Thus, the migrated oil was depleted in longer chain *n*-alkanes when continuing migration to shallower reservoirs such as the Garn Fm. This oil charge model is consistent with oil filling mechanism in other Haltenbanken regions proposed by Karlsen et al. (2004). The expelled oil migrated from deeper zones along faults into the Tilje Fm until an equilibrium between the pressure head of the Tilje petroleum charge in the reservoir and the pressure head of the petroleum in the fault zone was reached. Afterwards the petroleum pressure head in the fault may build up with sufficient buoyancy to further ascend the fault and to cause filling of the adjacent shallower Garn Fm (Karlsen et al., 2004).

3.6.4.2 Oil leakage and recharge of the Garn Fm

In contrast to the Tilje Fm, biomarker results gained from the current reservoir Ad oils in the Garn Fm show significant differences compared to the corresponding FI oils (in maturation and source indicators). Generally, in a system of continuous charge from the same source, the reservoir petroleum should have approximately the same or a slightly higher maturity level than the initial oil, since the source rock and thus the expelled oil might become more mature during progressive burial. This is true for the Tilje Fm where the oil from FIs is similar in facies and maturity to the Ad oil found in the Tilje reservoir, which clearly indicates that there was only one oil charge in the Tilje Fm.

In contrast, in the Garn Fm the Ad oils show lower maturity and different source characteristics compared to the corresponding FI oils. Since oil FIs usually formed in high oil saturations (George et al., 1998), differences between FI and Ad oils in the Garn Fm imply that the initial oil trapped in the reservoir during the first charge (also filling the Tilje Fm) has been lost in the Garn Fm by leakage and that the Garn reservoir was recharged or mixed with another oil (current Ad oil). Asphaltene-rich residues in the Garn reservoir were considered of being the result of an upwards

leakage of gas from an underlying gas condensate in the North Sea (Dahl and Speers, 1985; Ehrenberg et al., 1995). Such residues were observed in the shallower sample G1 by microscopy, which contained more NSO-compounds than the Ad oil samples G2 and G3 (Fig. 3.2 and Table 3.1). This observation supports that oil and gas leakage has occurred in the Garn Fm. Additionally, reservoir oil with similar geochemical characterization to the Skarv oils was found in the Gråsel field, a Cretaceous reservoir unit partly congruent with the Skarv field (Fig. 3.10b), which could support the vertical leakage. Thus, Ad oils from the Garn Fm represent a later oil charge (G1: 0.78 %Rc, G2 and G3: 0.73 %Rc), which is confirmed by the lower maturity compared to the first charged oil (0.80–0.83 %Rc). The geochemical data of the Ad oils from the Garn Fm indicate that post-charged oil originated from another source region (not the western fault zone) in the Spekk Fm, having lower maturity and different facies characteristics. Heum et al. (1986) proposed that oil expulsion in the Spekk Fm is initiated at a maturity of about 0.7 %Rc, which is consistent with the maturity of the Ad oils (0.73 %Rc) from the Garn Fm. This supports that the Ad oil in the Garn reservoir has been expelled from a different area of the Spekk Fm being in the early expulsion stage and being influenced by facies heterogeneities. Such depositional heterogeneities in the Spekk Fm have been described by Karlsen et al. (1995) and Pedersen et al. (2006) before. The burial history at well 6507/5-1 in the Skarv A segment showed accelerated burial in the past 5 Ma (Kazankapov, 2019), which may have caused oil generation and expulsion from shallower buried Spekk Fm source rocks. Spekk Fm source rock directly located at well 6507/5-1 shows only a maturity level of approximately 0.5 %Ro. However, deeper Spekk Fm source rocks from the footwall of the adjacent fault such as the saddle between the Skarv and Idun field might have reached the oil expulsion stage of 0.7 %Rc (Figs. 3.1b and 3.10b). Thus, it is reasonable to deduce that recharged oil in the Garn Fm was sourced from mature Spekk Fm due to the accelerated burial during the last 5 Ma. Refilling of leaked traps has been documented by Karlsen et al. (2004) in other Haltenbanken region as well. These dry Garn reservoirs communicated with petroleum generating source rock areas, where the Spekk Fm was mature enough for petroleum expulsion.

In contrast to the reservoir oils in the Garn and Tilje Fms, which were most likely derived from the upper-Jurassic/lower-Cretaceous marine, anoxic source rock facies of the Spekk Fm, the adjacent Idun field (Fig. 3.1) have been suggested to be sourced at least partly from a terrigenous source rock facies presumably the Åre Fm (Xu, 2003). The carbon isotopic gas compositions indicate higher gas maturity (approx. 1.6–1.7 %Ro-equivalent) for the Idun field (J. Rinna, Aker BP, personal communication) compared to the Skarv field (approx. 1.1–1.2 %Ro-equivalent). However, the maturity level of the Skarv field deduced from the gas isotopic composition is significantly higher than those inferred from the oil phase biomarkers (0.73–0.84 %Rc, Table 3.2). This suggests that at least part of the gas phase in the Skarv field was derived also from the more mature Åre Fm. More analyses of suitable sample material are needed including samples from the Idun field to elucidate the interconnections of the Skarv and Idun petroleum systems.

3.7 Conclusions and outlook

(1) Biomarker, stable carbon isotope and NSO-compound analyses indicate that FI oils from the Garn and Tilje Fms and Ad oil from the Tilje Fm in the Skarv field were derived from the same marine source rock most likely the Spekk Fm. In contrast, the Ad oil from the Garn Fm is suggested to originate from a different less mature source rock of the Spekk Fm, which was deposited under higher salinity conditions.

(2) Geochemical similarities and differences between FI and Ad oils imply that the oil charge and leakage history of the Garn and Tilje reservoirs are relatively complex. The initially charged oil was generated from deeply buried Spekk Fm source rocks in an extensively faulted region west of the Skarv field. The petroleum has migrated along faults and charged both the Tilje and Garn reservoirs.

(3) While the initially charged oil in the Tilje reservoir was preserved, in the Garn reservoir the initial oil was lost by leakage and the reservoir was recharged. The recharged oil in the Garn Fm presumably originates from another less mature kitchen area of the Spekk Fm, becoming mature enough for oil expulsion due to rapid burial over the past 5 Ma.

3.8 Acknowledgements

The China Scholarship Council (CSC) is gratefully acknowledged for funding Yufu Han's research. The study is financially and scientifically supported by an Industry Partnership with Aker BP ASA Norway, and we are grateful for the permission to publish the outcome. We extend our gratitude to Cornelia Karger, Anke Kaminsky, Andrea Vieth-Hillebrand and Doreen Noack for their technical support. We thank the associate editor Xiaowen Guo and two anonymous reviewers for their careful and constructive reviews of this paper.

4. FRACTIONATION OF HYDROCARBONS AND NSO-COMPOUNDS DURING PRIMARY OIL MIGRATION REVEALED BY HIGH RESOLUTION MASS SPECTROMETRY: INSIGHTS FROM OIL TRAPPED IN FLUID INCLUSIONS[3]

4.1 Abstract

The composition of oil trapped in fluid inclusions (FI) occurring in mineral cements can provide valuable insights into oil migration. Here, FI oils in a calcite vein (representing expelled fluids) and source rock (SR) extracts (representing retained bitumen) from the Hosszúhetény Calcareous Marl Formation (HCMF) in the Mecsek Mountains area of Hungary are investigated to assess how organic compounds are fractionated during primary migration. Biomarkers analyzed by gas chromatography-mass spectrometry (GC-MS) and stable carbon isotope gas chromatography-isotope ratio mass spectrometry (GC-IRMS) were first used to demonstrate that the FI oils had been expelled from the HCMF marl. Fourier transform-ion cyclotron resonance-mass spectrometry (FT-ICR-MS) then provided insights into polar compound geochemistry, showing that O_1, N_1, N_1O_1 and S_1O_1 compound classes are preferentially retained in the source rock bitumen, while S_1 compounds are preferentially expelled. O_2 compounds and hydrocarbons (HCs) seem to show at first glance no preference, but on closer examination not only HC and O_2 compounds but also S_1, O_1, and N_1 compounds in the retained source rock bitumen are enriched in

3 This chapter has been published as: Han, Y., Noah, M., Lüders, V., Körmös S., Schubert F., Poetz S., Horsfield, B., Mangelsdorf, K. 2022. Fractionation of hydrocarbons and NSO-compounds during primary oil migration revealed by high resolution mass spectrometry: insights from oil trapped in fluid inclusions. International journal of Coal Geology, 254, 10397, https://doi.org/10.1016/j.coal.2022.103974. This is the preprint version.

compounds with higher double bond equivalents (DBEs). This reflects a higher aromaticity and a larger molecular size of the retained molecules in the bitumen. Thus, the functional groups and the degree of aromaticity are the two main factors affecting the migration and retention behavior of the petroleum HCs and NSO-compounds in the HCMF. Moreover, the enrichment of high DBE compounds with shorter alkyl chains in the SR extracts infers that shielding effects also could have played a role for compounds retention and expulsion. These findings confirm the earlier work that functional groups, aromaticity, and alkylation degree of HCs and NSO-compounds are main factors affecting compositional fractionation of petroleum during primary migration.

Keywords: FI oil, NSO-compounds; oil primary migration, FT-ICR-MS, Hosszúhetény Calcareous Marl Formation, fractionation

4.2 Introduction

During primary oil migration, petroleum is expelled from the source rock into the surrounding or adjacent carrier lithology. During this process the expelled fluids become enriched in saturated hydrocarbons, while the retained bitumen is enriched in asphaltenes and resins (Tissot and Welte, 1984). The expulsion sequence saturated hydrocarbons > aromatic hydrocarbons > polar compounds has been confirmed using experiments and modelling in many studies (Tissot and Welte, 1984; Leythaeuser et al., 1988a; Sandvik et al., 1992; Kelemen et al., 2006; Han et al., 2015). The preferential expulsion of saturated hydrocarbons and aromatic compounds has been widely examined using gas chromatography either coupled to a flame ionization detector (GC-FID) or a mass spectrometer (GC-MS) (Mackenzie et al., 1983; Leythaeuser et al., 1988b, 1998c; Han et al., 2015). For example, Mackenzie et al. (1983) showed that a preferential expulsion of lower carbon number *n*-alkanes occurs during migration. Han et al. (2015) elucidated the preferential retention of polar compounds, aromatic hydrocarbons and saturated hydrocarbons in this order within the Barnett shale. Additionally, compositional fractionation processes during migration can be assessed by nitrogen, sulfur and oxygen (NSO)-containing

compounds, e.g., methylcarbazoles and xanthones (Larter and Aplin, 1995; Li et al., 1995; Larter et al., 1996; Taylor et al., 1997; Clegg et al., 1998; Oldenburg et al., 2002; Bennett et al., 2004), because, due to their polarity, these compounds are most strongly influenced by physical and chemical interaction processes with the pore fluids and the surrounding mineral and organic matrix. The relative enrichment of nitrogen-shielded and nitrogen-exposed benzocarbazole isomers were used to elucidate the fractionation during migration (Li et al., 1995; Larter et al., 1996), although a strong link to maturity occurs in the case of vertically charged petroleum systems (Clegg et al., 1998; Horsfield et al., 1998). Phenols and its alkylated homologues can alter wetting properties of mineral surface, and subsequently allowing the adsorption of larger hydrophobic molecules (Larter and Aplin, 1995; Taylor et al., 1997; Bennett et al., 2004). While these low molecular weight NSO-containing compounds have intensively been investigated to study oil migration processes (Leythaeuser et al., 1988c; Yamamoto et al., 1991; Li et al., 1995; Peters et al., 2018), studies on high molecular weight NSO-compounds are almost lacking.

Fourier transform-ion cyclotron resonance-mass spectrometry (FT-ICR-MS) has broadened the analytical window for NSO-compounds and aromatic hydrocarbons (HCs) (Marshall and Rodgers, 2008). The ultra-high mass resolution allows the elemental composition of thousands of previously inaccessible organic compounds to be determined and thus allows new insights into compositional fractionation processes to be gained. Numerous studies have been conducted to address the HC and NSO-compound fractionation during oil migration by investigating the free petroleum phase using Electrospray Ionization (ESI) and Atmospheric Pressure Photoionization (APPI) FT-ICR-MS (Mahlstedt et al., 2016; Han et al., 2018a, 2018b, 2021; Ziegs et al., 2018; Poetz et al., 2020; Yue et al., 2021). The migration related fractionation is controlled by the elemental classes of their functional groups or polarity (Han et al., 2018a, 2018b, 2021; Ziegs et al., 2018; Poetz et al., 2020; Yue et al., 2021). Han et al. (2018a, 2018b) pointed out that the N_y compounds were selectively retained in the Mississippian Barnett Shale, while the N_yO_x compounds were preferentially expelled. The opposite case has also been reported in Eagle Ford oil system that pyrrolic nitrogen compounds are more enriched in crude oil, while high contents of N_yO_x and

S_zO_x compounds in source rock (Poetz et al., 2020). Retention of NSO-compounds in source rock also depends on their molecular size and aromaticity (Mahlstedt et al., 2016; Poetz et al., 2020). Mahlstedt et al. (2016) revealed that the aromaticity and molecular size of NSO-compounds increased much more pronouncedly with increasing maturity for retained than for expelled oil. The lithofacies of source rock was considered to play a significant role on oil expulsion as well. For instance, Yue et al. (2021) reported that nitrogen-containing compounds are preferentially retained by biogenic quartz of Barnett Shale, while the more polar acidic oxygen-containing compounds are preferably retained by clay-rich Posidonia Shale, exhibiting various retention capacities of NSO-compounds by mineralogical compositions.

Oil-bearing fluid inclusions (FIs) hosted in mineral cements contain aliquots of oil that were trapped either within cavities during crystal growth, in which case they are termed primary FIs, or during subsequent recrystallization, in which case they are termed secondary FIs (Burruss, 1981). The great advantage of investigating FI oils is that the oil is physically isolated, and therefore its composition is not affected by later secondary geological transformation processes (Volk and George, 2019). The geochemical information they contain has been used to compare present oil properties with those of paleo-oils (early oil charges) and to examine the impact of migration and alteration processes on oil composition (Horsfield and McLimans, 1984; Bodnar, 1990; Jochum et al., 1995b; Volk et al., 2002; George et al., 2007a; Cobbold et al., 2013; Volk and George, 2019). Recently, a procedural and analytical protocol for analyzing HCs and NSO-compounds in FI oils using FT-ICR-MS has been reported (Noah et al., 2018; Han et al., 2020). The ultra-high mass resolution allows the elemental composition of thousands of newly accessible organic compounds to be identified.

In the study reported here, we have compared the solvent extracts from the Hosszúhetény Calcareous Marl Formation (HCMF) (Hungary) marl source rock (SR) with FI oils hosted in a calcite vein cutting the HCMF in order to unravel the compositional fractionation of NSO-compounds during oil primary migration. In a first step, biomarker and stable carbon isotope analyses were conducted using GC-MS

and gas chromatography-isotope ratio mass spectrometry (GC-IRMS) to establish compositional relationships between SR extracts (retained bitumen) and FI oils (expelled oil). In addition to these conventional methods, FT-ICR-MS in the APPI positive (+) mode was then applied to reveal effects of migration-induced fractionation on the petroleum HCs and NSO-compounds.

4.3 Geological setting and sample set

4.3.1 Geological setting

The Pannonian Basin is surrounded by the Dinarides, Alps and Carpathians (Fig. 4.1a). The Mecsek Mountains are located in the southwestern part of the Pannonian Basin. The mountain range forms part of the Tisza Mega-unit (Csontos, 1995; Csontos et al., 2002). This area became part of the European continent at the end of the Variscan orogeny, and rifted off the European shelf at the end of the Jurassic (Haas et al., 1999; Csontos et al., 2002). The complex movement of crustal plates resulted in amalgamation and the Tisza Mega-unit reached its current position during the Palaeogene and Neogene (Csontos et al., 2002). An extensional half-graben formed during the Rhaetian to Hettangian time, and coal-bearing fluvial-deltaic swamp sediments of the Mecsek Coal Formation were deposited (Haas, 2012). In the early Sinemurian, the subsidence of the Mecsek Basin resulted in the deposition of shallow marine sandstones and marls of the Zobákpuszta Sandstone Formation and Vasas Marl Formation, respectively (Raucsik, 2012a; 2012b). Due to a rise in eustatic see level a bioturbated, hemipelagic series of mixed carbonate and siliciclastic sediments were deposited, comprising the HCMF (Raucsik, 2012c). The Upper Pliensbachian and Lower Toarcian succession are characterized by monotonous bioturbated, spotted marl with turbiditic sandstone intercalations (Mecseknádasd Sandstone Formation) and limestone beds (Kecskehát Limestone Formation), representing depositional conditions controlled by tectonism, sea level fluctuation and climate change (Raucsik and Varga, 2008). The lower Toarcian strata also contain organic-rich and laminated sediments of the Rékavölgy Siltstone Formation (Varga et al., 2007; Raucsik, 2012d). Spotted marl deposition succeeded black shale deposition in the remaining Toarcian

(Komló Calcarous Marl Formation) (Raucsik, 2012e) (Fig. 4.1b).

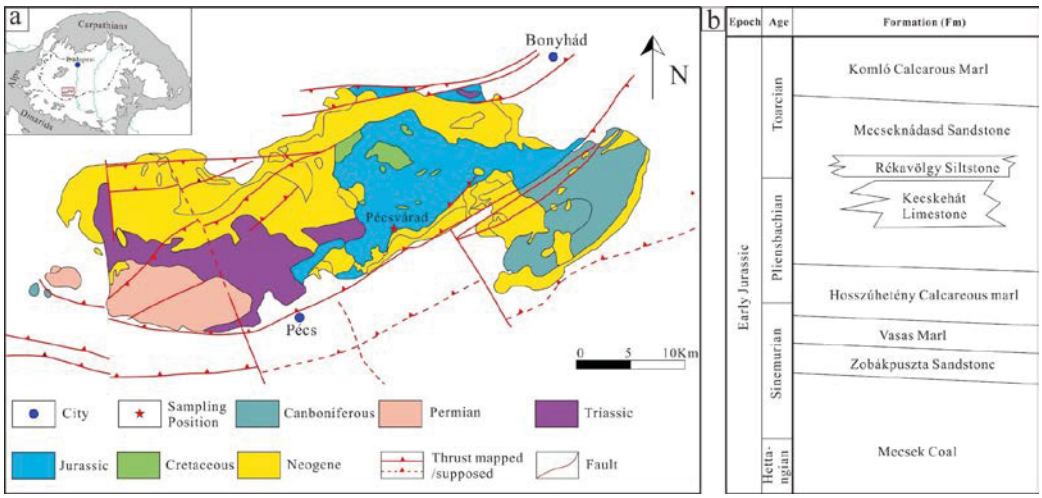

Figure 4.1. a) Geological map of Mecsek Mountains in Hungry and sampling outcrop position (revised from Csontos et al. (2002) and Raucsik and Varga (2008)); b) Chronostratigraphic chart of Early Jurassic formations of Mecsek Mountain in Hungry (revised from Főzy (2012)).

The focus of the study is the Lower Jurassic Hosszúhetény Calcareous Marl Formation calcite-filled fractures up to 40 cm thick crosscut the thick-bedded HCMF, where abundant oil FIs have been discovered (Lukoczki et al., 2012). Although there are several potential source rocks in the Mecsek Mountains, such as the Mecsek Coal Formation, Vasas Marl Formation, Hosszúhetény Calcareous Marl Formation, and the Rékavölgy Siltstone Fm (Fig. 4.1b), it is the HCMF marl which is the most likely SR for the FI oils, because the calcite vein cuts through this formation and is sub-perpendicular to the HCMF marl (Fig. 4.2). The measured vitrinite reflectance values (Ro = 0.69%–0.73%) suggest that the sediments and incorporated organic matter are within the oil window (Lukoczki et al., 2012).

4.3.2 Sample set

Two source rock (named as SR-1 and SR-2) and six pure milky-gray FI-bearing calcites (named as FI-1 to FI-6) from a vein within the HCMF were collected from an abandoned quarry close to the city of Pécsvárad in the Mecsek Mountains, Hungary (Fig. 4.2). Massive calcite fills the HCMF fractures with tens of meters in length and several to tens of centimeters in width (Fig. 4.2a). Calcite vein material could easily be obtained and split into small pieces (Fig. 4.2b).

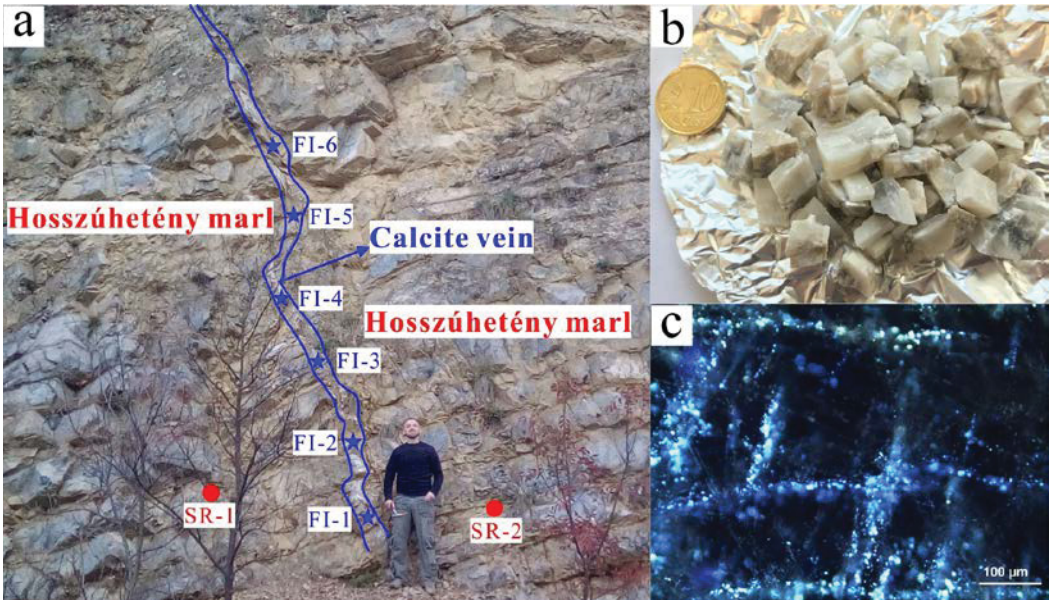

Figure 4.2. Sample material: a) Calcite vein (outlined in blue) filling a HCMF fracture with red dots representing source rock and blue stars representing calcite sampling positions. b) Calcite vein material from the HCMF fracture. c) Photomicrograph of fluid inclusion trails under UV light showing the presence of petroleum by pale-blue and yellowish-blue fluorescence.

4.4 Methods

4.4.1 Sample preparation

Two powdered marl SR samples (SR-1 and SR-2) were extracted by a mixture of dichloromethane (DCM) and methanol (99:1, v/v) at 50 °C using Soxhlet extraction for 24 h, the extracts termed SR extracts. Six calcite crystal concentrates (FI-1 to FI-6) were cleaned using the rigorous clean-up protocols developed by Han et al. (2020). In brief, host minerals were washed with a Waller solution containing 33% sodium dithionite, 28% sodium bicarbonate, 59% sodium citrate in distilled water. Then the host minerals were transferred into a Soxhlet extraction thimble and washed twice (24 h) with DCM mixed with methanol (99:1, v/v) at 50 °C. Afterwards, the minerals were washed with three different organic solvents in the following order: methanol, blend of dichloromethane (DCM) and methanol (93:7, v/v), and DCM. The DCM extract from the last cleaning step was collected and residual particles were removed using a pre-cleaned thimble. This DCM extract was used as procedural blank for the respective sample. Before continuing, the procedural blanks were measured by GC-

MS and FT-ICR-MS and controlled for the amounts of remaining bitumen. The washing procedure was repeated until the cleaning of the outer mineral surfaces from bitumen residues was deemed successful. Afterwards the cleaned calcite crystals were crushed in a small metal cylinder with two stainless steel balls, and finally, the inclusion oil (named as FI oil) in the powdered sample was extracted by a mixture of DCM and methanol (99:1, v/v) using Soxhlet extraction.

The source rock extracts (SR-1 and SR-2) were split into two parts: one for GC-MS and GC-IRMS and the other for FT-ICR-MS analysis. Due to the fact that only low amounts of FI oils were anticipated, the six FI oil samples from the HCMF calcite vein were divided into two sets: FI-1 and FI-2 were used for GC-MS and GC-IRMS analysis, and FI-3 to FI-6 were used for FT-ICR-MS. The extracts for FI-1 and FI-2 were deasphaltened to obtain the *n*-hexane-soluble maltene fraction. Subsequently, the maltenes were further separated into aliphatic, aromatic and NSO-compound fractions using a medium pressure liquid chromatography (MPLC) system (Radke et al., 1980). The extracts FI-3 to FI-6 were analysed directly by FT-ICR-MS with no prior treatment.

4.4.2 Microscopy

FI analysis were conducted on doubly polished thin sections, with thickness of ca. 150 µm to ensure the transparency of the calcite in transmitted. The sections were used to investigate the oil FIs using a BX50 Olympus microscope with various objectives (5×, 10×, 20×, 50×) connected to a UV light source.

4.4.3 GC-MS

The aliphatic and aromatic fractions of two SR extracts (SR-1 and SR-2) and two FI oils (FI-1 and FI-2) were selected for GC-MS analysis using a Trace GC Ultra coupled to a DSQ mass spectrometer (Thermo Electron Corp.). The Agilent 6890 Serie GC instrument was equipped with a Thermo PTV injection system and a SGE BPX5 fused silica capillary column (50 m × 0.22 mm ID and 0.25 µm film thickness). Helium was used as a carrier gas. The GC oven was programmed from 50 to 310 °C at a rate of 3 °C min^{-1}, followed by an isothermal phase of 30 min. The MS was

operated in electron impact ionization mode (EI) at 70 eV. Full scan mass spectra for compound identification were recorded from *m/z* 50 to 600 Da in the aliphatic fraction, and from 50 to 330 Da in the aromatic fraction at a scan rate of 2.5 scans/second. In addition to the full scan mode, aliphatic fractions were also measured in the SIM (single ion monitoring) mode to improve the sensitivity for specific biomarkers such as hopanes (*m/z* 191) and steranes (*m/z* 217).

4.4.4 GC-IRMS

The *n*-alkanes in the aliphatic fraction of the two source rock extracts (SR-1 and SR-2) and the combined FI oils (FI-1 and FI-2) were analyzed by GC-IRMS using a GC unit (7890N, Agilent Technology, USA) connected to a GC-Isolink that is coupled via open split with a Delta V Plus mass spectrometer (ThermoFisher Scientific, Germany). For carbon isotope analysis, the organic compounds of the GC effluent stream were oxidized to CO_2 on a CuO/Ni/Pt catalyst in the combustion furnace held at 940 °C. 3 µL of saturated fraction were injected to the injector, working in splitless mode and held at a constant temperature of 300 °C. The aliphatic fractions were separated on a fused silica capillary column (HP Ultra 1, 50 m × 0.2 mm ID, 0.33 µm FT, Agilent Technology, Germany). The temperature program started at 80 °C, held for 2 minutes. Temperature was increased at a rate of 5 °C min^{-1} to 320 °C, and with a lower rate of 1 °C min^{-1} increased to 325 °C, held for 15 minutes. Helium, set to a flow rate of 1.3 mL min^{-1}, was used as carrier gas. All aliphatic hydrocarbon fractions were measured in triplicate and the standard deviation was ≤ 0.5‰ for most of the compounds and samples for ^{13}C. The quality of the isotope measurements was checked regularly by measuring different *n*-alkane standards with known isotopic composition (provided by Campro Scientific, Germany and Arndt Schimmelmann, Indiana University, USA).

4.4.5 FT-ICR-MS

Two SR extracts (SR-1 and SR-2) and four FI oils (FI-3 to FI-6) were selected for FT-ICR-MS analysis. Samples were measured using a 12 Tesla Solarix FT-ICR-MS from Bruker Daltonik GmbH (Bremen, Germany) in APPI (+) mode, which can

ionize mainly aromatic compounds of low-polarity (Huba et al., 2016a). A standard solution of the extract with a concentration of 1 mg/mL in a mixture of methanol and hexane (9:1, v/v) was diluted with the same solvent mixture to give a final concentration of 20 µg/mL. The solutions were injected into the APPI source at a flow rate of 20 µL/h using a syringe pump (Hamilton) where the analytes were ionized using a krypton lamp at 10.6 eV. The instrumental parameters on APPI (+) mode were as follows: dry gas (N_2) flow rate 3 L min and temperature 210 °C, nebulizing gas (N_2) 2.3 bar, capillary voltage 1000 V, additional collision-induced dissociation voltage of 30 V, ions accumulation time 0.03 s, transfer time 1 ms, 4 megaword data sets. A total of 300 mass spectra were accumulated in a mass range from *m/z* 147 to 1200.

In each spectrum, signals with a signal-to-noise ratio ≥ 8 were included into the further data assessment. Formula assignment was done using the isotopes ^{1}H, ^{12}C, ^{13}C, ^{14}N, ^{16}O, and ^{32}S, with the upper thresholds N ≤ 2, O ≤ 8, and S ≤ 2; C and H were unlimited. If no chemical formula within the allowed mass error of 0.5 ppm was found, the peak was not included into the mass/formula list. For each $C_cH_hN_nO_oS_s$ compound, its double bond equivalent (DBE) value was obtained by calculating DBE = c – h/2 + n/2 + 1, where c is carbon number, h is hydrogen number and n is nitrogen number. Each DBE refers to the number of unsaturation or rings in the individual compound structure (Poetz et al., 2014).

4.5 Results

4.5.1 Microscopic characterization

Calcites from the investigated HCMF marl fracture host numerous oil inclusions, occurring in clusters and along trails cross-cutting the host mineral crystals, and with lengths less than 20 µm. The FI can be classified as secondary fluid inclusions which were trapped along a healed fracture (Goldstein and Reynolds, 1994). The oil FIs show mainly pale-blue and yellowish-blue fluorescence under UV light (Fig. 4.2c), corresponding to predominantly aromatic and aliphatic compositions, respectively (Hagemann and Hollerbach, 1986). According to a previous study (Lukoczki et al., 2012), the variation in fluorescence spectral properties of the present oil inclusion

trails was not caused by maturity differences, but by oil fractionation during trapping.

4.5.2 Biomarkers

Trace chromatograms of the hopanes and steranes from the SR extracts and the two FI oils FI-1 and FI-2 are shown in Figure 4.3. All biomarker ratios quoted in this study were calculated from SIM data (Table 4.1). 18α-trisnorneohopane (Ts) and C_{30} αβ-hopane or 18α-30-norneohopane (C_{29}Ts) are the most abundant hopanes in both SR extracts and FI oils investigated. The C_{31} αβ-22S/(22S + 22R) hopanes values (~ 0.59) are very similar in SR extracts and FI oils. The C_{35} homohopanes presented in a significant proportion can be seen from Figure 4.3 and C_{35} homohopane index (Table 4.1).

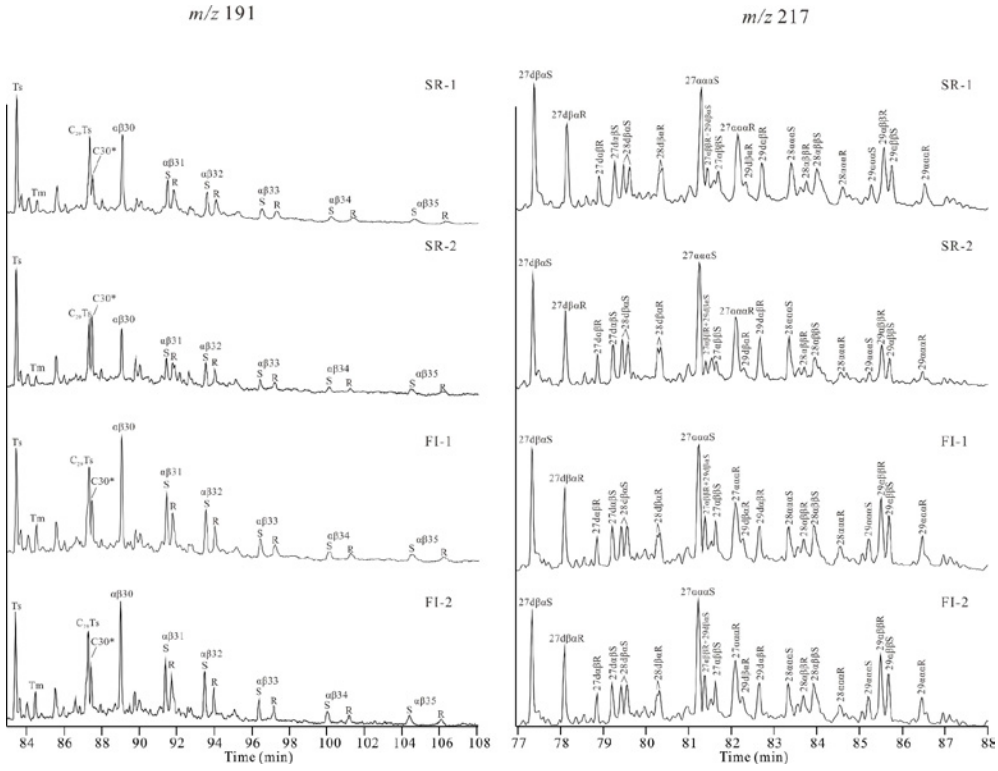

Figure 4.3. Comparison of the hopane (*m/z* 191) and sterane (*m/z* 217) mass traces of the two source rocks (SR) extracts SR-1 and SR-2 and the two inclusion (FI) oils FI-1 and FI-2 from the HCMF marl in the Mecsek Mountains, Hungary. Ts = 18α-trisnorneohopane; Tm = 17α-trisnorhopane; C_{29}Ts = 18α-30-norneohopane; C_{30}* = 17α-diahopane.

Table 4.1. Aliphatic and aromatic hydrocarbon parameters for the two fluid inclusion (FI) oils FI-1 and FI-2 and source rock (SR) extracts SR-1 and SR-2 from the HCMF marl in the Mecsek Mountains, Hungary.

Parameters	SR-1	SR-2	FI-1	FI-2
Hopanes/Terpanes				
Ts/(Ts + Tm)	0.79	0.9	0.77	0.79
C_{29}Ts/C_{29} αβ hopane	0.72	0.87	0.74	0.76
22S/(22S + 22R)	0.59	0.59	0.59	0.58
C_{35} homohopane index	0.12	0.15	0.12	0.15
Steranes				
20S/(20S + 20R)	0.42	0.4	0.42	0.43
ββ/(ββ + αα)	0.69	0.71	0.65	0.65
C_{27}/C_{29} sterane	3.25	5.22	2.27	2.48
Diasteranes/steranes	0.73	0.72	0.64	0.63
Steranes/17α-hopanes	1.21	1.46	1	1.08
Aromatics				
MPI-1	0.58	0.57	0.57	0.58
Calculated Rc (%)	0.75	0.74	0.74	0.75

Note: Ts = 18α-trisnorneohopane; Tm = 17α-trisnorhopane; C_{29}Ts = 18α-30-norneohopane; 22S/(22S + 22R) = C_{31} αβ-22S/(22S + 22R) hopanes; C_{35} homohopane index = C_{35}/(C_{31}–C_{35}) homohopanes; 20S/(20S + 20R) = C_{29} ααα-20S/(20S + 20R) steranes; ββ/(ββ + αα) = C_{29} αββ/(αββ + ααα) steranes; C_{27}/C_{29} sterane = C_{27} ααα-20R/C_{29} ααα-20R sterane; diasteranes/steranes = C_{27} βα-diasteranes/C_{27} (ααα + αββ) steranes; steranes/17α-hopanes = C_{27}–C_{29} steranes/C_{29}–C_{35} 17α-hopanes; methylphenanthrene index (MPI-1) = 1.5 × (3MP + 2MP)/(P + 9MP + 1MP); calculated vitrinite reflectance (Rc) = 0.6 × MPI-1 + 0.4 (for 0.65% < Ro < 1.35%; Radke and Welte, 1983).

The SR extracts and FI oils show quite similar sterane and diasterane distributions, in which the C_{27} steranes and diasteranes are more abundant than the C_{28} and C_{29} congeners. The C_{29} ααα-20S/(20S + 20R) sterane ratios show similar values (~ 0.42) in SR extracts and FI oils (Fig. 4.3). In contrast, the C_{29} αββ/(αββ + ααα) sterane ratios and diasteranes/steranes ratios in SR extracts are slightly higher than in FI oils. One further difference is that SR extracts contain more steranes, relative to the hopanes, than the FI oils.

Aromatic compounds such as phenanthrene, alkylphenanthrenes and alkyldibenzothiophenes are also present in the two SR extracts and the two selected FI oils. The distribution pattern of aromatic hydrocarbons changes with an increasing degree of maturation (Radke and Welte, 1983) and thus, provides indication on the maturity level of the respective sample. Here, the phenanthrene maturity ratios such as MPI-1 and calculated vitrinite reflectance (Rc) point to similar maturity stages for the two SR and FI oil samples (Table 4.1).

4.5.3 Stable carbon isotope

In Figure 4.4 the $\delta^{13}C$ values of the *n*-alkanes from the two SR extracts (SR-1 and SR-2) and two FI oils (FI-1 and FI-2) are plotted against the carbon numbers. The $\delta^{13}C$ values of *n*-alkanes in SR extracts range from –32.8‰ to –35.4‰, which partly overlaps with the $\delta^{13}C$ values of the *n*-alkanes in the FI oils ranging from –31.1‰ to –34.1‰. In general, the SR extracts and FI oils show a similar variability in the isotopic compositions of *n*-alkanes, however, long chain *n*-alkanes (> C_{29}) in SR extracts are slightly enriched in ^{13}C compared to those in the FI oils.

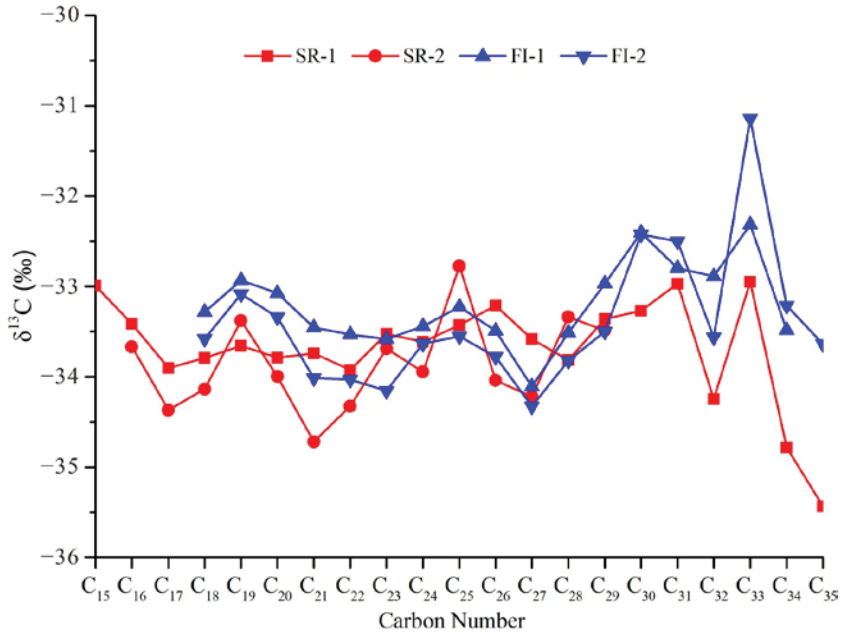

Figure 4.4. Compound specific carbon isotope compositions of the *n*-alkanes of the aliphatic fractions in the source rock extracts (SR, blue lines) and inclusion oils (FI, red lines) from the HCMF marl in the Mecsek Mountains, Hungary.

4.5.4 General characterization of hydrocarbons and NSO-compounds by FT-ICR-MS

Two SR extracts (SR-1 and SR-2) and four FI oils (FI-3 to FI-6) from the calcite vein were characterized using FT-ICR-MS in APPI (+) mode. The abundances of individual compound classes show significant differences between the SR extracts and FI oils (Fig. 4.5). In the following, percentages of the total monoisotopic ion abundance (%TMIA) are used to express the relative abundances of compound classes (Hughey et al., 2002; Poetz et al., 2014). The HC class is the dominant compound group within both the FI oils (42.5% to 44 %TMIA) and SR extracts (34.1% to 41.8 %TMIA). The N_1 compound class shows a slightly higher abundance in the SR extracts (average value 15.8 %TMIA) compared to the FI oils (average value 12.1 %TMIA). In contrast, the O_1, N_1O_1 and S_1 compound classes show a stronger variability between FI oils and SR samples. The O_1 class is the most abundant O_x class in all samples, showing a significant enrichment in the SR extracts (average value 17 %TMIA) compared to the FI oils (average value 12.5 %TMIA). The same trend can be observed for the N_1O_1 class with on average 7.2 %TMIA for the SR extracts and 2.9 %TMIA for the FI oils. In contrast, the S_1 compound class exhibits an opposite trend with enrichment in the FI oils of on average 12 %TMIA compared to 7 %TMIA in the SR extracts. There is less difference within the O_2 class between SR extracts and FI oils (both ~ 5 %TMIA). The relative abundance of the remaining compound classes e.g., O_3, O_4, $N_1O_{2\text{-}8}$ and $S_1O_{2\text{-}8}$, are lower than 5 %TMIA and will, therefore, not be discussed here in detail.

Figure 4.6 displays the average double bond equivalents (DBE) values and carbon numbers of all assessed compounds in the SR extracts and FI oils. The mean DBE values in the SR extracts (15.5 on average) are higher than those in the FI oils (11.2 on average) which suggests that compounds in the retained bitumen show a higher aromatic character and molecular size. The mean carbon number of compounds in SR extracts (38.4 on average) is similar to that in the FI oils (37.9 on average) implying that there is no preferential expulsion of compounds with a specific carbon number range.

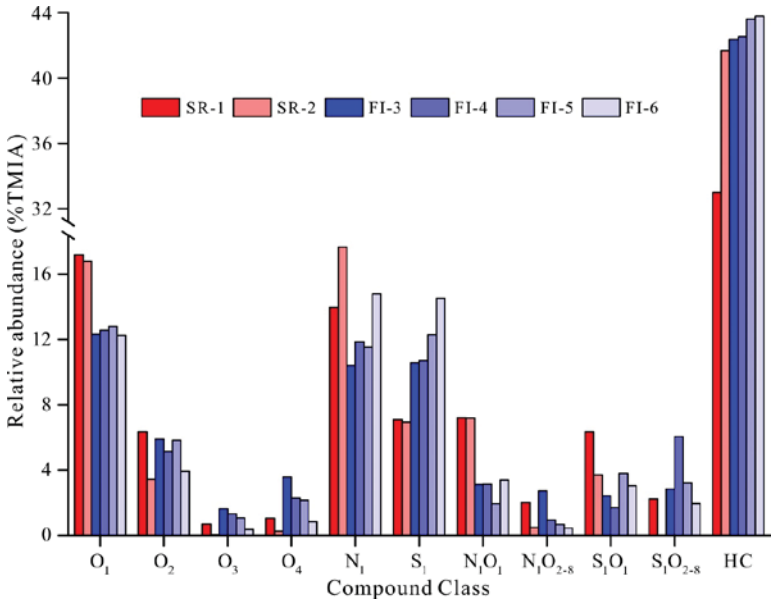

Figure 4.5. Relative abundances of the main compound classes within the source rock (SR) extracts and fluid inclusion (FI) oils from the HCMF marl in the Mecsek Mountains (Hungary) measured by FT-ICR-MS in APPI (+) mode. HC = hydrocarbons.

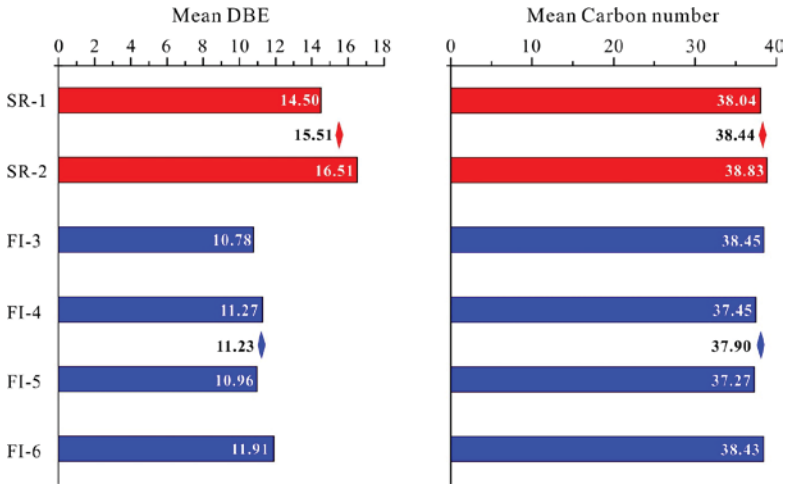

Figure 4.6. Mean double bond equivalents (DBE) values and carbon numbers of all assessed compounds detected by FT-ICR-MS in APPI (+) mode in source rock (SR) extracts and fluid inclusion (FI) oils from the HCMF marl in the Mecsek Mountains, Hungary. Colored rhombus represents the average mean value of each sample type.

4.5.5 Compositional changes of individual compound classes using FT-ICR-MS

In addition to the quantitative changes of individual compound classes presented above, the FT-ICR-MS technique allows compositional changes within the compound

classes to be assessed with regard to their carbon number range and DBE distributions. Thus, in the following sections, the main compound classes (HC, S_1, O_1, O_2, and N_1) were described in more detail to reveal fractionation within each of these classes during primary oil migration. Here, the normalized abundance (%) within a DBE or carbon number distribution is expressed relative to the total monoisotopic ion abundance of each individual compound and DBE class, respectively.

4.5.5.1 HC compounds

The APPI (+) mode ionizes mainly aromatic HC compounds (DBE ≥ 4) with small amounts of non-aromatic cyclic compounds (Huba et al., 2016a). A closer look into the HC DBE distribution (Fig. 4.7a) reveals that the HC species in the SR extracts cover a DBE range from 3 to 35 with a maximum at DBE 10 or 11, followed by a gradual decrease with an intermediate smaller maximum at DBE 20. In contrast, FI oils show a DBE range from 3 to 30 with a maximum at DBE 9 or 10, followed by a steep and asymptotic decrease (Fig. 4.7a).

Based on their DBE values, the HC compounds are sorted into three groups, $DBE_{1–5}$, $DBE_{6–15}$ and DBE_{15+}, termed low, medium and high DBE compound groups, which represent compounds with different level of aromaticity and molecular size (the classification is the same for other compound classes described below). The relative abundances of the three HC DBE groups are plotted in Figure 4.7b. The FI oils are dominated by the $DBE_{6–15}$ group (on average 67.4%) followed by the DBE_{15+} (on average 22.4%) and the $DBE_{1–5}$ (on average 10.2%) groups. The SR extracts consist of almost equal amounts of the $DBE_{6–15}$ group (on average 48.9%) and the DBE_{15+} group (on average 46.1%). The $DBE_{1–5}$ group occurs only in relatively low abundance in the SR extracts (on average 5.0%). Obviously, the SR extracts are more enriched in DBE_{15+} compounds relative to the FI oils, while the FI oils contain a higher proportion of low and medium DBE group compounds. Moreover, HC compounds with high $DBE_{30–35}$ are absent in FI oils.

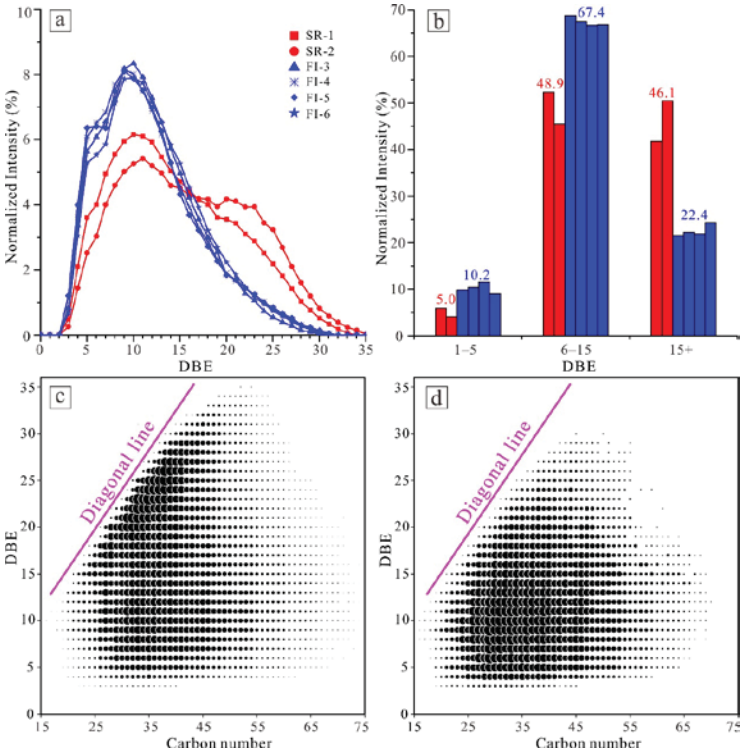

Figure 4.7. a) Double bond equivalent (DBE) distributions of hydrocarbon (HC) in the two source rocks (SR-1 and SR-2) extracts (red) and four fluid inclusion (FI-3 to FI-6) oils (blue). b) Normalized intensity of the low ($DBE_{1–5}$), medium ($DBE_{6–15}$) and high (DBE_{15+}) DBE groups of HCs in the SR extracts (red) and FI oils (blue) with numbers indicating average values. c) DBE versus carbon number plot of HCs in a representative SR extract (SR-2). d) DBE versus carbon number plot of HCs in a representative FI oil (FI-6). The normalized intensity (%) is expressed relative to the total monoisotopic ion abundance of the HC class. The magenta colored diagonal line delineates the minimum carbon number of a non-alkylated planar polycyclic aromatic core molecule within every DBE class.

Looking into the carbon number distributions depicted by the DBE versus carbon number plots of one representative SR extract and one FI oil (Figs. 4.7c and 4.7d), the higher DBE classes (15–30) in the SR extract are dominated by compounds with carbon numbers between 25 and 45 close to a diagonal line which represents the minimum carbon number of a non-alkylated planar polycyclic aromatic core molecule within the respective DBE class. Compounds along this line are therefore aromatic compounds with a low degree of alkylation (Poetz et al., 2014; Mahlstedt et al., 2016). In contrast, the carbon number distributions in the FI oil per DBE class is shifted to higher carbon numbers showing a Gaussian distribution maximizing at carbon number

ranges that represent polycyclic aromatic compounds with medium alkylation degree.

4.5.5.2 S_1 compounds

The APPI (+) method is also sensitive for the ionization of organosulfur compounds from crude oil and sediment extracts (Purcell et al., 2006). S_1 compounds appear to be significantly more enriched in FI oils than in SR extracts (Fig. 4.5). The DBE distribution of the S_1 class in FI oils and SR extracts are significantly different (Fig. 4.8a). A bimodal DBE distribution with DBE values from 2 to 26 is displayed for the FI oils. The DBE distribution reveals two maxima: a smaller one at DBE 6 and a larger one at DBE 10. By comparison, the DBE values range from 6 to 31 in the SR extracts and show only one broad maximum between 12 and 23. The DBE $\geq$ 3 S_1 compounds are most likely aromatic compounds that bear a thiophene unit, while S_1 compounds with lower DBE number can be interpreted to represent alkyl thiolanes (tetrahydrothiophenes) or alkyl thianes (tetrahydrothiopyrans) (Liu et al., 2018).

As for the HCs, the S_1 compounds are separated into three DBE groups. The SR extracts do not contain any $DBE_{1–5}$ S_1 compounds, but significant proportions of $DBE_{6–15}$ (on average 43.2%) and especially DBE_{15+} compounds (on average 56.8%). In contrast, FI oils exhibit the highest content of $DBE_{6–15}$ compounds (on average 70.9%), and significantly lower amounts of DBE_{15+} S_1 compounds (on average 19.3%). $DBE_{1–5}$ S_1 compounds occur at least with an average share of 9.8%. Comparing the two sample types, the low and medium DBE S_1 groups are dominant in the FI oils, while the high DBE group is most abundant among the S_1 compounds in the SR extracts. Moreover, S_1 compounds with DBEs from 27 to 31 are not observed in the FI oils.

Looking into the DBE versus carbon number distributions of one representative SR extract and one FI oil (Figs. 4.8c and 4.8d), the higher DBE classes (15–31) in the SR extract are dominated by compounds with carbon numbers between 22 and 43 close to the diagonal line, indicating a low alkylation degree of the polyaromatic system. In contrast, the carbon number distributions in the FI oil are shifted to higher carbon numbers showing a Gaussian distribution and thus a higher degree of

alkylation of the polyaromatic ring system. In the SR extract high molecular weight S_1 compounds with carbon number above 50 are missing in all DBE classes. However, this is due to instrumental limitation: the resolving power of the FT-ICR-MS instrument in the broadband mode is for this sample too low to separate the signal of these S_1 compounds from another compound group in the high molecular mass range.

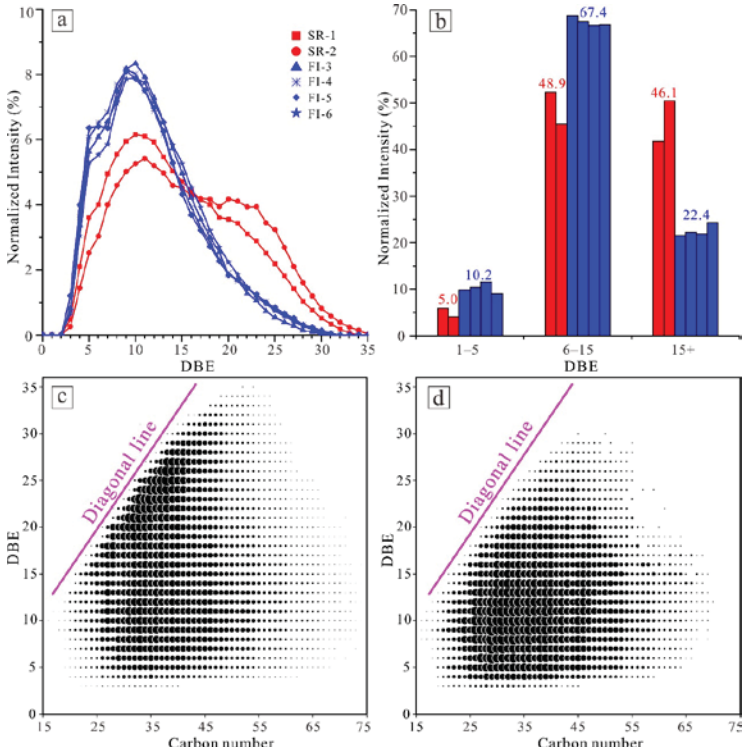

Figure 4.8. a) Double bond equivalent (DBE) distributions of the S_1 compound class in the two source rocks (SR-1 and SR-2) extracts (red) and four fluid inclusion (FI-3 to FI-6) oils (blue). b) Normalized intensity distribution of the three DBE groups $DBE_{1–5}$ (low), $DBE_{6–15}$ (medium) and DBE_{15+} (high) of S_1 class in the SR extracts (red) and FI oils (blue) with average value indicated. c) DBE versus carbon number plot of the S_1 class in a representative SR extract (SR-2). d) DBE versus carbon number plot of the S_1 class in a representative FI oil (FI-6). The normalized intensity (%) is expressed relative to the total monoisotopic ion abundance of the S_1 class. The magenta colored diagonal line delineates the minimum carbon number of a non-alkylated planar polycyclic aromatic core molecule within every DBE class. Note that S_1 compounds with carbon numbers above 50 in the SR extract are not included due to instrumental resolving power limitations for S_1 compounds in the here investigated SR sample (see text).

4.5.5.3 O_1 compounds

O_1 compounds detected with APPI (+) mode are suspected to be aliphatic and aromatic aldehydes, alcohols, ketones and furans (Huba et al., 2016a). The O_1 compounds are the most abundant oxygen-containing compounds in both the SR extracts and FI oils and the relative abundance of O_1 species is higher in the SR extracts than in the FI oils (Fig. 4.5). The clear increase of oxygenated hydrocarbons in crude oils with weathering has been reported by Huba et al. (2016b), but this is not the case here since fresh HCMF marl samples were collected from abandoned quarry. For the O_1 class, the SR extracts have a monomodal DBE distribution with DBE values in the range between 1 and 32 (Fig. 4.9a). In comparison, the FI oils show a DBE distribution between 1 and 27 DBE, and exhibit an odd-over-even carbon number predominance in the DBE 1 to 9 range (except for sample FI-4) with a maximum at DBE 1 and an additional maximum between DBE 10 and 15.

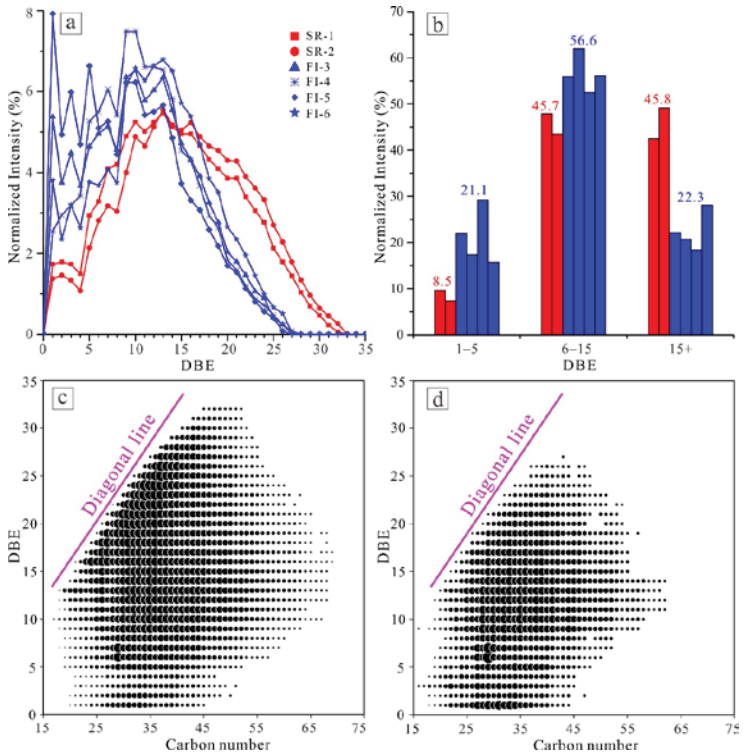

Figure 4.9. a) Double bond equivalent (DBE) distributions of the O_1 compound class in the two source rocks (SR-1 and SR-2) extracts (red) and four fluid inclusion (FI-3 to FI-6) oils (blue). b) Normalized intensity distribution of the three DBE groups $DBE_{1–5}$ (low), $DBE_{6–15}$ (medium) and DBE_{15+} (high) for the O_1 class in the SR extracts (red) and FI oils (blue) with average value

indicated. c) DBE versus carbon number plot of the O_1 class in a representative SR extract (SR-2). d) DBE versus carbon number plot of the O_1 class in a representative FI oil (FI-6). The normalized intensity (%) is expressed relative to the total monoisotopic ion abundance of the O_1 class. The magenta colored diagonal line delineates the minimum carbon number of a non-alkylated planar polycyclic aromatic core molecule within every DBE class.

Figure 4.9b exhibits the intensity distribution of the three classified DBE groups. The FI oils are dominated by O_1 compounds in the $DBE_{6–15}$ group (on average 56.6%) followed by O_1 compounds in the DBE_{15+} (on average 22.3%) and $DBE_{1–5}$ groups (on average 21.1%). The SR extract show high abundances of O_1 compounds within the DBE_{15+} (on average 45.8%) and $DBE_{6–15}$ (on average 45.7%) groups followed by compounds from the $DBE_{1–5}$ group (on average 8.5%). In comparison, the SR extracts are dominated by the medium and high DBE group compounds, while the FI oils are dominated by the medium DBE group compounds.

In the DBE versus carbon number plot the maximum of O_1 species in the representative SR extract is also located close to the diagonal line with higher DBEs and lower carbon numbers (Fig. 4.9c). In contrast, in the FI oil O_1 compounds are more centered at lower DBE numbers: one center is in the DBE range from 9 to 18 and carbon numbers in the range between 20 and 50 and another center is in the DBE range from 1 to 6 and carbon numbers ranging from 20 to 40 (Fig. 4.9d).

4.5.5.4 O_2 compounds

The O_2 compounds are the second abundant oxygen class (Fig. 4.5). O_2 compounds detected in ESI (–) mode are regarded as tools to assess the level of biodegradation (Kim et al., 2005; Hughey et al., 2007). However, in APPI (+) mode they are not well studied, and they could be mixed aliphatic and aromatic dialdehydes, dialcohols, diketones and difurans or carboxylic acids (Huba et al., 2016a). The FI oils have a monomodal DBE distribution with DBE values in the range between 1 and 22, with a maximal relative abundance at DBE 2. The SR extracts show a wider DBE range from 2 to 28 and there is no apparent predominance of certain DBEs (Fig. 4.10a).

The FI oils show high relative O_2 compound abundances in the $DBE_{1–5}$ (on average 52.0%) and $DBE_{6–15}$ groups (on average 39.8%) followed by the DBE_{15+} group (on average 8.2%). In contrast, the SR extracts show highest abundance in the DBE_{15+} (on average 46.4%) and $DBE_{6–15}$ (on average 43.6%) groups and low abundance in the $DBE_{1–5}$ group (on average 10.1%) (Fig. 4.10b). Interestingly, all of the DBE 1 compounds are absent in SR extracts but present in FI oils. Moreover, DBE 2 compounds are very dominant in FI oils in contrast to the SR extracts (Fig. 4.10a).

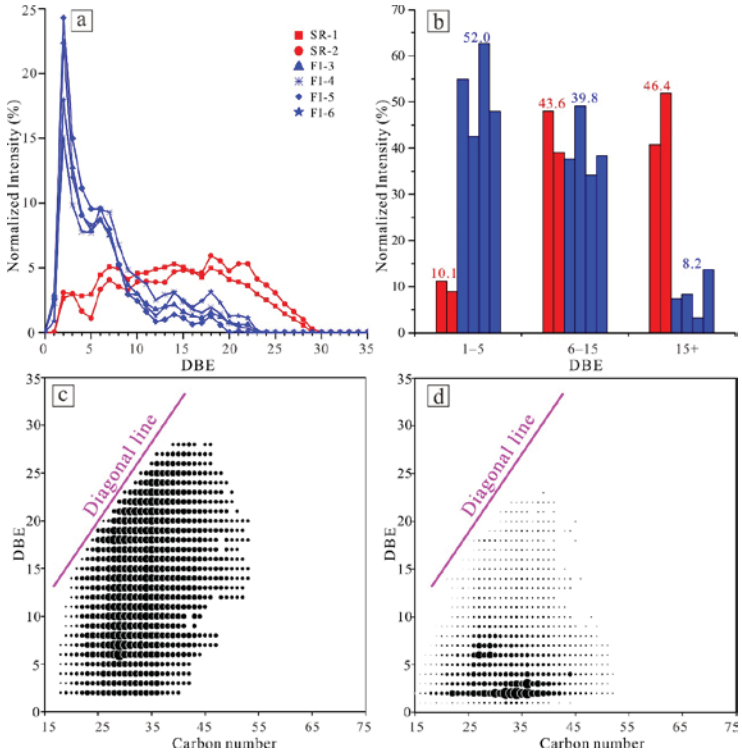

Figure 4.10. a) Double bond equivalent (DBE) distributions of the O_2 compound class in the two source rocks (SR-1 and SR-2) extracts (red) and four inclusion (FI-3 to FI-6) oils (blue). b) Normalized intensity distribution of the three DBE groups $DBE_{1–5}$ (low), $DBE_{6–15}$ (medium) and DBE_{15+} (high) for the O_2 class in SR extracts (red) and FI oils (blue) with average value indicated. c) DBE versus carbon number plot of the O_2 class in a representative SR extract (SR-1). d) DBE versus carbon number plot of the O_2 class in a representative FI oil (FI-3). The normalized intensity (%) is expressed relative to the total monoisotopic ion abundance of O_2 class. The magenta colored diagonal line delineates the minimum carbon number of a non-alkylated planar polycyclic aromatic core molecule within every DBE class.

The DBE versus carbon number plots indicate that high molecular weight compounds from C_{16} to C_{54} with higher DBEs ranging from 2 to 29 are preferentially present in the SR extract (Fig. 4.10c), while high molecular weight O_2 compounds ranging from C_{16} to C_{52} with low DBEs from 2 to 8 are preferentially found in the FI oil (Fig. 4.10d).

4.5.5.5 N_1 compounds

Both pyrrolic (with nitrogen in a five-membered ring) and pyridinic (with nitrogen in a six-membered ring) compounds can be ionized and identified by APPI (+) mode (Marshall and Rodgers, 2008). The relative ion abundances of the N_1 compounds are quite variable between the two SR extracts but especially among the FI oils. Overall, N_1 compound abundance might be a bit higher in the SR extracts than in the FI oils (Fig. 4.5). However, there are significant differences within the DBE distributions (Fig. 4.11a). Both show a monomodal distribution, but in the FI oils the DBEs range from 5 to 27 with a maximum around DBE 12 and in the SR extracts DBEs range from 7 to 34 with a maximum around DBE 19 or 21.

A closer look into the three classified DBE groups (Fig. 4.11b) shows that the FI oils are dominated by N_1 compounds in the $DBE_{6–15}$ group (on average 63.6%), followed by the DBE_{15+} group (on average 36.3%) and only very low amounts in the $DBE_{1–5}$ (on average 0.1%) group. The SR extracts are dominated by N_1 compounds in the DBE_{15+} (on average 67.9%) followed by the $DBE_{6–15}$ group (on average 32.1%). As already seen for the other compound classes also the N_1 compounds in the SR extracts show their highest proportion in the DBE_{15+} class while in the FI oil the $DBE_{6–15}$ class is the most abundant. Also, the predominance of N_1 compound in the SR extract in the DBE versus carbon number plot is shifted close to the diagonal line in the higher DBE range (Fig. 4.11c). Generally, high $DBE_{28–34}$ compounds are only retained in SR and are not expelled. In contrast, the DBE versus carbon number distribution in the FI oil show a Gaussian distribution shifted to higher carbon numbers and maximizing at carbon number ranges similar to HC class (Fig. 4.11d).

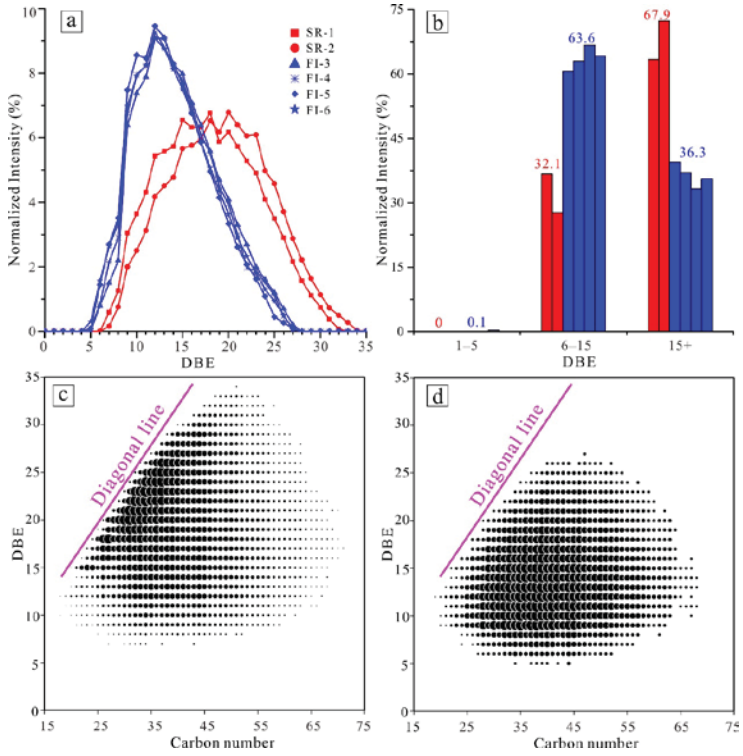

Figure 4.11. a) Double bond equivalent (DBE) distributions of the N_1 compound class in the two source rocks (SR-1 and SR-2) extracts (red) and four inclusion (FI-3 to FI-6) oils (blue). b) Normalized intensity distribution of the three DBE groups $DBE_{1–5}$ (low), $DBE_{6–15}$ (medium) and DBE_{15+} (high) for N_1 class in SR extracts (red) and FI oils (blue) with average value indicated. c) DBE versus carbon number plot of the N_1 class in a representative SR extract (SR-2). d) DBE versus carbon number plot of the N_1 class in a representative FI oil (FI-6). The normalized intensity (%) is expressed relative to the total monoisotopic ion abundance of the N_1 class. The magenta colored line represents the diagonal line indicating the minimum carbon number of a non-alkylated planar polycyclic aromatic core molecule within every DBE class.

4.6 Discussion

4.6.1 Correlation of SR extracts and FI oils by facies biomarkers, maturity indicators and stable carbon isotopes

Hopanes and steranes were widely used for tracing facies differences and similarities of the SR extracts and FI oils (Peters et al., 2005). High steranes/17α-hopanes ratio in both SR extracts and FI oils reflects an origin of marine organic matter (OM) with major contributions from planktonic and/or benthic algae material (Moldowan et al., 1985; Peters et al., 2005). The predominance of C_{27} steranes and

the significant amount C_{35} homohopane suggests OM with a high proportion of microalgae deposited in dysoxic to anoxic environments (Moldowan et al., 1985; Peters and Moldowan, 1991). High diasteranes/steranes ratios commonly indicate clay-rich source rocks (Peters et al., 2005), while the reverse can be observed in some organic-lean carbonate rocks (Clark and Philp, 1989). The diasteranes/steranes values of the SR extracts are in accordance with their marly lithofacies typical for calcareous deposits with a distinct clay content (Clark and Philp, 1989). Overall, the source-related parameters suggest that the FI oils are derived from SRs deposited under anoxic marine environmental conditions, which is in agreement with a previous study showing that HCMF marl was deposited in an open marine, relatively deep basin (Raucsik, 2012c).

Concerning their level of maturity both the SR extracts and FI oils are beyond the early oil generation window, as indicated by similar C_{31}αβ-22S/(22S + 22R) hopane ratios having reached its equilibrium (0.59) (Seifert and Moldowan, 1980). The similar C_{29}ααα-20S/(20S + 20R) sterane ratios confirm the similar maturity stages of SR extracts and FI oils. The same is true for the Ts/(Ts + Tm) ratios, although the value of SR-1 is lower than SR-2 which might reflect some compositional heterogeneity in the source rock facies. However, the C_{29}αββ/(αββ + ααα) sterane ratios are equivocal, exhibiting slightly higher maturity levels for the SR extracts than for the FI oils. The maturity-related parameters can be affected by source OM input (Peters et al., 2005), but FI oils should have been derived from the same source rock deposited under similar marine environmental conditions. Fractionation induced by oil migration has also been debated for steranes and hopanes for long time (Seifert and Moldowan, 1981; Han et al., 2017), which can lead to different sterane and hopane ratios in expelled fluids compared to the retained bitumen. In addition to the hopane and sterane derived maturity parameters, further thermal maturity information can be gained from the phenanthrene maturity ratios, which are not affected by expulsion fractionation (Leythaeuser et al., 1988c). The substantially identical Rc values suggest that the maturity of FI oils are equal to SR extracts. Thus, although there are some individual variabilities in the biomarker maturity parameters, most parameters indicate equal maturation stages for the SR extracts and the FI oils.

The stable carbon isotopic compositions of the *n*-alkanes are useful for oil-source correlations, since the *n*-alkane isotope signatures of a crude oil are primarily controlled by the OM input (Sofer et al., 1984; Bjorøy et al., 1994; Murray et al., 1994). Figure 4.4 exhibits that the carbon isotopic signatures of *n*-alkanes in the SR extracts and FI oils are essentially in the same range, which points to an origin of the FI oils trapped in calcite veins from HCMF marl SRs. However, the increasing deviation of the carbon isotopic compositions in the long chain *n*-alkane range (> C_{29}) of the SR extracts and the FI oils (Fig. 4.4) might be caused by isotopic fraction that is induced by thermal maturation or migration during the generation and expulsion process (Sofer et al., 1984; Tissot and Welte, 1984; Clayton, 1991; Dzou and Hughes, 1993; Cramer et al., 1998; Liao and Geng, 2009). Since the thermal maturation of both SR extracts and FI oils has been shown to be in a similar range, it is suggested that the slightly heavier $\delta^{13}C$ signal of long chain *n*-alkanes in the expelled oils (FI oils) is the result of fluid migration. Higher molecular weight HCs are preferential adsorbed onto mineral surfaces (George et al., 1998) and it is suggested that such a preferential adsorption also leads to a slight isotopic fractionation with an enrichment of heavier *n*-alkanes in the FI oils.

Thus, based on the biomarker parameters and carbon isotope signatures presented here, the HCMF marl SRs correlate very well with the investigated FI oils. In consequence, it can be assumed that when the HCMF reached the oil window, oil expulsion occurred and the expelled oil was trapped in pre-formed calcite veins as secondary inclusions (Fig. 4.2c). These FI oils are suggested to preserve the original information of the expelled fluids from the HCMF marl. Due to the similar maturity levels between SR extracts and FI oils, the maturity of Rc 0.74% can be regarded as the onset of oil expulsion from the HCMF marl, otherwise the maturity level in the FI oils, representing early oil expulsion, should be lower than in the SR extracts. Although a bit higher, the onset of oil expulsion for HCMF marl is in the same range as other source rocks such as the Posidonia shale with a vitrinite reflectance (Ro) of 0.68% (Rullkötter et al., 1988; Mahlstedt et al., 2016) and the North Sea Spekk shale at a vitrinite reflectance equivalents (VRE) of 0.7% (Heum et al., 1986).

4.6.2 Compositional fractionation during primary migration revealed by FT-ICR-MS

The organic components distributed throughout the marl are variably partitioned between the oil and brine phases, and the carbonate and clay mineral surfaces (Mann et al., 1997). It is suggested that the migration behavior can depend on the functional group and its polarity, shielding effects concerning the functional group due to specific molecular configurations and on the molecular shape (e.g., aromatic system, alkyl branches etc.) and size (Li et al., 1995; Larter et al., 1996; Poetz et al., 2014, 2020; Mahlstedt et al., 2016; Han et al., 2018a, 2018b; Yue et al., 2021).

4.6.2.1 Fractionations of different compound classes

O_1, N_1, N_1O_1 and S_1O_1 compounds are relatively enriched in the HCMF marl SR extracts when compared to the FI oils (Fig. 4.5), suggesting that these compound classes are preferentially retained in the SRs. In contrast, especially the S_1 compounds are more abundant in the FI oils, pointing to an overall preferential expulsion of these compound classes. O_2 compounds seem to show no preference. The HC class is the most dominant class in the SR extracts and FI oils (Fig. 4.5). However, a preference is not clear due to the variable relative abundance of the HC class in the SR extracts, which points to some heterogeneity within the source rock unit. These differences are suggested to be the expression of different adsorption affinities of these different functional groups (e.g., hydroxy, carbonyl, carboxyl, pyrrolic, carbazolic, thiophenic and thiol groups), on mineral surfaces in the oil-water-rock system (Larter and Aplin, 1995; Adams, 2014). Previous experiment and computer simulation studies have revealed that oxygen- and particularly nitrogen-containing compounds exhibit a higher adsorption affinity onto surfaces than sulfur-containing compounds, since sulfur represents a significantly weaker dipole (López-Linares et al., 2006; González et al., 2007; Adams, 2014; Ataman et al., 2016). In addition to this, the acidic and alkalinic character of functional groups are suggested to affect the adsorption process (Drummond et al., 2004; Adams, 2014). For instance, experimental work suggested that pyridinic nitrogen compounds preferentially adsorb on mineral surfaces compared with pyrrolic compounds (Reed, 1968; Larter and Aplin, 1995). Besides

that, source rocks comprise organic and inorganic materials containing various active sites that significantly interact with functional groups in oil constituents (Stanford et al., 2007). For example, Yue et al. (2021) showed that N_y and N_yO_x compounds are preferably retained in the biogenic carbonate-rich Barnett and biogenic quartz-rich Niobrara shale (USA) compared with other compound classes.

4.6.2.2 Effect of compound aromaticity on compositional fractionations

The assessment of the quantitative fractionation of different compound classes provides a first insight into the expulsion and retention behavior of these compound classes with respect to their functional groups. However, a deeper view into the component inventory of the different compound classes show significant differences in the compound composition with regard to DBE and carbon numbers when comparing SR extracts and FI oils.

To visualize those compositional differences for the DBEs of SR extracts and FI oils, the abundances of three DBE groups $DBE_{1–5}$ (low), $DBE_{6–15}$ (medium) and DBE_{15+} (high) are depicted in a triangular plot in Figure 4.12. The data clearly show that the bitumen retained in the SR is enriched in HC, S_1, O_1, O_2 and N_1 compounds with a higher proportion of DBEs. In contrast, the expelled fluid in the FI oils is enriched in respective compounds with a low to medium content of DBEs. Thus, the data from the HCMF marl imply that compounds with a higher aromaticity and due to the larger ring system a higher molecular size are preferentially retained, while those with a low to medium aromaticity and smaller molecular size are preferentially expelled. This finding is in agreement with studies comparing reservoir and source rock units (Mahlstedt et al., 2016; Han et al., 2018b; Yue et al., 2021), suggesting a preferential removal of compounds with lower DBEs during primary migration, while compounds with higher DBEs are preferentially retained in source rock. Moreover, compared to these previous studies (Mahlstedt et al., 2016; Han et al., 2018b) which focused on the nitrogen-containing compounds, the current results indicate that this preferential behavior is also true for other compound classes. Former asphaltene (condensed polyaromatic backbone strewn with heteroatoms) adsorption experiments and computer simulations indicated that larger aromatic ring systems and thus

increased aromaticity allow surface active areas of heteroatoms to more favorably adsorb onto surfaces (López-Linares et al., 2009; Marchal et al., 2010). For example, Plancher et al. (1977) found that 5-aromatic ring structured compounds adsorbed more firmly to mineral surfaces than 2-aromatic ring structured compounds. Additionally, Yue at al. (2021) showed that depending on the micropore size of the host rock, lower DBE species, representing smaller molecular sizes, migrate more easily out of the source rock compared with higher DBE species, resulting into the retention of these compounds in source rock. The same can be observed in this study for HCs and NSO-compounds with a higher degree of aromaticity (high DBEs) which are preferentially retained in the SRs. This deeper data evaluation shows that in addition to the functional group, structural properties play a major role for the fractionation behavior.

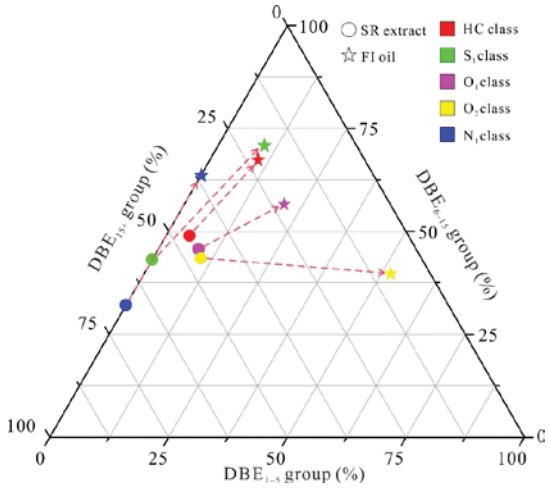

Figure 4.12. Ternary diagram of three double bond equivalents (DBE) groups $DBE_{1–5}$, $DBE_{6–15}$ and DBE_{15+} for hydrocarbon (HC), S_1, O_1, O_2, N_1 classes in source rock (SR) extracts (with average value) and fluid inclusion (FI-6) oils (with average value) from the HCMF (Hungary). Red arrow indicates the compositional changes between SR bitumen and expelled oil.

4.6.2.3 Effect of alkylation degrees on compositional fractionations

The degree of alkylation represents the length of alkyl side chains for a given compound class and/or DBE (Marshall and Rodgers, 2008). The shielding effect induced by aliphatic side chains, that could reduce interactions with the mineral active sites, was considered to affect the retention capacity (Li et al., 1995; Larter et al.,

1996; Mahlstedt et al., 2016; Yue et al., 2021). The FT-ICR-MS technique provides only information on the carbon number range (with regard to DBEs) and, therefore, maybe on the degree of alkylation, but gives no clue about the alkyl chain configuration within the molecule.

The carbon number range is in most cases comparable for the retained and expelled compounds, with exception of the S_1 compounds but this distribution is impaired by compound assignment problems as discussed above (Fig. 4.8). However, the data show that compounds with higher DBEs in the SR extracts are more enriched in the lower carbon number range (low alkylated species) close to the diagonal line which represents the minimum carbon number of a non-alkylated planar polycyclic aromatic core molecule within the respective DBE class (Figs. 4.7c–4.11c). Figure 4.13 exhibits the carbon number distribution of the representative DBE 12 (medium DBE range) and DBE 20 (high DBE range) classes of the N_1 and HC compounds in the SR extracts and FI oils. The medium DBE 12 class of the N_1 and HC compounds shows no preferential expulsion in terms of the carbon number (Fig. 4.13a). In contrast, in the higher DBE range (DBE 20) N_1 and HC compounds with shorter alkyl chains (lower carbon numbers) are preferentially retained in the SRs (Fig. 4.13b). This suggests that in these compounds the centers of increased interaction (hetero-atoms and aromatic rings) are less shielded by long alkyl chains in appropriate positions leading to their preferential retention in the SR.

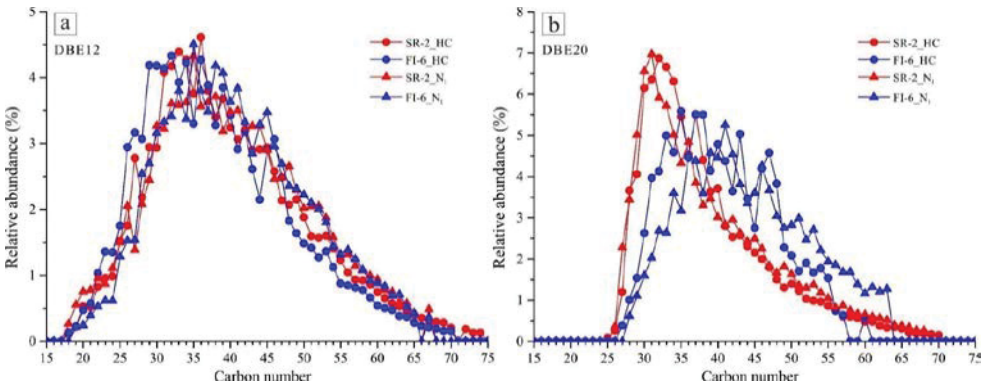

Figure 4.13. Carbon number distribution of a) the DBE 12 and b) DBE 20 class of N_1 and HC compounds in a representative source rock (SR-2) extract and fluid inclusion (FI-6) oil from the HCMF (Hungary). The relative abundance in percent is expressed relative to the total ion abundance of compounds for the DBE distribution.

Thus, although the FT-ICR-MS cannot provide direct structural information, the DBE versus carbon number plot can give insight into the alkylation degree of the retained and expelled compounds. The observation that those high DBE compounds with a lower degree of alkylation are preferentially retained suggests that shielding effects play an additional role for the retention and expulsion of the petroleum constituents.

4.7 Conclusions

The biomarker and stable carbon isotope data indicate that the investigated FI oils trapped in a calcite vein comprise expelled fluids from the adjacent HCMF marl source rock. On a functional group level the FT-ICR-MS measurements indicate that O_1, N_1, N_1O_1 and S_1O_1 compounds are preferentially retained in the source rock, while the S_1 compounds are preferentially expelled. O_2 compounds and HCs seem to show no clear preference. A deeper insight into the compound inventory shows that petroleum HCs and NSO-compounds with higher aromaticity are preferentially retained in the source rock during primary migration, which is especially true for high DBE compounds in the lower carbon number range which indicate a lower degree of alkylation and thus a less pronounced shielding effect.

4.8 Acknowledgements

The China Scholarship Council (CSC) is gratefully acknowledged for funding Yufu Han's research. Sophie Müller-Moewes and the Center for Junior Scholars (CJS) from the Technical University Berlin are also thanked for supporting me with a Short-term scholarship for foreign students (STIBET) degree completion grant enabling me to finish my thesis. We thank the National Research, Development and Innovation Office (grant no. K-138919) from Hungary for supporting this study. We extend our gratitude to Cornelia Karger, Anke Kaminsky, Andrea Vieth-Hillebrand and Doreen Noack for their technical support.

5. SUMMARY AND OUTLOOK

The main objective of this dissertation is to harness the full analytical potential of the Fourier transform-ion cyclotron resonance-mass spectrometry (FT-ICR-MS) technique for oil-bearing fluid inclusion (FI) research. Therefore, as a prerequisite, a suitable clean-up method for oil FI analysis had to be developed because of the high sensitivity of the FT-ICR-MS. The newly developed clean-up and crushing procedure for different host minerals enables the analysis of biomolecules and NSO-compounds in fluid inclusions using FT-ICR-MS (APPI (+) and ESI (–) modes) and GC-MS as well. At the same time, the FT-ICR-MS technique shifts the detectability of the biomolecules into the high molecular weight range, not accessible before. Another benefit of the presented procedure is that it can also be applied to carbonate mineral hosts since it does not employ acids.

To test the analytical potential of the FT-ICR-MS in FI research two geological case studies were conducted examining inclusion oils and sediment extracts by FT-ICR-MS in APPI (+) mode in combination with approaches such as microscopic, GC-MS and GC-IRMS analyses to address two petroleum systems related scientific questions. The first issue is to reconstruct the oil charge and leakage history in the North Sea Skarv oil field A segment using biomarkers, stable carbon isotope data and NSO-compounds in FI oils and Ad oil (reservoir oil remains). The second issue addresses the potential of HCs and NSO-compounds to discover compound fractionation processes during oil primary migration by comparing FI oils and source rock extracts.

5.1 Newly developed clean-up method for FI-ICR-MS research

Preliminary experiments indicate that previous clean-up methods developed for conventional analytical instruments (e.g., GC-FID and GC-MS) in FI oil research are not suitable for the FT-ICR-MS analysis with its ultra high sensitivity. Thus, a set of different oil FI containing host minerals comprising two quartz samples from

Germany (GE) and Pakistan (PK) and two fluorite samples from Tunisia (TN) and Mexico (MX) were investigated to develop a new protocol. Similar to the conventional clean-up method, the host minerals are cleaned by Soxhlet and ultrasonication in a several step process with pure and mixed organic solvents in sequence. However, in contrast to the conventional clean-up method applying strong acids for non-carbonate minerals and organic solvents for carbonate minerals, in the new protocol a Waller solution (33% sodium dithionite, 28% sodium bicarbonate, 59% sodium citrate in distilled water) was added to oxidize iron and organic matter on the surface of the host mineral fragments allowing the analysis of carbonate and non-carbonate host minerals with the same method. Afterwards, the outer surface of the host minerals is cleaned with organic solvents in an iterative process. The final washing step was measured on the FT-ICR-MS as procedural blank (P-blank), and pure solvent was measured as system blank (S-blank) of the FT-ICR-MS. Finally, the cleanness of the host mineral was examined by the comparison of S-blank and P-blank, which is different to the conventional clean-up method where an internal standard was used to check for the sample purity in the final solvent extract. Cleaned host minerals were crushed in a crushing cylinder equipped with two stainless steel balls by shaking. After crushing, the PK quartz sample showed the highest and the GE fluorite sample the lowest extraction yield, while the MX fluorite and TN quartz samples showed intermediate concentrations.

Despite of the rigorous cleaning measure contamination could not completely be avoided for all compound classes measured by the FT-ICR-MS. However, by comparing the compound classes and double bond equivalent (DBE) distributions within the samples with those from the P- and S-blank, the method allows to assess the cleanness of the samples concerning external contamination. Three different assessment categories were defined: Assessment category I represents a high contamination level, category II a low contamination level and category III a non-contamination level. In accordance with these three categories, the compound classes of the samples can be assessed as fully suitable (category III) or conditionally suitable (categories II) or unsuitable (category I) for further interpretation.

The data evaluation showed that the main (most abundant) compound classes are less affected by external contamination especially in APPI (+) mode and that external contamination plays an important role in low abundant compound classes. Thus, established parameters developed for characterizing petroleum by FT-ICR-MS can be determined for the main compound classes from FI oils as well. For instance, in the MX sample maturity indicators based on N_1, S_1 and HC compounds can be used to investigate the maturation stage of FI oil. In addition to the maturity parameters established biodegradation parameter based on O_2 compounds can be applied to FI oil analysis.

Overall, the newly developed clean-up methods enable the application of the FT-ICR-MS technique in FI research and to exploit the full potential of the FT-ICR-MS to solve geological issues trapped in FIs. Thus, to test this new analytical procedure for studying oil FIs, the new method was applied in two case studies to examine the oil charge and leakage history and compound fractionation processes during primary migration in natural petroleum systems.

5.2 Applications of hydrocarbons and NSO-compounds

5.2.1 Oil charge and leakage history

High frequency of oil FIs trapped in quartz cements from the Garn (Middle Jurassic) and Tilje (Early Jurassic) Formation (Fm) sandstones in in the Skarv field A segment in the Haltenbanken region, offshore Norway, represent paleo charged oils, while their corresponding adsorbed (Ad) oil residues from the outer mineral surfaces can also represent a later oil charge of the reservoir. The newly developed clean-up and crushing method, suitable for GC-MS, GC-IRMS and FT-ICR-MS, were applied to study these FI and Ad oils from the Skarv field to elucidate the charging and leakage history of the Garn and Tilje Fm.

The source-related biomarker parameters and specific stable carbon isotopic compositions of *n*-alkanes indicate that FI oils from the Garn and Tilje Fm and reservoir Ad oil from the Tilje Fm are derived from the same marine source rock,

while the Ad oil from the Garn Fm originated from another source rock which was deposited under slightly higher salinity conditions. The maturity-related biomarker parameters also show that the maturity of Ad and FI oils from the Tilje Fm are similar to the FI oils from the Garn Fm, while Ad oils from the Garn Fm are of lower maturity. Thus, Ad and FI oils from Tilje Fm and FI oil from Garn Fm are suggested to derive from the same charge, while the Ad oil from the Garn Fm is sourced from another less mature source. The similarity of FI oil in the Garn and Tilje Fm is also pointed out by NSO-compounds measured by FT-ICR-MS when comparing individual compound classes ($O_{1–3}$, N_1, N_1O_1 classes) using van Krevelen diagrams. Due to the low number of NSO-compounds measured by FT-ICR-MS in the Ad oils, differences to the Garn Ad oil, as indicated by the biomarker results, could not be confirmed by the FT-ICR-MS technique in this case.

The geological setting of Haltenbanken regions indicates that the initial oil charge was generated from Spekk Fm in the western area, where the Fm is subsided to deeper depth. The oil has migrated upwards along fault zones and charged both the Garn and Tilje reservoirs. While the initial oil charge in the Tilje reservoir was preserved, in the Garn reservoir it leaked and the Garn Fm was recharged by less mature oil. The recharged oil in Garn Fm is suggested to originate from another less mature kitchen area of the Spekk Fm, where petroleum was expelled during the rapid burial over the past 5 Ma.

In this comparison study, the application of the FT-ICR-MS technique is restricted due to the low number of detected NSO-compounds in the Ad oils from the Garn and Tilje reservoirs forming an important end member for the comparison. Nevertheless, the similarity of the FI oils from the Garn and Tilje Fm, assessed from the biomarkers, could also be confirmed by the FT-ICR-MS data. Thus, although the FT-ICR-MS technique could not deploy its full analytical potential in this study, it shows that NSO-compounds in FI can in principle be used to address geological issues in natural petroleum systems.

5.2.2 Compositional fractionation during primary migration

Calcite veins cut through the Hosszúhetény Calcareous Marl Formation (HCMF) in the Mecsek Mountains in Hungary, containing high abundance of oil FIs, which represent secondary fluid inclusions that were trapped in healed fractures showing pale bule and yellowish fluorescence under UV light. Oil FIs from these calcite veins are compared to adjacent source rock samples from the HCMF marl.

The source-related biomarker parameters suggest that FI oils derive from source rock deposited under anoxic marine environmental conditions, confirming that the FI oil derived from the adjacent HCMF marl source rock. Most of the maturity-related biomarker parameters from aliphatic and aromatic compounds indicate similar maturation stage of FI oils and HCMF SR extracts supporting this oil-source rock correlation. Additionally, stable carbon isotopic composition of *n*-alkanes in the FI oils and HCMF SR extracts are essentially in the same range. Thus, the oil trapped in the calcite veins most likely was expelled fluid from the HCMF marl source rock. Therefore, the FI oils represent expelled oils and the source rock extracts from the adjacent HCMF marl represent retained bitumen in this oil primary migration system.

To evaluate compositional fractionation during primary migration, the HCs and NSO-compounds in the FI oils and SR extracts from the HCMF were measured and compared using FT-ICR-MS in APPI (+) mode. The data revealed different retention and expulsion behaviors for individual compound classes. While O_1, N_1, N_1O_1 and S_1O_1 compounds are more relatively enriched in SR extracts suggesting a preferential retention, the S_1 compounds are more enriched in the FI oils pointing to an overall preferential expulsion. O_2 and HC compounds seem to show no preference. Moreover, the DBE distributions separated into three groups, $DBE_{1–5}$ (low), $DBE_{6–15}$ (medium) and DBE_{15+} (high), of the HC, S_1, O_1, O_2 and N_1 compounds show that the SR bitumen is enriched in compounds with higher numbers of DBEs, while the FI oils are enriched in respective compounds with a low to medium numbers of DBEs. In this context the DBE to carbon number relation suggest a higher aromaticity of the retained compounds in the bitumen. The carbon number range of compounds in the SR extracts and FI oils is comparable for the retained and expelled compounds.

Thus, the migration and retention of high molecular weight compounds in the HCMF during primary migration mainly depends on their functional groups with its different polarity and adsorption behaviors onto surfaces. Oxygen- and particularly nitrogen-containing compounds show higher adsorption affinity onto surfaces than sulfur-containing compounds. Furthermore, compounds with a higher degree of aromaticity show an increased retention ability, since the enhanced degree of aromatic rings and aromaticity allows a more favorably adsorption on active surface areas. On a first view, the molecular size indicated by the carbon number range seems to play a minor role. However, increased abundance of aromatic structures in the lower carbon number range (shorter alkyl chains) infers a less pronounced shielding effect of the heterocyclic aromatic ring systems by alkyl chains, which might support the retention of these compounds in the SR bitumen.

In contrast to the case study on the charging and leakage history, which was mainly driven by the biomarkers with only minor contributions of FT-ICR-MS data, in this study on the compound fractionation during primary migration the FT-ICR-MS data provide the main insight into the compositional changes of the oil fluids during the migration process. Therefore, this is an excellent example to show as to how the analytical potential of the FT-ICR-MS technique can be applied to FI research and to provide in-depth compositional information on the trapped petroleum. Thus, although this method still shows some limitation when it comes to very low compound amounts concerning compound detectability and contamination impact, the presented examples demonstrate the added value this newly developed method can provide to the conventional methods applied in FI research and how these different methods can be combined to gain a more sophisticated view on natural petroleum systems.

5.3 Outlook

The presented newly developed clean-up method opens the window for a new field of applications in FI research using the FT-ICR-MS technique as already indicated by the two presented case studies. The FT-ICR-MS significantly broadens the inventory of meaningful biomolecules in FI research into the high molecular

weight HC and NSO-compound range allowing a more comprehensive insight into petroleum systems. Thus, in a next step the new method should be tested in many different settings impacted by secondary processes to comprehensively investigate the potential of the new procedure to provide in-depth information into petroleum system evolution. For instance, the investigation of the original oil charge trapped in FI in petroleum reservoirs affected by biodegradation could be a very interesting next research target.

Furthermore, during oil exploration reservoir samples can be influenced by oil-based drilling mud contaminants interfering with the compositional evaluation of crude oils and reservoir oil extracts. Since oil trapped in FIs is not influenced by drilling mud, drilling mud contaminants attached on mineral surface can be removed by the rigorous clean-up method. Thus, the presented method provides a promising opportunity to investigate the original oil charge in drilling mud contaminated reservoir samples or cuttings.

Studies on biomarkers from FIs in Precambrian host minerals have been conducted to obtain information on the early evolution of life (Dutkiewicz et al., 2004; George et al., 2007a). It is exciting to imagine how fundamentally important studies on early life could in the future be significantly extended in scope and detail, if the methods presented in this thesis, namely concerning the collection of pristine samples and applying FT-ICR MS to elucidate polar compound geochemistry, are utilized.

REFERENCES

Adams, J.J., 2014. Asphaltene adsorption, a literature review. Energy & Fuels 28, 2831–2856.

Andersen, S.I., Speight, J.G., 2001. Petroleum resins: separation, character, and role in petroleum. Petroleum science and technology 19, 1–34.

Aplin, A.C., Macleod, G., Larter, S.R., Pedersen, K.S., Sorensen, H., Booth, T., 1999. Combined use of confocal laser scanning microscopy and PVT simulation for estimating the composition and physical properties of petroleum in fluid inclusions. Marine and Petroleum Geology 16, 97–110.

Ataman, E., Andersson, M.P., Ceccato, M., Bovet, N., Stipp, S.L.S., 2016. Functional group adsorption on calcite: II. Nitrogen and sulfur containing organic molecules. The Journal of Physical Chemistry C 120, 16597–16607.

Baron, M., Parnell, J., Mark, D., Carr, A., Przyjalgowski, M., Feely, M., 2008. Evolution of hydrocarbon migration style in a fractured reservoir deduced from fluid inclusion data, Clair Field, west of Shetland, UK. Marine and Petroleum Geology 25, 153–172.

Barwise, T., Hay, S., 1996. Predicting oil properties from core fluorescence. In: Schumacher, D., Abrams, M.A. (Eds.), Hydrocarbon Migration and its Nearsurface Expression. AAPG Memoir, pp. 363–371.

Bejaoui, J., Bouhlel, S., Barca, D., 2013. Geology, mineralogy and fluid inclusions investigation of the fluorite deposit at Jebel Kohol, northeastern Tunisia. Period Mineral 82, 217–237.

Benchilla, L., Guilhaumou, N., Mougin, P., Jaswal, T., Roure, F., 2003. Reconstruction of palaeo-burial history and pore fluid pressure in foothill areas: a sensitivity test in the Hammam Zriba (Tunisia) and Koh-i-Maran (Pakistan) ore deposits. Geofluids 3, 103–123.

Bennett, B., Buckman, J.O., Bowler, B.F.J., Larter, S.R., 2004. Wettability alteration in petroleum systems: the role of polar non-hydrocarbons. Petroleum Geoscience 10, 271–277.

Betz, D., Führer, F., Greiner, G., Plein, E., 1987. Evolution of the Lower Saxony basin. Tectonophysics 137, 127–170.

Bhullar, A.G., Karlsen, D.A., Backer-Owe, K., Seland, R.T., Le Tran, K., 1999. Dating reservoir filling–a case history from the North Sea. Marine and Petroleum Geology 16, 581–603.

Bjorøy, M., Hall, P.B., Moe, R.P., 1994. Stable carbon isotope variation of *n*-alkanes in Central Graben oils. Organic Geochemistry 22, 355–381.

Blanc, P., Connan, J., 1994. Preservation, degradation, and destruction of trapped oil. In: Magoon, L.B., Dow, W.G. (Eds.), The Petroleum System-From Source to Trap. AAPG Memoir 60, pp. 237–247.

Bodnar, R.J., 1990. Petroleum migration in the Miocene Monterey Formation, California, USA: constraints from fluid inclusion studies. Mineralogical Magazine 54, 295–304.

Bodnar R.J., 2003. Introduction to aqueous fluid systems. In: Samson, I., Anderson, A., Marshall, D. (Eds.), Fluid Inclusions: Analysis and Interpretation. Mineral. Assoc. Canada, Short Course 32, 81–99.

Bouhlel, S., Fortuné, J.P., Guilhaumou, N., Touray, J.C., 1988. Les minéralisations stratiformes à F-Ba de Hammam Zriba, Jebel Guébli (Tunisie nord orientale): l'apport des études d'inclusions fluides à la modélisation génétique. Mineralium Deposita 23, 166–173.

Bourdet, J., Eadington, P., Volk, H., George, S.C., Pironon, J., Kempton, R., 2012. Chemical changes of fluid inclusion oil trapped during the evolution of an oil reservoir: Jabiru-1A case study (Timor Sea, Australia). Marine and Petroleum Geology 36, 118–139.

Burruss, R.C., 1981. Hydrocarbon fluid inclusions in studies of sedimentary diagenesis. In: Hollister, L.S., Crawford, M.L. (Eds.), Fluid inclusions: Applications to Petrology, vol. 6. Mineralogical Association of Canada Short Course Notes, pp. 138–156.

Burruss, R.C., Cercone, K.R., Harris, P.M., 1985. Timing of hydrocarbon migration: evidence from fluid inclusions in calcite cements, tectonics, and burial history. Society of Economic Paleontologists and Mineralogists Special Publication 36, 277–289.

Burruss, R.C., 1987. Crushing cell, capillary column gas chromatography of petroleum inclusions: method and application to petroleum source beds, reservoirs and low hydrothermalores. In: Roedder, E., Kozlowski, A. (Eds.), Fluid Inclusion Research 20, p. 59.

Burruss, R.C., 2003. Petroleum fluid inclusions, an introduction. In: Samson, I., Anderson, A., Marshall, D. (Eds.), Fluid Inclusions: Analysis and Interpretation. Short Course Series, vol. 32. Mineralogical Association of Canada, Ottawa, pp. 159–174.

Cao, J., Yao, S., Jin, Z., Hu, W., Zhang, Y., Wang, X., Zhang, Y., Tang, Y., 2006. Petroleum migration and mixing in the northwestern Junggar Basin (NW China): constraints from oil-bearing fluid inclusion analyses. Organic Geochemistry 37, 827–846.

Cathles, L.M., Smith, A.T., 1983. Thermal constraints on the formation of Mississippi Valley-type lead-zinc deposits and their implications for episodic basin dewatering and deposit genesis. Economic Geology 78, 983–1002.

Chen, Y., Zou, C., Mastalerz, M., Hu, S., Gasaway, C., Tao, X., 2015. Applications of micro-fourier transform infrared spectroscopy (FTIR) in the geological sciences—a review. International journal of molecular sciences 16, 30223–30250.

Clark, J.P., Philp, R.P., 1989. Geochemical characterization of evaporite and carbonate depositional environments and correlation of associated crude oils in the Black Creek Basin, Alberta. Bulletin of Canadian Petroleum Geology 37, 401–416.

Clayton, C.J., 1991. Effect of maturity on carbon isotope ratios of oils and condensates. Organic Geochemistry 17, 887–899.

Clegg, H., Wilkes, H., Oldenburg, T., Santamaría-orozco, D., Horsfield, B., 1998. Influence of maturity on carbazole and benzocarbazole distributions in crude oils and source rocks from the Sonda de Campeche, Gulf of Mexico. Organic Geochemistry 29, 183–194.

Clementz, D.M., 1976. Interaction of petroleum heavy ends with montmorillonite. Clays and Clay Minerals 24, 312–319.

Cobbold, P.R., Zanella, A., Rodrigues, N., Løseth, H., 2013. Bedding-parallel fibrous veins (beef and cone-in-cone): Worldwide occurrence and possible significance in terms of fluid overpressure, hydrocarbon generation and mineralization. Marine and Petroleum Geology 43, 1–20.

Cohen, M.J., Dunn, M.E., 1987. The hydrocarbon habitat of the Haltenbank-Traenabank area offshore Mid-Norway. In: Brooks, J., Glennie, K. (Eds.), Geology of north west Europe: London. Graham and Trotman, pp. 1091–1104.

Comisarow, M.B., Marshall, A.G., 1974a. Fourier transform ion cyclotron resonance spectroscopy. Chemical Physics Letters, 25, 282–283.

Comisarow, M.B., Marshall, A.G., 1974b. Frequency-sweep Fourier transform ion cyclotron resonance spectroscopy. Chemical Physics Letters, 26, 489–490.

Conliffe, J., Burden, E.T., Wilton, D.H., 2017. The use of integrated fluid inclusion studies for constraining petroleum charge history at Parsons Pond, Western Newfoundland, Canada. Minerals 7, 39.

Connan, J., 1984. Biodegradation of crude oils in reservoirs. In: Brooks, J., Welte, D.H. (Eds.), Advances in Petroleum Geochemistry, vol. 1. Academic Press, London, pp. 299–335.

Cramer, B., Krooss, B.M., Littke, R., 1998. Modeling isotope fractionation during primary cracking of natural gas: a reaction kinetic approach. Chemical Geology 149, 235–250.

Crocker, M.E., Marchin, L.M., 1988. Wettability and adsorption characteristics of crude-oil asphaltene and polar fractions. Journal of Petroleum Technology 40, 470–474.

Cross, M.M., Manning, D.A., Bottrell, S.H., Worden, R.H., 2004. Thermochemical sulphate reduction (TSR): experimental determination of reaction kinetics and implications of the observed reaction rates for petroleum reservoirs. Organic Geochemistry 35, 393–404.

Csontos, L., 1995. Tertiary tectonic evolution of the Intra-Carpathian area: a review. Acta Vulcanol 7, 1–13.

Csontos, L., Benkovics, L., Bergerat, F., Mansy, J., Wórum, G., 2002. Tertiary deformation history from seismic section study and fault analysis in a former European Tethyan margin (the Mecsek-Villány area, SW Hungary). Tectonophysics 357, 81–102.

Cui, D., Li, J., Zhang, X., Zhang, L., Chang, H., Wang, Q., 2021. Pyrolysis temperature effect on compositions of basic nitrogen species in Huadian shale oil using positive-ion ESI FT-ICR MS and GC-NCD. Journal of Analytical and Applied Pyrolysis 153, 104980.

Dahl, B., Speers, G.C., 1985. Organic Geochemistry of the Oseberg Field (1). In: Graham & Trotman. (Eds.), Petroleum geochemistry in exploration of the Norwegian shelf. Norwegian Petroleum Society, pp. 185–196.

de Hoffmann, E., Stroobant, V., 2007. Mass Spectrometry: Principles and Applications, 3rd ed.; John Wiley & Sons, Ltd.: Chichester, U.K.

Dickinson, E.M., 1980. Structural comparison of petroleum fractions using proton and ^{13}C n.m.r. spectroscopy. Fuel 59, 290–294.

dos Santos Rocha, Y., Pereira, R.C.L., Mendonça Filho, J.G., 2018. Geochemical characterization of lacustrine and marine oils from off-shore Brazilian sedimentary basins using negative-ion electrospray Fourier transform ion cyclotron resonance mass spectrometry (ESI FTICR-MS). Organic Geochemistry 124, 29–45.

Drummond, C., Israelachvili, J., 2004. Fundamental studis of crude oil–surface water interactions and its relationship to reservoir wettability. Journal of Petroleum Science and Engineering 45, 61–81.

Dubey, S.T., Waxman, M.H., 1991. Asphaltene adsorption and desorption from mineral surfaces. SPE Reservoir Engineering 6, 389–395.

Dutkiewicz, A., Volk, H., Ridley, J., George, S.C., 2004. Geochemistry of oil in fluid inclusions in a middle Proterozoic igneous intrusion: implications for the source of hydrocarbons in crystalline rocks. Organic Geochemistry 35, 937–957.

Dzou, L.I., Hughes, W.B., 1993. Geochemistry of oils and condensates, K Field, offshore Taiwan: a case study in migration fractionation. Organic Geochemistry 20, 437–462.

Ehrenberg, S.N., 1990. Relationship between diagenesis and reservoir quality in sandstones of the Garn Formation, Haltenbanken, mid-Norwegian continental shelf. AAPG Bulletin 74, 1538–1558.

Ehrenberg, S.N., Skjevrak, I., Gilje, A.E., 1995. Asphaltene-rich residues in sandstone reservoirs of Haltenbanken province, mid-Norwegian continental shelf. Marine and Petroleum Geology 12, 53–69.

England, W.A., Mackenzie, A.S., Mann, D.M., Quigley, T.M., 1987. The movement and entrapment of petroleum fluids in the subsurface. Journal of the Geological Society of London 144, 327–347.

Etminan, H., Hoffmann, C.F., 1989. Biomarkers in fluid inclusions: A new tool in constraining source regimes and its implications for the genesis of Mississippi Valley-type deposits. Geology 17, 19–22.

Fenn, J.B., Mann, M., Meng, C.K., Wong, S.F., Whitehouse, C.M., 1989. Electrospray ionization for mass spectrometry of large biomolecules. Science 246, 64–71.

Főzy, I., 2012. Magyarország litosztratigráfiai alapegységei. Jura. Hungarian Geological Society, Budapest, pp. 10. (in Hungarian)

Gan, S., Guo, P., Wu, Y., Zhao, Y., 2021. A Novel Method for Unraveling the Black Box of Dissolved Organic Matter in Soils by FT-ICR-MS Coupled with Induction-Based Nanospray Ionization. Environmental Science & Technology Letters. 8, 356–361.

George, S.C., Lisk, M., Eadington, P.J., Quezada, R.A., Krieger, F.W., Greenwood, P.F., Wilson, M.A., 1996. Comparison of palaeo oil charges with currently reservoired hydrocarbons using the geochemistry of oil-bearing fluid inclusions. Society of Petroleum Engineers, Asia Pacific Oil and Gas Conference, SPE paper 36980, Adelaide, Australia, pp. 159–171.

George, S.C., Greenwood, P.F., Logan, G.A., Quezada, R.A., Pang, L.S.K., Lisk, M., Krieger, F.W., Eadington, P.J., 1997a. Comparison of palaeo oil charges with currently reservoired hydrocarbons using molecular and isotopic analyses of oil bearing fluid inclusions: Jabiru oil field, Timor Sea. Australian Petroleum Production and Exploration Association Journal 37, 490–504.

George, S.C., Krieger, F.W., Eadington, P.J., Quezada, R.A., Greenwood, P.F., Eisenberg, LI., Hamilton, P.J., Wilson, M. A., 1997b. Geochemical comparison of oil-bearing fluid inclusions and produced oil from the Toro sandstone, Papua New Guinea. Organic Geochemistry 26, 155–173.

George, S.C., Lisk, M., Summons, R.E., Quezada, R.A., 1998. Constraining the oil charge history of the South Pepper oilfield from the analysis of oil-bearing fluid inclusions. Organic Geochemistry 29, 631–648.

George, S.C., Ruble, T.E., Dutkiewicz, A., Eadington, P.J., 2001. Assessing the maturity of oil trapped in fluid inclusions using molecular geochemistry data and visually-determined fluorescence colours. Applied Geochemistry 16, 451–473.

George, S.C., Volk, H., Ruble, T.E., Brincat, M.P., Lisk, M., 2002. Evidence for an unusual oil family in the Nancar Trough area, Timor Sea. The Australian Petroleum Production and Exploration Association Journal 42, 387–404.

George, S.C., Ruble, T.E., Volk, H., Lisk, M., Brincat, M.P., Dutkiewicz, A., Ahmed, M., 2004a. Comparing the geochemical composition of fluid inclusion and crude oils from wells on the Laminaria High, Timor Sea. In: Ellis, G.K., Baillie, P.W., Munson, T.J. (Eds.), Timor Sea Petroleum Geoscience, Proceedings of The Timor Sea Symposium, Darwin, Northern Territory, 19–20 June 2003. Northern Territory Geological Survey, Special Publication, vol. 1, pp. 203–230.

George, S.C., Ahmed, M., Liu, K., Volk, H., 2004b. The analysis of oil trapped during secondary migration. Organic Geochemistry 35, 1489–1511.

George, S.C., Volk, H., Ahmed, M., 2007a. Geochemical analysis techniques and geological applications of oil-bearing fluid inclusions, with some Australian case studies. Journal of Petroleum Science and Engineering 57, 119–138.

George, S.C., Volk, H., Ahmed, M., Pickel, W., Allan, T., 2007b. Biomarker evidence for two sources for solid bitumens in the Subu wells: implications for the petroleum prospectivity of the East Papuan Basin. Organic Geochemistry 38, 609–642.

Germann, A., Jochum, J., Friedrich, G., Horsfield, B., 1995. The sandstone-hosted lead–zinc deposits of Maubach/Mechernich—a new genetic model based on thermochemical sulfate reduction. Zentralblatt für Geologie und Paläontologie, Teil I, 1995.11/12, 1133–1139.

Goldstein, R.H., Reynolds, T.J., 1994. Systematics of fluid inclusions in diagenetic minerals. SEPM Short Course 31, 1–199.

Goldstein, R.H., 2003. Petrographic analysis of fluid inclusions. In: Samson, I., Anderson, A., Marshall, D. (Eds.), Fluid inclusions: Analysis and interpretation. Short Course Series, vol. 32. Mineralogical Association of Canada, Ottawa, pp. 9–55.

González, M.F., Stull, C.S., López-Linares, F., Pereira-Almao, P., 2007. Comparing asphaltene adsorption with model heavy molecules over macroporous solid surfaces. Energy & Fuels 21, 234–241.

González-Partida, E., Carrillo-Chávez, A., Grimmer, J.O.W., Pironon, J., 2002. Petroleum-rich fluid inclusions in fluorite, Purisima mine, Coahuila, Mexico. International Geology Review 44, 755–764.

González-Partida, E., Carrillo-Chávez, A., Grimmer, J.O.W., Pironon, J., Mutterer, J., Levresse, G., 2003. Fluorite deposits at Encantada-Buenavista, Mexico: products of Mississippi Valley type processes. Ore Geology Reviews 23, 107–124.

Grantham, P.J., Posthuma, J., de Groot, K., 1980. Variation and significance of the C_{27} and C_{28} triterpane content of a North Sea core and various North Sea crude oils. Physics and Chemistry of the Earth 12, 29–38.

Greenwood, P.F., George, S.C., Hall, K., 1998. Applications of laser micropyrolysis– gas chromatography–mass spectrometry. Organic Geochemistry 29, 1075–1089.

Griffiths, M.T., Da Campo, R., O'Connor, P.B., Barrow, M.P., 2014. Throwing light on petroleum: simulated exposure of crude oil to sunlight and characterization using atmospheric pressure photoionization Fourier transform ion cyclotron resonance mass spectrometry. Analytical Chemistry 86, 527–534.

Guan, S., Marshall, A.G., Scheppele, S.E., 1996. Resolution and chemical formula identification of aromatic hydrocarbons and aromatic compounds containing sulfur, nitrogen, or oxygen in petroleum distillates and refinery streams. Analytical chemistry 68, 46–71.

Guigue, J., Harir, M., Mathieu, O., Lucio, M., Ranjard, L., Lévêque, J., Schmitt-Kopplin, P., 2016. Ultrahigh-resolution FT-ICR mass spectrometry for molecular characterisation of pressurised hot water-extractable organic matter in soils. Biogeochemistry 128, 307–326.

Guilhaumou, N., Szydlowskii, N., Pradier, B., 1990. Characterization of hydrocarbon fluid inclusions by infra-red and fluorescence microspectrometry. Mineralogical Magazine 54, 311–324.

Guilhaumou, N., Ellouz, N., Jaswal, T.M., Mougin, P., 2000. Genesis and evolution of hydrocarbons entrapped in the fluorite deposit of Koh-i-Maran, (North Kirthar Range, Pakistan). Marine and Petroleum Geology 17, 1151–1164.

Haas, J., Hámor, G., Korpás, L., 1999. Geological setting and tectonic evolution of Hungary. Geologica Hungarica. Series Geologica 24, 179–196.

Haas, J., 2012. Geology of Hungary. Springer Science & Business Media.

Hagemann, H.W., Hollerbach, A., 1986. The fluorescence behaviour of crude oils with respect to their thermal maturation and degradation. Organic Geochemistry 10, 473–480.

Han, Y., Mahlstedt, N., Horsfield, B., 2015. The Barnett Shale: Compositional fractionation associated with intraformational petroleum migration, retention, and expulsion. AAPG Bulletin 99, 2173–2202.

Han, Y., Horsfield, B., Curry, D.J., 2017. Control of facies, maturation and primary migration on biomarkers in the Barnett Shale sequence in the Marathon 1 Mesquite well, Texas. Marine and Petroleum Geology 85, 106–116.

Han, Y., Poetz, S., Mahlstedt, N., Karger, C., Horsfield, B., 2018a. Fractionation and origin of NyOx and Ox compounds in the Barnett Shale sequence of the Marathon 1 Mesquite well, Texas. Marine and Petroleum Geology 97, 517–524.

Han, Y., Poetz, S., Mahlstedt, N., Karger, C., Horsfield, B., 2018b. Fractionation of pyrrolic nitrogen compounds during primary migration of petroleum within the Barnett Shale sequence of Marathon 1 Mesquite Well, Texas. Energy & Fuels 32, 4638–4650.

Han, Y., Noah, M., Lüders, V., Horsfield, B., Mangelsdorf, K., 2020. NSO-compounds in oil-bearing fluid inclusions revealed by FT-ICR-MS in APPI (+) and ESI (–) modes: A new method development. Organic Geochemistry 149, 104113 .

Han, Y., Horsfield, B., Mahlstedt, N., Noah, M., 2021. Chemostatistic allocation of shale oil production using acidic heterocompounds. AAPG Bulletin 105, 2207–2219.

Hayes, J., Freeman, K.H., Popp, B.N., Hoham, C.H., 1990. Compound-specific isotopic analyses: a novel tool for reconstruction of ancient biogeochemical processes. Organic Geochemistry 16, 1115–1128.

Harayama, S., Kishira, H., Kasai, Y., Shutsubo, K., 1999. Petroleum biodegradation in marine environments. Journal of Molecular Microbiology and Biotechnology 1, 63–70.

Heum, O.R., Dalland, A., Meisingset, K.K., 1986. Habitat of hydrocarbons at Haltenbanken (PVT-modelling as a predictive tool in hydrocarbon exploration). In: Spencer, A.M. (Ed.), Habitat of hydrocarbons on the Norwegian continental shelf. Graham & Trotman, pp. 259–274.

Hirasaki, G.J., Lo, S.W., Zhang, Y., 2003. NMR properties of petroleum reservoir fluids. Magnetic Resonance Imaging 21, 269–277.

Ho, T.Y., Rogers, M.A., Drushel, H.V., Koons, C.B., 1974. Evolution of sulfur compounds in crude oils. AAPG Bulletin 58, 2338–2348.

Horsfield, B., McLimans, R.K., 1984. Goethermometry and geochemistry of aqueous and oil-bearing fluid inclusions from Fateh Field, Dubai. Organic Geochemistry 6, 733–740.

Horsfield, B., 1989. Practical criteria for classifying kerogens: some observations from pyrolysis-gas chromatography. Geochimica et Cosmochimica Acta 53, 891–901.

Horsfield, B., 1997. The bulk composition of first-formed petroleum in source rocks, Petroleum and basin evolution. Springer, pp. 335–402.

Horsfield, B., Clegg, H., Wilkes, H., Santamaria-Orozco, D., 1998. Effect of maturity on carbazole distributions in petroleum systems: new insights from the Sonda de Campeche, Mexico, and Hils Syncline, Germany. Naturwissenschaften 85, 233–237.

Horstad, I., Larter, S.R., Dypvik, H., Aagaard, P., Bjørnvik, A.M., Johansen, P.E., Eriksen, S., 1990. Degradation and maturity controls on oil field petroleum column heterogeneity in the Gullfaks field, Norwegian North Sea. Organic Geochemistry 16, 497–510.

Hosseini, S.H., Horsfield, B., Poetz, S., Wilkes, H., Yalçın, M.N., Kavak, O., 2017. Role of maturity in controlling the composition of solid bitumens in veins and vugs from SE Turkey as revealed by conventional and advanced geochemical tools. Energy & Fuels 31, 2398–2413.

Hsu, C.S., Liang, Z., Campana, J.E., 1994. Hydrocarbon characterization by ultrahigh resolution Fourier transform ion cyclotron resonance mass spectrometry. Analytical Chemistry 66, 850–855.

Huba, A.K., Huba, K., Gardinali, P.R., 2016a. Understanding the atmospheric pressure ionization of petroleum components: The effects of size, structure, and presence of heteroatoms. Science of The Total Environment 568, 1018–1025.

Huba, A.K., Gardinali, P.R., 2016b. Characterization of a crude oil weathering series by ultrahigh-resolution mass spectrometry using multiple ionization modes. Science of the Total Environment 563, 600–610.

Hughey, C.A., Rodgers, R.P., Marshall, A.G., Qian, K., Robbins, W.K., 2002. Identification of acidic NSO compounds in crude oils of different geochemical origins by negative ion electrospray Fourier transform ion cyclotron resonance mass spectrometry. Organic Geochemistry 33, 743–759.

Hughey, C.A., Rodgers, R.P., Marshall, A.G., Walters, C.C., Qian, K., Mankiewicz, P., 2004. Acidic and neutral polar NSO compounds in Smackover oils of different thermal maturity revealed by electrospray high field Fourier transform ion cyclotron resonance mass spectrometry. Organic Geochemistry 35, 863–880.

Hughey, C.A., Galasso, S.A., Zumberge, J.E., 2007. Detailed compositional comparison of acidic NSO compounds in biodegraded reservoir and surface crude oils by negative ion electrospray Fourier transform ion cyclotron resonance mass spectrometry. Fuel 86, 758–768.

Islam, A., Ahmed, A., Hur, M., Thorn, K., Kim, S., 2016. Molecular-level evidence provided by ultrahigh resolution mass spectrometry for oil-derived DOC in groundwater at Bemidji, Minnesota. Journal of Hazardous Materials 320, 123–132.

Jackson, J.S., Hastings, D.S., 1986. The role of salt movement in the tectonic history of Haltenbanken and Trænabanken and its relationship to structural style. In: Spencer, A.M. (Ed.), Habitat of hydrocarbons on the Norwegian continental shelf. Graham & Trotman, pp. 241–257.

Jensenius, J., Burruss, R.C., 1990. Hydrocarbon-water interactions during brine migration: evidence from hydrocarbon inclusions in calcite cements from Danish North Sea oil fields. Geochimica et Cosmochimica Acta 54, 705–713.

Jiang, B., Tian, Y., Zhai, Z., Zhan, Z., Liao, Y., Zou, Y., Peng, P., 2021. Characterisation of heteroatomic compounds in free and bound bitumen from different source rocks by ESI FT-ICR MS. Organic Geochemistry 151, 104147.

Jin, Z., Cao, J., Hu, W., Zhang, Y., Yao, S., Wang, X., Zhang, Y., Tang, Y., Shi, X., 2008. Episodic petroleum fluid migration in fault zones of the northwestern Junggar Basin (northwest China): Evidence from hydrocarbon-bearing zoned calcite cement. AAPG Bulletin 92, 1225–1243.

Jochum, J., Germann, A., Friedrich, G., Horsfield, B., Pickel, W., 1995a. Mechanical decrepitation coupled with gas chromatography—A new method for the determination of hydrocarbons in ore minerals, Mineral deposits: from their origin to their environmental impacts. Proceedings of the third biennial SGC meeting. Praha, pp. 560–757.

Jochum, J., Friedrich, G., Leythaeuser, D., Littke, R., Ropertz, B., 1995b. Hydrocarbon-bearing fluid inclusions in calcite-filled horizontal fractures from mature Posidonia Shale (Hils Syncline, NW Germany). Ore Geology Reviews 9, 363–370.

Jones, R.W., 1987. Organic facies. In: Brooks, J., Welte, H.D. (Eds.), Advances in Petroleum Geochemistry, Academic Press, London, 1–90.

Jones, D.M., Macleod, G., 2000. Molecular analysis of petroleum in fluid inclusions: a practical methodology. Organic Geochemistry 31, 1163–1173.

Karlsen, D.A., Nedkvitne, T., Larter, S.R., Bjørlykke, K., 1993. Hydrocarbon composition of authigenic inclusions: application to elucidation of petroleum reservoir filling history. Geochimica et Cosmochimica Acta 57, 3641–3659.

Karlsen, D.A., Nyland, B., Flood, B., Ohm, S.E., Brekke, T., Olsen, S., Backer-Owe, K., 1995. Petroleum geochemistry of the Haltenbanken, Norwegian continental shelf. Geological Society, London, Special Publications 86, 203–256.

Karlsen, D.A., Skeie, J.E., Backer-Owe, K., Bjørlykke, K., Olstad, R., Berge, K., Cecchi, M., Vik, E., Schaefer, R.G., 2004. Petroleum migration, faults and overpressure. Part II. Case history: the Haltenbanken Petroleum Province, offshore Norway. In: Cubitt, J.M., England, W.A., Larter, S.R. (Eds.), Understanding Petroleum Reservoirs: Towards an Integrated Reservoir Engineering and Geochemical Approach, Geological Society Special Publication 237. Geological Society Publishing House, London, pp. 305–372.

Karlsen, D.A., Skeie, J.E., 2006. Petroleum migration, faults and overpressure, part I: calibrating basin modelling using petroleum in traps—a review. Journal of Petroleum Geology 29, 227–256.

Kazankapov, A., 2019. Geochemistry of Natural Gases in the Vøring and Møre Basins, Norwegian Sea. Colorado School of Mines. Arthur Lakes Library.

Kelemen, S.R., Walters, C.C., Ertas, D., Freund, H., Curry, D.J., 2006. Petroleum expulsion part 3. A model of chemically driven fractionation during expulsion of petroleum from kerogen. Energy & Fuels 20, 309–319.

Kim, S., Kramer, R.W., Hatcher, P.G., 2003. Graphical method for analysis of ultrahigh-resolution broadband mass spectra of natural organic matter, the van Krevelen diagram. Analytical Chemistry 75, 5336–5344.

Kim, S., Stanford, L.A., Rodgers, R.P., Marshall, A.G., Walters, C.C., Qian, K., Wenger, L.M., Mankiewicz, P., 2005. Microbial alteration of the acidic and neutral polar NSO compounds revealed by Fourier transform ion cyclotron resonance mass spectrometry. Organic Geochemistry 36, 1117–1134.

Klein, G.C., Kim, S., Rodgers, R.P., Marshall, A.G., Yen, A., 2006. Mass spectral analysis of asphaltenes. II. Detailed compositional comparison of asphaltenes deposit to its crude oil counterpart for two geographically different crude oils by ESI FT-ICR MS. Energy & Fuels 20, 1973–1979.

Koch, B.P., Ludwichowski, K.U., Kattner, G., Dittmar, T., Witt, M., 2008. Advanced characterization of marine dissolved organic matter by combining reversed-phase liquid chromatography and FT-ICR-MS. Marine Chemistry 111, 233–241.

Kvenvolden, K.A., Roedder, E., 1971. Fluid inclusions in quartz crystals from South- West Afrika. Geochimica et Cosmochimica Acta 35, 1209–1229.

Larter, S.R., Aplin, A.C., 1995. Reservoir geochemistry: methods, applications and opportunities. In: Cubitt, J.M., England, W.A. (Eds.), The Geochemistry of Reservoirs. Geological Society of London, Special Publication, pp. 5–32.

Larter, S.R., Bowler, B.F.J., Li, M., Chen, M., Brincat, D., Bennett, B., Noke, K., Donohoe, P., Simmons, D., Kohnen, M., 1996. Molecular indicators of secondary oil migration distances. Nature 383, 593.

Lawrence, E.O., Edlefsen, N.E., 1930. On the production of high speed protons. Science 72, 376.

Lewan, M.D., 1997. Experiments on the role of water in petroleum formation. Geochimica et Cosmochimica Acta 61, 3691–3723.

Leythaeuser, D., Littke, R., Radke, M., Schaefer, R.G., 1988a. Geochemical effects of petroleum migration and expulsion from Toarcian source rocks in the Hils syncline area, NW-Germany. Organic Geochemistry 13, 489–502.

Leythaeuser, D., Schaefer, R.G., Radke, M., 1988b. Geochemical effects of primary migration of petroleum in Kimmeridge source rocks from Brae field area, North Sea. I: Gross composition of C_{15+}-soluble organic matter and molecular composition of C_{15+}-saturated hydrocarbons. Geochimica et Cosmochimica Acta 52, 701–713.

Leythaeuser, D., Radke, M., Willsch, H., 1988c. Geochemical effects of primary migration of petroleum in Kimmeridge source rocks from Brae field area, North Sea. II: Molecular composition of alkylated naphthalenes, phenanthrenes, benzo-and dibenzothiophenes. Geochimica et Cosmochimica Acta 52, 2879–2891.

Li, M., Larter, S.R., Stoddart, D., Bjorøy, M., 1995. Fractionation of pyrrolic nitrogen compounds in petroleum during migration: derivation of migration-related geochemical parameters. Geological Society, London, Special Publications 86, 103–123.

Li, S., Pang, X., Shi, Q., Zhang, B., Zhang, H., Pan, N., Zhao, M., 2011. Origin of the unusually high dibenzothiophene concentrations in Lower Ordovician oils from the Tazhong Uplift, Tarim Basin, China. Petroleum Science 8, 382–391.

Liao, Y., Geng, A., 2009. Stable carbon isotopic fractionation of individual *n*-alkanes accompanying primary migration: Evidence from hydrocarbon generation–expulsion simulations of selected terrestrial source rocks. Applied Geochemistry 24, 2123–2132.

Liao, Y., Shi, Q., Hsu, C.S., Pan, Y., Zhang, Y., 2012. Distribution of acids and nitrogen-containing compounds in biodegraded oils of the Liaohe Basin by negative ion ESI FT-ICR MS. Organic Geochemistry 47, 51–65.

Lisk, M., George, S.C., Summons, R.E., Quezada, R.A., O'Brien, G.W., 1996. Mapping hydrocarbon charge histories: detailed characterisation of the South Pepper oil field, Carnarvon Basin. Australian Petroleum Production and Exploration Association Journal 36, 445–464.

Liu, P., Xu, C., Shi, Q., Pan, N., Zhang, Y., Zhao, S., Chung, K.H., 2010. Characterization of sulfide compounds in petroleum: selective oxidation followed by positive ion electrospray Fourier transform ion cyclotron resonance mass spectrometry. Analytical Chemistry 82, 6601–6606.

Liu, P., Li, M., Jiang, Q., Cao, T., Sun, Y., 2015. Effect of secondary oil migration distance on composition of acidic NSO compounds in crude oils determined by negative-ion electrospray Fourier transform ion cyclotron resonance mass spectrometry. Organic Geochemistry 78, 23–31.

Liu, W., Liao, Y., Pan, Y., Jiang, B., Zeng, Q., Shi, Q., Hsu, C.S., 2018. Use of ESI FT-ICR MS to investigate molecular transformation in simulated aerobic biodegradation of a sulfur-rich crude oil. Organic Geochemistry 123, 17–26.

López-Linares, F., Carbognani, L., González, M.F., Sosa-Stull, C., Figueras, M., Pereira-Almao, P., 2006. Quinolin-65 and violanthrone-79 as model molecules for the kinetics of the adsorption of C_7 athabasca asphaltene on macroporous solid surfaces. Energy & Fuels 20, 2748–2750.

López-Linares, F., Carbognani, L., Sosa-Stull, C., Pereira-Almao, P., Spencer, R.J., 2009. Adsorption of virgin and visbroken residue asphaltenes over solid surfaces. 1. Kaolin, smectite clay minerals, and athabasca siltstone. Energy & Fuels 23, 1901–1908.

Lüders, V., Plessen, B., di Primio, R., 2012. Stable carbon isotopic ratios of CH_4-CO_2-bearing fluid inclusions in fracture-fill mineralization from the Lower Saxony Basin (Germany) – a tool for tracing gas sources and maturity. Marine and Petroleum Geology 30, 174–183.

Lüders, V., Plessen, B., 2015. Stable carbon isotope ratios of CH_4-rich gas inclusions in shale-hosted fracture-fill mineralization: a tool for tracing hydrocarbon generation and migration in shale plays for oil and gas. Marine and Petroleum Geology 63, 68–81.

Lukoczki, G., Schubert, F., Hámor-Vidó, M., 2012. Traces of hydrocarbon migration near Pécsvárad (Mecsek Mts.). Földtani Közlöny 142, 229–241.

Mackenzie, A.S., Leythaeuser, D., Schaefer, R.G., Bjorøy, M., 1983. Expulsion of petroleum hydrocarbons from shale source rocks. Nature 301, 506–509.

Macleod, G., Petch, G.S., Larter, S.R., Aplin, A.C., 1993. Investigations of the composition of hydrocarbon fluid inclusions. Abstracts of the 205th ACS National Meeting, Division of Geochemistry 86.

Mahlstedt, N., Horsfield, B., Wilkes, H., Poetz, S., 2016. Tracing the impact of fluid retention on bulk petroleum properties using nitrogen-containing compounds. Energy & Fuels 30, 6290–6305.

Mann, U., Hantschel, T., Schaefer, R.G., Krooss, B., Leythaeuser, D., Littke, R., Sachsenhofer, R.F., 1997. Petroleum migration: mechanisms, pathways, efficiencies and numerical simulations. In: Welte, D., Horsfield, B., Baker, D. (Eds.), Petroleum and Basin Evolution. Springer Berlin Heidelberg, pp. 403–520.

Manzano, B.K., Fowler, M.G., Machel, H.G., 1997. The influence of thermochemical sulphate reduction on hydrocarbon composition in Nisku reservoirs, Brazeau river area, Alberta, Canada. Organic Geochemistry 27, 507–521.

Marchal, C., Abdessalem, E., Tayakout-Fayolle, M., Uzio, D., 2010. Asphaltene diffusion and adsorption in modified NiMo alumina catalysts followed by ultraviolet (UV) spectroscopy. Energy & Fuels 24, 4290–4300.

Marshall, A.G., Rodgers, R.P., 2004. Petroleomics: the next grand challenge for chemical analysis. Accounts of Chemical Research 37, 53–59.

Marshall, A.G., Rodgers, R.P., 2008. Petroleomics: Chemistry of the underworld. Proceedings of the National Academy of Sciences 105, 18090–18095.

Martins, L.L., Pudenzi, M.A., da Cruz, G.F., Nascimento, H.D.L., Eberlin, M.N., 2017. Assessing biodegradation of Brazilian crude oils via characteristic profiles of O_1 and O_2 compound classes: Petroleomics by negative-ion mode electrospray ionization Fourier transform ion cyclotron resonance mass spectrometry. Energy & Fuels 31, 6649–6657.

McLimans, R.K., 1987. The application of fluid inclusions to migration of oil and diagenesis in petroleum reservoirs. Applied Geochemistry 2, 585–603.

Meredith, W., Kelland, S.J., Jones, D.M., 2000. Influence of biodegradation on crude oil acidity and carboxylic acid composition. Organic Geochemistry 31,1059–1073.

Minor, E.C., Steinbring, C.J., Longnecker, K., Kujawinski, E.B., 2012. Characterization of dissolved organic matter in Lake Superior and its watershed using ultrahigh resolution mass spectrometry. Organic Geochemistry 43, 1–11.

Mitchell, D.L., Speight, J.G., 1973. The solubility of asphaltenes in hydrocarbon solvents. Fuel 52, 149–152.

Moldowan, J.M., Seifert, W.K., Gallegos, E.J., 1985. Relationship between petroleum composition and depositional environment of petroleum source rocks. AAPG Bulletin 69, 1255–1268.

Munz, I.A., 2001. Petroleum inclusions in sedimentary basins: systematics, analytical methods and applications. Lithos 55, 195–212.

Murray, A.P., Summons, R.E., Boreham, C.J., Dowling, L.M., 1994. Biomarker and *n*-alkane isotope profiles for Tertiary oils: relationship to source rock depositional setting. Organic Geochemistry 22, 521–526.

Murray, R.C., 1957. Hydrocarbon fluid inclusions in quartz. AAPG Bulletin 41, 950–956.

Nedkvitne, T., Karlsen, D.A., Bjørlykke, K., Larter, S.R., 1993. Relationship between reservoir diagenetic evolution and petroleum emplacement in the Ula Field, North Sea. Marine and Petroleum Geology 10, 255–270.

Nichols, D., 2019. How to clean rocks and crystals. https://www.canoncitygeologyclub.com/uploads/4/5/5/2/45523343/how_to_clean_minerals_and_crystals.pdf.

Noah, M., Poetz, S., Vieth-Hillebrand, A., Wilkes, H., 2015. Detection of residual oil-sand-derived organic material in developing soils of reclamation sites by ultra-high-resolution mass spectrometry. Environmental Science & Technology 49, 6466–6473.

Noah, M., Volk, H., Schubert, F., Horsfield, B., 2018. First analysis of polar compounds trapped in fluid inclusions using ultra high resolution mass spectrometry – A proof of concept demonstrated on a case study from the Pannonian Basin (Hungary). Latin American Association of Organic Geochemistry (ALAGO), Salvador, Bahia, Brazil.

Noah, M., Volk, H., Schubert, F., Horsfield, B., 2019. Identification of NSO compounds trapped in fluid inclusions using FT-ICR-MS – A case study from the Pannonian Basin (Hungary). 29th International Meeting on Organic Geochemistry, Gothenburg, Sweden.

Noah, M., Horsfield, B., Han, S., Wang, C., 2020. Precise maturity assessment over a broad dynamic range using polycyclic and heterocyclic aromatic compounds. Organic Geochemistry 148, 104099.

O'Malley, V. P., Abrajano, T. A., Jr and Hellou, J. 1994. Determination of the $^{13}C/^{12}C$ ratios of individual PAH from environmental samples: can PAH sources be apportioned? Organic Geochemistry, 21, 809–22.

Ohno, T., He, Z., Sleighter, R.L., Honeycutt, C.W., Hatcher, P.G., 2010. Ultrahigh resolution mass spectrometry and indicator species analysis to identify marker components of soil- and plant biomass-derived organic matter fractions. Environmental Science & Technology, 44, 8594–8600.

Ohno, T., Parr, T.B., Gruselle, M.-C.I., Fernandez, I.J., Sleighter, R.L., Hatcher, P.G., 2014. Molecular composition and biodegradability of soil organic matter: a case study comparing two new England forest types. Environmental Science & Technology, 48, 7229–7236.

Oldenburg, T.B., Wilkes, H., Horsfield, B., Van Duin, A.C., Stoddart, D., Wilhelms, A., 2002. Xanthones—novel aromatic oxygen-containing compounds in crude oils. Organic Geochemistry 33, 595–609.

Oldenburg, T.B.P., Brown, M., Bennett, B., Larter, S.R., 2014. The impact of thermal maturity level on the composition of crude oils, assessed using ultra-high resolution mass spectrometry. Organic Geochemistry 75, 151–168.

Oldenburg, T.B.P., Jones, M., Huang, H., Bennett, B., Shafiee, N.S., Head, I., Larter, S.R., 2017. The controls on the composition of biodegraded oils in the deep subsurface – Part 4. Destruction and production of high molecular weight non-hydrocarbon species and destruction of aromatic hydrocarbons during progressive in-reservoir biodegradation. Organic Geochemistry 114, 57–80.

Oliveros, J.C., 2007. Venny. An interactive tool for comparing lists with Venn Diagrams. http://bioinfogp.cnb.csic.es/tools/venny/index.html.

Orr W.L., 1974. Changes in sulfur content and isotopic-ratios of sulfur during petroleum maturation–study of Big Horn Basin Paleozoic oils. AAPG Bulletin 58, 2295–2318.

Palmer, S.E., 1993. Effect of biodegradation and water washing on crude oil composition. In: Engel, M. H., Macko S. A. (Eds.), Organic Geochemistry, Plenum Press, New York, pp. 511–533.

Pan, C., Yang, J., Fu, J., Sheng, G., 2003. Molecular correlation of free oil and inclusion oil of reservoir rocks in the Junggar Basin, China. Organic Geochemistry 34, 357–374.

Pan, Y., Liao, Y., Shi, Q., Hsu, C.S., 2013. Acidic and neutral polar NSO compounds in heavily biodegraded oils characterized by negative-ion ESI FT-ICR MS. Energy & Fuels 27, 2960–2973.

Pan, Y., Li, M., Sun, Y., Li, Z., Liu, P., Jiang, B., Liao, Y., 2019. Characterization of free and bound bitumen fractions in a thermal maturation shale sequence. Part 1: Acidic and neutral compounds by negative-ion ESI FT-ICR MS. Organic Geochemistry 134, 1–15.

Pang, L.S.K., George, S.C., Quezada, R.A., 1998. A study of the gross compositions of oil-bearing fluid inclusions using high performance liquid chromatography. Organic Geochemistry 29, 1149–1161.

Parnell, J., Carey, P., Duncan, W., 1998. History of hydrocarbon charge on the Atlantic margin: Evidence from fluid-inclusion studies, West of Shetland. Geology 26, 807–810.

Parnell, J., Honghan, C., Middleton, D., Haggan, T., Carey, P., 2000. Significance of fibrous mineral veins in hydrocarbon migration: fluid inclusion studies. Journal of Geochemical Exploration 69, 623–627.

Parnell, J., Middleton, D., Chen, H., Hall, D., 2001. The use of integrated fluid inclusion studies in constraining oil charge history and reservoir compartmentation: examples from the Jeanne d'Arc Basin, offshore Newfoundland. Marine and Petroleum Geology 18, 535–549.

Pearson, C.D., Gharfeh, S.G., 1986. Automated high-performance liquid chromatography determination of hydrocarbon types in crude oil residues using a flame ionization detector. Analytical Chemistry 58, 307–311.

Pedersen, J.H., Karlsen, D.A., Backer-Owe, K., Lie, J.E., Brunstad, H., 2006. The geochemistry of two unusual oils from the Norwegian North Sea: implications for new source rock and play scenario. Petroleum Geoscience 12, 85–96.

Pestilho, A.L.S., Monteiro, L.V.S., Carbonezi, C.A., Jorge, S.B., Santos Neto, E.V., 2018. Linking the geochemistry of crude oils and petroleum inclusions in the Ubarana and Lorena oilfields, Potiguar Basin, Brazilian Equatorial Margin. Organic Geochemistry 124, 133–150.

Peters, C.A., Hallmann, C., George, S.C., 2018. Phenolic compounds in oil-bearing fluid inclusions: implications for water-washing and oil migration. Organic Geochemistry 118, 36–46.

Peters, K.E., Moldowan, J.M., 1991. Effects of source, thermal maturity, and biodegradation on the distribution and isomerization of homohopanes in petroleum. Organic Geochemistry 17, 47–61.

Peters, K.E., Walters, C.C., Moldowan, J.M., 2005. The Biomarker Guide: Biomarkers and Isotopes in Petroleum Exploration and Earth History, second ed. Cambridge University Press, Cambridge, UK.

Pironon, J., Barrés, O., 1990. Semi-quantitative FT-IR microanalysis limits: evidence from synthetic hydrocarbon fluid inclusions in sylvite. Geochimica et Cosmochimica Acta 54, 509–518.

Pironon, J., Canals, M., Dubessy, J., Walgenwitz, F., Laplace-Builhe, C., 1998. Volumetric reconstruction of individual oil inclusions by confocal scanning laser microscopy. European Journal of Mineralogy 10, 1143–1150.

Plancher, H., Dorrence, S.M., and Petersen, J.C., 1977. Identification of chemical types in asphalts strongly absorbed at the asphalt-aggregate interface and their relative displacement by water. Journal of Association of Asphalt PavingTechnologists 46, 151–175.

Poetz, S., Horsfield, B., Wilkes, H., 2014. Maturity-driven generation and transformation of acidic compounds in the organic-rich Posidonia shale as revealed by electrospray ionization Fourier transform ion cyclotron resonance mass spectrometry. Energy & Fuels 28, 4877–4888.

Poetz, S., Kuske, S., Song, Y., Jweda, J., Michael, E., Horsfield, B., 2020. Using polar nitrogen-, sulphur-and oxygen-compound compositions from ultra-high resolution mass spectrometry for petroleum fluid assessment in the Eagle Ford Formation, Texas. Geological Society, London, Special Publications 484, 71–96.

Potter, J., Longstaffe, F.J., 2007. A gas-chromatograph, continuous flow-isotope ratio mass-spectrometry method for $\delta^{13}C$ and δD measurement of complex fluid inclusion volatiles: examples from the Khibina alkaline igneous complex, northwest Russia and the South Wales coalfields. Chemical Geology 244, 186–201.

Purcell, J.M., Hendrickson, C.L., Rodgers, R.P., Marshall, A.G., 2006. Atmospheric pressure photoionization Fourier transform ion cyclotron resonance mass spectrometry for complex mixture analysis. Analytical Chemistry 78, 5906–5912.

Purcell, J.M., Juyal, P., Kim, D.-G., Rodgers, R.P., Hendrickson, C.L., Marshall, A.G., 2007. Sulfur speciation in petroleum: atmospheric pressure photoionization or chemical derivatization and electrospray ionization Fourier transform ion cyclotron resonance mass spectrometry. Energy & Fuels 21, 2869–2874.

Qian, K., Rodgers, R.P., Hendrickson, C.L., Emmett, M.R., Marshall, A.G., 2001. Reading chemical fine print: Resolution and identification of 3000 nitrogen-containing aromatic compounds from a single electrospray ionization Fourier transform ion cyclotron resonance mass spectrum of heavy petroleum crude oil. Energy & Fuels 15, 492–498.

Radke, M., Willsch, H., Welte, D.H., 1980. Preparative hydrocarbon group type determination by automated medium pressure liquid chromatography. Analytical Chemistry 52, 406–411.

Radke, M., Welte, D.H., 1983. The methylphenanthrene index (MPI): A maturity parameter based on aromatic hydrocarbons. In: Bjorøy, M. (Ed.), Advances in Organic Geochemistry. Wiley, Chichester, pp. 504–512.

Rathsack, P., Kroll, M.M., Otto, M., 2014. Analysis of high molecular compounds in pyrolysis liquids from a german brown coal by FT-ICR-MS. Fuel 115, 461–468.

Raucsik, B., Varga, A., 2008. Climato-environmental controls on clay mineralogy of the Hettangian–Bajocian successions of the Mecsek Mountains, Hungary: an evidence for extreme continental weathering during the early Toarcian oceanic anoxic event. Palaeogeography, Palaeoclimatology, Palaeoecology 265, 1–13.

Raucsik, B., 2012a. Zobákpuszta Sandstone Formation, In: Fozy, I. (Ed.), Jurassic Lithostratigraphic Units in Hungary, Hungarian Geological Society, Budapest, pp. 149–151. (in Hungarian)

Raucsik, B., 2012b. Vasas Marl Formation. In: Fozy, I. (Ed.), Jurassic Lithostratigraphic Units in Hungary, Hungarian Geological Society, Budapest, pp. 152–154. (in Hungarian)

Raucsik, B., 2012c. Hosszúhetény Calcarous Marl Formation. In: Fozy, I. (Ed.), Jurassic Lithostratigraphic Units in Hungary, Hungarian Geological Society, Budapest, pp. 155–158. (in Hungarian)

Raucsik, B., 2012d. Rékavölgy Siltstone Formation. In: Fozy, I. (Ed.), Jurassic Lithostratigraphic Units in Hungary, Hungarian Geological Society, Budapest, pp. 164–167. (in Hungarian)

Raucsik, B., 2012e. Komló Calcareous Marl Formation. In: Fozy, I. (Ed.), Jurassic Lithostratigraphic Units in Hungary, Hungarian Geological Society, Budapest, pp. 174–176. (in Hungarian)

Reed, M.G., 1968. Retention of crude oil bases by clay-containing sandstone. Clay and Clay Minerals 16, 173–178.

Reese, C.L., 1898. Petroleum inclusions in quartz crystals. Journal of the American Chemical Society 20, 795–797.

Riis, F., Wolff, A., 2020. Use of pore pressure data from the Norwegian continental shelf to characterize fluid flow processes in geological time scales. Geological Society, London, Special Publications 495, 176.

Robb, D.B., Covey, T.R., Bruins, A.P., 2000. Atmospheric pressure photoionization: an ionization method for liquid chromatography – mass spectrometry. Analytical Chemistry 72, 3653–3659.

Robbins, W.K., Hsu, C.S., 2000. Petroleum, composition. Kirk-Othmer Encyclopedia of Chemical Technology.

Robinson, A., Gluyas, J., 1992. Duration of quartz cementation in sandstones, North Sea and Haltenbanken Basins. Marine and Petroleum Geology 9, 324–327.

Rodgers, R.P., Marshall, A.G., 2007. Petroleomics: Advanced characterization of petroleum-derived materials by Fourier transform ion cyclotron resonance mass spectrometry (FT-ICR MS), Asphaltenes, Heavy Oils, and Petroleomics. In: Mullins, O.C., Sheu, E.Y., Hammami, A., Marshall, A.G. (Eds.), Asphaltenes, Heavy Oils, and Petroleomics. Springer, New York, pp. 63–93.

Roedder, E., 1984. Fluid inclusions. Mineralogical Society of America. Revues in Mineralogy 12, 1–644.

Rossel, P.E., Bienhold, C., Boetius, A., Dittmar, T., 2016. Dissolved organic matter in pore water of Arctic Ocean sediments: environmental influence on molecular composition. Organic Geochemistry 97, 41–52.

Ruble, T.E., George, S.C., Lisk, M., Quezada, R.A., 1998. Organic compounds trapped in aqueous fluid inclusions. Organic Geochemistry 29, 195–205.

Rullkötter, J., Leythaeuser, D., Horsfield, B., Littke, R., Mann, U., Müller, P.J., Radke, M., Schaefer, R.G., Schenk, H.J., Schwochau, K., Witte, E.G., Welte, D.H., 1988. Organic matter maturation under the influence of a deep intrusive heat source: A natural experiment for quantitation of hydrocarbon generation and expulsion from a petroleum source rock (Toarcian shale, northern Germany). Organic Geochemistry 13, 847–856.

Sandvik, E.I., Young, W.A., Curry, D.J., 1992. Expulsion from hydrocarbon sources: the role of organic absorption. Organic Geochemistry 19, 77–87.

Sarowha, S.L.S, Sharma, B.K., Sharma, C.D., Bhagat, S.D, 1997. Characterization of petroleum heavy distillates using HPLC and spectroscopic methods. Energy & Fuels 11, 566–569.

Schmidt, F., Koch, B.P., Witt, M., Hinrichs, K.-U., 2014. Extending the analytical window for water-soluble organic matter in sediments by aqueous Soxhlet extraction. Geochimica et Cosmochimica Acta 141, 83–96.

Schubert, F., Diamond, L.W., Tóth, T.M., 2007. Fluid-inclusion evidence of petroleum migration through a buried metamorphic dome in the Pannonian Basin, Hungary. Chemical Geology 244, 357–381.

Schwark, L., Stoddart, D., Keuser, C., Spitthoff, B., Leythaeuser, D., 1997. A novel sequential extraction system for whole core plug extraction in a solvent flow-through cell – application to extraction of residual petroleum from an intact pore-system in secondary migration studies. Organic Geochemistry 26, 19–31.

Seidel, M., Kleindienst, S., Dittmar, T., Joye, S.B., Medeiros, P.M., 2016. Biodegradation of crude oil and dispersants in deep seawater from the Gulf of Mexico: Insights from ultra-high resolution mass spectrometry. Deep Sea Research Part II: Topical Studies in Oceanography 129, 108–118.

Seifert, W.K., Moldowan, J.M., 1980. The effect of thermal stress on source-rock quality as measured by hopane stereochemistry. Physics and Chemistry of the Earth 12, 229–237.

Seifert, W.K., Moldowan, J.M., 1981. Paleoreconstruction by biological markers. Geochimica et Cosmochimica Acta 45, 783–794.

Shariatinia, Z., Feiznia, S., Shafiei, A., Haghighi, M., Mousavi Dehghani, A., Memariani, M., Farhadian, N., 2013. Multiple hydrocarbon charging events in Kuh-e-Mond oil field, Coastal Fars: evidence from biomarkers in oil inclusions. Geofluids 13, 594–609.

Shepherd, T.J., Rankin, A.H., Alderton, D.H.M.A., 1985. A Practical Guide to Fluid Inclusion Studies. Blackie, Chapman & Hall.

Shi, Q., Zhao, S., Xu, Z., Chung, K., Zhang, Y., Xu, C., 2010. Distribution of acids and neutral nitrogen compounds in a Chinese crude oil and its fractions: characterized by negative-ion electrospray ionization fourier transform ion cyclotron resonance mass spectrometry. Energy & Fuels 24, 4005–4011.

Siljeström, S., Lausmaa, J., Sjovall, P., Broman, C., Thiel, V., Hode, T., 2010. Analysis of hopanes and steranes in single oil-bearing fluid inclusions using time-of-flight secondary ion mass spectrometry (TOF-SIMS). Geobiology 8, 37–44.

Siljeström, S., Volk, H., George, S.C., Lausmaa, J., Sjövall, P., Dutkiewicz, A., Hode, T., 2013. Analysis of single oil-bearing fluid inclusions in mid-Proterozoic sandstones (Roper Group, Australia). Geochimica et Cosmochimica Acta 122, 448–463.

Sinninghe Damste, J.S., Kenig, F., Koopmans, M.P., Koster, J., Schouten, S., Hayes, J.M., de Leeuw, J.W., 1995. Evidence for gammacerane as an indicator of water-column stratification. Geochimica et Cosmochimica Acta 59, 1895–1900.

Sofer, Z., 1984. Stable carbon isotope compositions of crude oils: application to source depositional environments and petroleum alteration. AAPG Bulletin 68, 31–49.

Speight, J.G., 2001. Handbook of petroleum analysis. Wiley-Interscience New York, NY, USA.

Stanford, L.A., Rodgers, R.P., Marshall, A.G., Czarnecki, J., Wu, X.A., 2007. Compositional characterization of bitumen/water emulsion films by negative-and positive-ion electrospray ionization and field desorption/ionization Fourier transform ion cyclotron resonance mass spectrometry. Energy & Fuels 21, 963–972.

Stasiuk, L.D., Snowdon, L.R., 1997. Fluorescence micro-spectrometry of synthetic and natural hydrocarbon fluid inclusions: crude oil chemistry, density and application to petroleum migration. Applied Geochemistry 12, 229–241.

Suchý, V., Dobeš, P., Sýkorová, I., Machovič, V., Stejskal, M., Kroufek, J., Chudoba, J., Matějovský, L., Havelcová, M., Matysová, P., 2010. Oil-bearing inclusions in vein quartz and calcite and, bitumens in veins: Testament to multiple phases of hydrocarbon migration in the Barrandian basin (lower Palaeozoic), Czech Republic. Marine and Petroleum Geology 27, 285–297.

Taylor, P., Larter, S., Jones, M., Dale, J., Horstad, I., 1997. The effect of oil-water-rock partitioning on the occurrence of alkylphenols in petroleum systems. Geochimica et cosmochimica acta 61, 1899–1910.

Theuerkorn, K., Horsfield, B., Wilkes, H., di Primio, R., Lehne, E., 2008. A reproducible and linear method for separating asphaltenes from crude oil. Organic Geochemistry 39, 929–934.

Thiel, V., Heim, C., Arp, G., Hahmann, U., Sjovall, P., Lausmaa, J., 2007. Biomarkers at the microscopic range: TOF-SIMS molecular imaging of archaea-derived lipids in a microbial mat. Geobiology 5, 413–421.

Thomson, J.J., 1913. Rays of Positive Electricity and Their Application to Chemical Analysis, Longmans Green, London.

Tissot, B.P., Durand, B., Espitalié, J., Combaz, A., 1974. Influence of nature and diagenesis of organic matter in formation of petroleum. AAPG Bulletin 58, 499–506.

Tissot, B.P., Welte, D.H., 1984. Petroleum formation and occurrence. Springer Science & Business Media, New York, NY.

Tritlla, J., González-Partida, E., Levresse, G., Banks, D., Pironon, J., 2004. ‘‘Fluorite deposits at Encantada-Buenavista, Mexico: products of Mississippi Valley type processes” [Ore Geol. Rev. 23 (2003), 107–124] – a reply. Ore Geology Reviews 25, 329–332.

Tseng, H.Y., Pottorf, R.J., 2003. The application of fluid inclusion PVT analysis to studies of petroleum migration and reservoirs. Journal of Geochemical Exploration 78–79, 433–436.

Ulrich, W., 1989. The quartz crystals of Herkimer County and its environs. Rocks & Minerals 64, 108–122.

van Krevelen, D.W., 1961. Coal: Typology – Chemistry – Physics– Constitution, first ed. Elsevier, The Netherlands.

Vandenbroucke, M., Largeau, C., 2007. Kerogen origin, evolution and structure. Organic Geochemistry 38, 719–833.

Varga, A., Raucsik, B., Hámor-Vidó, M., Rostási, Á., 2007. Isotope geochemistry and characterization of hydrocarbon potential of black shale from Óbánya Siltstone Formation. Bulletin of the Hungarian Geological Society, 137. 449–472.

Volk, H., George, S.C., Lisk, M., Killops, S.D., Ahmed, M., Quezada, R.A., 2001. Charge histories of petroleum reservoirs in the Gippsland and Taranaki Basins – evidence from the analysis of oil inclusions and crude oils. In: Hill, K.C., Bernecker, T. (Eds.), Eastern Australasian Basins Symposium, A Refocused Energy Perspective for the Future. Petroleum Exploration Society of Australia, Special Publication, Melbourne, pp. 413–422.

Volk, H., Horsfield, B., Mann, U., Suchý, V., 2002. Variability of petroleum inclusions in vein, fossil and vug cements – a geochemical study in the Barrandian Basin (Lower Palaeozoic, Czech Republic). Organic Geochemistry 33, 1319–1341.

Volk, H., Dutkiewicz, A., George, S.C., Ridley, J., 2003. Oil migration in the Middle Proterozoic Roper Superbasin, Australia: evidence from fluid inclusions and their geochemistries. Journal of Geochemical Exploration 78–79, 437–441.

Volk, H., George, S.C., Boreham, C.J., Kempton, R.H., 2004. Geochemical and compound specific carbon isotopic characterisation of fluid inclusion oils from the offshore Perth Basin (Western Australia): implications for recognizing effective oil source rocks. The Australian Petroleum Production and Exploration Association Journal 44, 223–239.

Volk, H., George, S.C., Middleton, H., Schofield, S., 2005a. Geochemical comparison of fluid inclusion and present-day oil accumulations in the Papuan Foreland – evidence for previously unrecognised petroleum source rocks. Organic Geochemistry 36, 29–51.

Volk, H., George, S.C., Dutkiewicz, A., Ridley, J., 2005b. Characterisation of fluid inclusion oil in a Mid-Proterozoic sandstone and dolerite (Roper Superbasin, Australia). Chemical Geology 223, 109–135.

Volk, H., Fuentes, D., Fuerbach, A., Miese, C., Koehler, W., Bärsch, N., Barcikowski, S., 2010. First on-line analysis of petroleum from single inclusion using ultrafast laser ablation. Organic Geochemistry 41, 74–77.

Volk, H., George, S.C., 2019. Using petroleum inclusions to trace petroleum systems – A review. Organic Geochemistry 129, 99–123.

Walderhaug, O., 1990. A fluid inclusion study of quartz-cemented sandstones from offshore mid-Norway – possible evidence for continued quartz cementation during oil emplacement. Journal of Sedimentary Research 60, 203–210.

Walderhaug, O., 1994. Temperatures of quartz cementation in Jurassic sandstones from the Norwegian Continental Shelf – evidence from fluid inclusions. Journal of Sedimentary Research Section A - Sedimentary Petrology and Processes 64, 311–323.

Walters, C.C., Wang, F.C., Qian, K., Wu, C., Mennito, A.S., Wei, Z., 2015. Petroleum alteration by thermochemical sulfate reduction – A comprehensive molecular study of aromatic hydrocarbons and polar compounds. Geochimica et Cosmochimica Acta 153, 37–71.

Wan, Z., Li, S., Pang, X., Dong, Y., Wang, Z., Chen, X., Meng, X., Shi, Q., 2017. Characteristics and geochemical significance of heteroatom compounds in terrestrial oils by negative-ion electrospray Fourier transform ion cyclotron resonance mass spectrometry. Organic Geochemistry 111, 34–55.

Wanczek, K.P., Kanawati, B., 2019. Historical developments in Fourier transform ion cyclotron resonance mass spectrometry. Fundamentals and Applications of Fourier Transform Mass Spectrometry, 3–33.

Wang, Z., Fingas, M., Li, K., 1994. Fractionation of a light crude oil and identification and quantitation of aliphatic, aromatic, and biomarker compounds by GC-FID and GC-MS, part II. Journal of chromatographic science 32, 367–382.

Wang, Z., Fingas, M., 1997. Developments in the analysis of petroleum hydrocarbons in oils, petroleum products and oil-spill-related environmental samples by gas chromatography. Journal of Chromatography A 774, 51–78.

Well 6507/5-1 final well report, 1998. https://factpages.npd.no/pbl/wellbore_documents/3683_6507_5_1_COMPLETION_REPORT.pdf.

Wilhelms, A., Horstad, I., Karlsen, D., 1996. Sequential extraction—a useful tool for reservoir geochemistry? Organic Geochemistry 24, 1157–1172.

Wopenka, B., Pasteris, J.D., Freeman, J.J., 1990. Analysis of individual fluid inclusions by Fourier transform infrared and Raman microspectroscopy. Geochimica et Cosmochimica Acta 54, 519–533.

Wu, Z., Rodgers, R.P., Marshall, A.G., 2004. Compositional determination of acidic species in Illinois no. 6 coal extracts by electrospray ionization Fourier transform ion cyclotron resonance mass spectrometry. Energy & Fuels 18, 1424–1428.

Xu, B., 2003. Biodegradation and accumulation of oils and condensates in the Dønna region Norwegian offshore continental shelf (NOCS). Cand. Scient thesis, University of Oslo, Oslo, Norway.

Yamamoto, M., Taguchi, K., Sasaki, K., 1991. Basic nitrogen compounds in bitumen and crude oils. Chemical Geology 93, 193–206.

Yue, H., Vieth-Hillebrand, A., Han, Y., Horsfield, B., Schleicher, A.M., Poetz, S., 2021. Unravelling the impact of lithofacies on the composition of NSO compounds in residual and expelled fluids of the Barnett, Niobrara and Posidonia formations. Organic Geochemistry 155, 104225.

Zanella, A., Cobbold, P.R., Boassen, T., 2015. Natural hydraulic fractures in the Wessex Basin, SW England: widespread distribution, composition and history. Marine and Petroleum Geology 68, 438–448.

Zhang, Y., Liao, Y., Guo, S., Xu, C., Shi, Q., 2016. Molecular transformation of crude oil in confined pyrolysis system and its impact on migration and maturity geochemical parameters. Energy & Fuels 30, 6923–6932.

Zhang, Z., Greenwood, P., Zhang, Q., Rao, D., Shi, W., 2012. Laser ablation GC-MS analysis of oil-bearing fluid inclusions in petroleum reservoir rocks. Organic Geochemistry 43, 20–25.

Zhu, Y., Vieth-Hillebrand, A., Noah, M., Poetz, S., 2019. Molecular characterization of extracted dissolved organic matter from New Zealand coals identified by ultrahigh resolution mass spectrometry. International Journal of Coal Geology 203, 74–86.

Ziegs, V., Noah, M., Poetz, S., Horsfield, B., Hartwig, A., Rinna, J., Skeie, J.E., 2018. Unravelling maturity- and migration-related carbazole and phenol distributions in Central Graben crude oils. Marine and Petroleum Geology 94, 114–130.

SUPPLEMENTARY

In the following tables the data for the figures presented in the three main chapters 2, 3 and 4, which are not already shown in tables in these chapters, are listed.

Table S1. Relative abundance of the compound class data in figure 2.5.

	GE		TN		PK		MX	
Compounds class	APPI (+)	ESI (–)	APPI (+)	ESI (–)	APPI (+)	ESI (–)	APPI (+)	ESI (–)
	(%)		(%)		(%)		(%)	
HC	11.36	nd.	33.40	nd.	46.46	nd.	36.61	nd.
O_1	36.11	3.26	22.56	2.58	32.73	4.33	5.14	3.32
O_2	21.03	23.10	11.99	30.66	14.64	34.61	1.10	32.39
O_3	7.11	20.68	4.53	27.36	2.81	23.31	0.10	16.02
O_4	12.34	12.50	13.44	6.70	1.04	14.55	1.61	3.55
O_5	1.34	7.79	1.77	1.85	0.00	5.80	0.02	0.91
O_6	0.98	4.61	2.17	0.62	0.00	1.30	0.31	0.28
N_1	6.99	nd.	0.37	nd.	0.87	0.30	5.81	14.67
S_1	0.02	nd.	1.85	nd.	0.00	nd.	40.98	nd.
S_2	0.00	nd.	0.24	nd.	0.00	nd.	3.86	nd.
N_1S_1	0.00	0.00	0.00	0.07	0.00	0.00	0.00	2.16
N_1O_1	1.03	0.00	0.13	0.00	0.35	0.00	0.34	0.09
N_2O_2	0.80	1.64	1.23	2.80	0.09	0.35	0.08	3.29
S_1O_1	0.03	0.52	0.59	3.54	0.93	1.86	3.07	1.11

Note: nd. = not detectable or not determinable; HC = hydrocarbon; GE = Germany; TN = Tunisia; PK = Pakistan; MX = Mexico; APPI (+) = Atmospheric Pressure Photoionization in positive ion mode; ESI (–) = Electrospray Ionization in negative ion mode.

Table S2. Relative abundance of the DBE 5 groups of the hydrocarbon data in figure 2.9.

Carbon number	GE	TN	PK	MX	Carbon number	GE	TN	PK	MX
	(%)					(%)			
15	nd.	nd.	nd.	nd.	43	0.021783	nd.	0.081427	0.078196
16	0.015982	0.023378	0.018603	nd.	44	0.026877	nd.	0.083685	0.080736
17	0.019368	0.024656	0.024975	0.010024	45	nd.	nd.	0.069286	0.068222
18	0.038142	0.05327	0.03483	0.011554	46	nd.	nd.	0.062448	0.058262
19	0.039226	0.061901	0.045926	0.018888	47	nd.	nd.	0.058476	0.061246
20	0.051342	0.066618	0.05243	0.025537	48	nd.	nd.	0.051703	0.05445
21	0.050391	0.075151	0.057496	0.034518	49	nd.	nd.	0.047702	0.044956
22	0.056188	0.073889	0.070889	0.038442	50	nd.	nd.	0.044631	0.044113
23	0.068975	0.094031	0.082505	0.052355	51	nd.	nd.	0.046525	0.044531
24	0.086946	0.131107	0.100419	0.065305	52	nd.	nd.	0.036167	0.039991
25	0.07045	0.102524	0.100819	0.073686	53	nd.	nd.	0.029571	0.032897
26	0.082636	0.12875	0.132547	0.0915	54	nd.	nd.	0.027818	0.026569
27	0.079418	0.133179	0.12392	0.084898	55	nd.	nd.	0.024725	0.026285
28	0.08615	0.129637	0.14143	0.10884	56	nd.	nd.	0.025122	0.0256
29	0.128982	0.196716	0.142154	0.107656	57	nd.	nd.	0.021338	0.025117
30	0.077121	0.113453	0.147136	0.114028	58	nd.	nd.	0.024665	0.019083
31	0.0685	0.081881	0.129184	0.10365	59	nd.	nd.	0.018375	0.017623
32	0.077357	0.074878	0.154119	0.120801	60	nd.	nd.	nd.	0.015236
33	0.056922	0.051093	0.113907	0.096839	61	nd.	nd.	nd.	0.014952
34	0.061781	0.059961	0.136635	0.117184	62	nd.	nd.	nd.	0.011341
35	0.053843	0.044381	0.123267	0.10964	63	nd.	nd.	nd.	0.013493
36	0.040573	0.03528	0.10721	0.091594	64	nd.	nd.	nd.	0.010098
37	0.048125	0.035013	0.122189	0.109494	65	nd.	nd.	nd.	nd.
38	0.035163	nd.	0.114491	0.099616	66	nd.	nd.	nd.	nd.
39	0.032744	0.02201	0.100322	0.09532	67	nd.	nd.	nd.	nd.
40	0.035904	0.026457	0.113024	0.10772	68	nd.	nd.	nd.	nd.
41	0.026394	nd.	0.09283	0.084757	69	nd.	nd.	nd.	nd.
42	nd.	nd.	0.074301	0.071601	70	nd.	nd.	nd.	nd.

Note: nd. = not detectable or not determinable; GE = Germany; TN = Tunisia; PK = Pakistan; MX = Mexico.

Table S3. Relative abundance of *n*-alkane distribution data in figure 3.3.

Carbon number	G1		G2		G3		T1		T2	
	Ad	FI	Ad	FI	Ad	FI	Ad	FI	Ad	FI
13	4.81	nd.	7.01	nd.	6.23	0.00	0.75	nd.	3.66	nd.
14	17.12	nd.	21.89	nd.	20.49	0.00	4.08	nd.	13.32	nd.
15	50.38	1.92	67.60	nd.	60.51	10.62	32.81	nd.	58.30	2.27
16	100.00	29.39	96.47	nd.	100.00	39.48	66.05	nd.	78.69	24.53
17	93.96	80.27	100.00	30.73	99.10	95.36	100.00	15.25	100.00	100.00
18	72.31	100.00	69.26	58.25	68.99	95.25	45.22	34.44	35.92	91.05
19	50.56	89.51	47.19	96.48	47.40	100.00	13.03	45.88	9.35	69.34
20	31.84	67.43	27.93	99.25	27.70	91.19	5.72	59.86	2.68	66.32
21	19.21	47.04	16.34	100.00	16.26	82.22	4.98	81.58	1.63	69.42
22	11.43	34.32	9.70	93.17	9.94	73.03	4.02	90.22	1.53	72.83
23	6.30	23.98	4.93	88.23	5.82	60.48	3.48	85.49	1.38	70.51
24	3.75	32.80	2.41	82.27	2.91	60.72	3.17	100.00	1.31	72.70
25	1.99	12.76	0.96	70.69	1.18	47.15	2.62	74.62	1.02	66.38
26	0.81	12.02	0.43	62.16	0.62	42.14	2.41	64.88	0.84	65.76
27	0.87	8.65	0.31	52.54	0.35	38.04	2.04	63.46	0.79	61.17
28	0.77	8.87	nd.	44.62	0.29	31.81	2.13	60.52	0.62	58.19
29	0.57	6.44	nd.	39.64	nd.	33.36	1.77	58.97	0.61	52.84
30	nd.	4.36	nd.	26.71	nd.	19.74	1.13	43.58	0.43	41.43
31	nd.	3.50	nd.	20.33	nd.	17.73	0.85	34.41	0.34	33.75
32	nd.	3.64	nd.	16.60	nd.	9.75	0.54	28.74	0.22	24.38
33	nd.	2.50	nd.	13.16	nd.	8.19	0.37	24.12	0.16	18.80
34	nd.	2.13	nd.	11.51	nd.	5.92	0.22	16.17	0.09	12.53
35	nd.	nd.	nd.	7.73	nd.	4.16	0.13	16.18	0.07	10.82
36	nd.	nd.	nd.	3.08	nd.	3.63	0.13	9.13	nd.	7.18
37	nd.	nd.	nd.	5.22	nd.	2.06	nd.	4.62	nd.	4.63
38	nd.	nd.	nd.	nd.	nd.	nd.	nd.	nd.	nd.	4.08

Note: nd. = not detectable or not determinable; G = Garn Formation; T = Tilje Formation; Ad = adsorbed oil; FI = inclusion oil.

Table S4. Relative abundance of the compound class data in figure 3.5.

Compound class	G1-FI	G2-FI	T1-FI
		(%)	
O_1	8.20	11.54	6.12
O_2	6.27	11.96	6.39
O_3	2.81	5.10	3.10
O_4	8.10	14.25	20.17
O_5	2.61	2.74	5.15
O_6	2.33	2.59	2.31
O_7	1.09	0.23	1.48
O_8	0.92	0.25	1.72
N_1	23.01	8.37	13.58
N_2	0.39	0.19	1.01
N_1O_1	13.71	5.34	6.05
N_1O_2	5.27	2.47	3.21
N_1O_3	3.92	2.74	2.03
N_1O_4	2.95	2.65	1.98
N_1O_{5-8}	6.20	5.94	5.31
N_2O_{1-2}	1.43	2.35	3.12
S_1	0.78	1.93	2.32
S_2	0.17	0.14	0.20
S_1O_1	0.96	2.10	2.28
S_1O_2	0.96	1.14	0.78
S_1O_{3-8}	0.38	1.14	0.77
HC	7.55	14.85	10.19

Note: G = Garn Formation; T = Tilje Formation; FI = inclusion oil; HC = hydrocarbon.

Table S5. Compound specific carbon isotopic composition of *n*-alkane data in figure 3.6.

Carbon number	G1-Ad	G2-Ad	T1-Ad
	$\delta^{13}C$ (‰)		
14	-30.85	-30.89	nd.
15	-30.74	-32.5	nd.
16	-31.82	-30.94	-35.11
17	-31.06	-30.38	-33.99
18	-30.49	-30.34	-33.58
19	-30.36	-29.88	-34.02
20	-30.25	-30.1	-33.82
21	-30.15	-30.19	-32.73
22	-29.93	-29.86	-31.84
23	-30.38	-29.7	-30.25
24	-31.29	-29.7	-28.58
25	-27.92	-27.3	-27.22
26	-31.02	-30.1	-28.82
27	-30.83	-29.95	-28.76
28	-30.01	-29.95	-29.46
29	nd.	nd.	-26.9
30	nd.	nd.	-28.65
31	nd.	nd.	-29.52
32	nd.	nd.	-29.58

Note: G = Garn Formation; T = Tilje Formation; Ad = adsorbed oil.

Table S6. Compound specific carbon isotopic composition of *n*-alkane data in figure 4.4.

Carbon number	SR-1	SR-2	FI-1	FI-2
	$\delta^{13}C$ (‰)			
15	-32.99	nd.	nd.	nd.
16	-33.41	-33.67	nd.	nd.
17	-33.9	-34.37	nd.	nd.
18	-33.79	-34.14	-33.28	-33.58
19	-33.66	-33.38	-32.93	-33.08
20	-33.79	-34	-33.08	-33.34
21	-33.74	-34.72	-33.45	-34.02
22	-33.92	-34.33	-33.53	-34.03
23	-33.53	-33.69	-33.58	-34.16
24	-33.61	-33.95	-33.44	-33.63
25	-33.43	-32.77	-33.23	-33.55
26	-33.21	-34.04	-33.49	-33.78
27	-33.58	-34.22	-34.11	-34.33
28	-33.82	-33.34	-33.51	-33.82
29	-33.36	-33.49	-32.97	-33.5
30	-33.27	nd.	-32.41	-32.42
31	-32.97	nd.	-32.8	-32.5
32	-34.25	nd.	-32.89	-33.56
33	-32.95	nd.	-32.32	-31.14
34	-34.78	nd.	-33.49	-33.21
35	-35.43	nd.	nd.	-33.64

Note: nd. = not detectable or not determinable; SR = source rock extract; FI = inclusion oil.

Table S7. Relative abundance of the compound class data in figure 4.5.

Compound class	SR-1	SR-2	FI-3	FI-4	FI-5	FI-6
O_1	17.46	16.78	12.32	12.57	12.78	12.24
O_2	6.33	3.45	5.91	5.13	5.84	3.94
O_3	0.68	0.07	1.64	1.33	1.08	0.37
O_4	1.57	0.27	3.58	2.30	2.18	0.84
N_1	13.53	17.65	10.39	11.86	11.53	14.77
S_1	6.98	6.95	10.58	10.71	12.29	14.53
N_1O_1	6.74	7.18	3.12	3.14	1.94	3.40
$N_1O_{2\text{-}8}$	1.81	0.50	2.74	0.97	0.69	0.46
S_1O_1	5.85	3.72	2.43	1.71	3.81	3.05
$S_1O_{2\text{-}8}$	2.95	0.02	2.84	6.05	3.20	1.96
HC	33.88	41.80	42.50	42.58	43.90	43.97

Note: nd. = not detectable or not determinable; HC = hydrocarbon; SR = source rock extract; FI = inclusion oil.

Table S8. Normalized abundance of compound data in figure 4.13.

Carbon number	DBE 12				DBE 20			
	SR-2_HC	FI-6_HC	SR-2_N1	FI-6_N1	SR-2_HC	FI-6_HC	SR-2_N1	FI-6_N1
	(%)							
15	nd.	nd.	nd.	nd.	nd.	nd.	nd.	nd.
16	nd.	nd.	nd.	nd.	nd.	nd.	nd.	nd.
17	nd.	nd.	nd.	nd.	nd.	nd.	nd.	nd.
18	0.11	0.13	0.27	nd.	nd.	nd.	nd.	nd.
19	0.22	0.23	0.56	0.21	nd.	nd.	nd.	nd.
20	0.53	0.47	0.75	0.25	nd.	nd.	nd.	nd.
21	0.52	0.58	0.78	0.39	nd.	nd.	nd.	nd.
22	0.82	1.03	0.95	0.53	nd.	nd.	nd.	nd.
23	0.96	1.36	0.87	0.62	nd.	nd.	nd.	nd.
24	0.98	1.35	1.11	0.62	nd.	nd.	nd.	nd.
25	1.52	1.76	1.50	1.29	0.09	nd.	nd.	nd.
26	1.75	2.95	2.05	1.53	0.26	nd.	0.36	nd.
27	2.78	3.17	1.39	1.54	1.20	0.39	2.28	nd.
28	2.18	3.07	2.08	2.54	3.66	1.01	3.44	0.62
29	2.94	4.19	2.45	2.70	4.06	1.54	5.01	1.11
30	2.94	4.18	3.27	3.16	6.15	2.63	6.56	1.60
31	4.08	4.14	3.22	3.33	6.36	3.97	6.97	2.03
32	4.17	4.33	3.61	3.41	6.87	4.13	5.91	2.69
33	4.39	3.92	3.58	3.80	6.66	4.99	5.72	2.64
34	4.27	4.22	3.62	3.37	6.31	4.59	5.01	3.61
35	3.76	3.30	4.32	4.50	5.45	5.58	4.32	3.18
36	4.61	4.27	3.56	3.80	4.53	4.46	4.84	4.49
37	3.80	3.88	3.63	3.48	5.49	5.51	3.85	4.38
38	3.40	3.28	3.71	4.18	4.40	5.50	3.31	3.59
39	3.68	3.85	3.19	4.07	3.64	4.14	3.47	4.58
40	3.24	3.42	3.48	3.63	3.70	4.78	3.02	4.46
41	3.06	2.91	3.50	3.84	2.80	4.37	2.84	5.26
42	3.17	3.20	3.24	3.32	2.53	3.64	2.96	4.54
43	2.90	2.61	3.27	2.85	2.57	5.03	2.63	3.82
44	2.91	2.15	3.27	3.29	2.30	3.46	2.43	3.35
45	2.94	2.90	2.90	3.48	2.15	2.75	2.49	3.61
46	2.58	3.07	2.46	2.96	2.00	4.19	2.25	4.26
47	2.14	2.49	2.48	2.69	1.80	4.58	1.83	3.67
48	2.07	1.83	2.65	2.36	1.50	3.83	1.67	3.05
49	2.15	1.64	2.29	2.31	1.30	2.28	1.82	2.76
50	1.88	1.48	2.02	2.22	1.40	2.08	1.63	2.83
51	1.59	1.42	2.05	2.11	1.22	1.70	1.36	2.99
52	1.57	1.27	2.05	2.00	1.04	1.90	1.29	2.47
53	1.60	1.37	1.87	1.80	0.99	1.67	1.38	2.71
54	1.41	1.12	1.58	1.44	0.96	1.78	1.18	2.21
55	1.23	0.88	1.32	1.31	0.86	1.54	1.05	1.94
56	1.04	0.85	1.32	1.39	0.74	0.74	0.82	1.86
57	0.93	0.81	1.14	1.25	0.60	0.64	0.87	1.69
58	0.92	0.78	1.07	1.09	0.60	nd.	0.75	1.68
59	0.86	0.66	1.00	0.92	0.57	nd.	0.67	1.39

60	0.75	0.54	0.94	0.88	0.48	0.59	0.66	1.17
61	0.65	0.50	0.78	0.84	0.47	nd.	0.60	1.32
62	0.58	0.47	0.75	0.69	0.38	nd.	0.56	1.21
63	0.53	0.38	0.59	0.71	0.33	nd.	0.52	1.27
64	0.44	0.37	0.58	0.52	0.35	nd.	0.40	nd.
65	0.39	0.28	0.44	0.42	0.31	nd.	0.38	nd.
66	0.36	0.23	nd.	nd.	0.21	nd.	0.34	nd.
67	0.31	0.21	0.49	0.36	0.19	nd.	0.27	nd.
68	0.29	0.19	nd.	nd.	0.18	nd.	0.27	nd.
69	0.28	0.16	nd.	nd.	0.17	nd.	nd.	nd.
70	0.20	0.15	nd.	nd.	0.15	nd.	nd.	nd.
71	nd.	nd.	nd.	nd.	nd.	nd.	nd.	nd.
72	0.19	nd.	nd.	nd.	nd.	nd.	nd.	nd.
73	0.13	nd.	nd.	nd.	nd.	nd.	nd.	nd.
74	0.13	nd.	nd.	nd.	nd.	nd.	nd.	nd.
75	nd.	nd.	nd.	nd.	nd.	nd.	nd.	nd.
76	0.13	nd.	nd.	nd.	nd.	nd.	nd.	nd.
77	nd.	nd.	nd.	nd.	nd.	nd.	nd.	nd.
78	nd.	nd.	nd.	nd.	nd.	nd.	nd.	nd.
79	nd.	nd.	nd.	nd.	nd.	nd.	nd.	nd.
80	nd.	nd.	nd.	nd.	nd.	nd.	nd.	nd.

Note: nd. = not detectable or not determinable; DBE = Double bond equivalent; HC = hydrocarbon; SR = source rock extract; FI = inclusion oil.